Dissecting Proteostatic Regulation of $CD8^+$ T cell Immunity

by

Luis Correa

A dissertation submitted in partial fulfillment
of the requirements for the degree of
Doctor of Philosophy
(Immunology)
in the University of Michigan
2024

Doctoral Committee:

Assistant Professor Shannon A. Carty Co-Chair
Professor Cheong-Hee Chang Co-Chair
Associate Professor Costas A. Lyssiotis
Professor Bethany B. Moore
Associate Professor Stephen C.J. Parker

Luis Correa

lcorrea@umich.edu

ORCID iD: 0000-0002-0345-5938

Dedication

To my family

Acknowledgements

Similar to how extrinsic signals and environments allow for T cells to persist through challenging times, this thesis work could not have been completed without the environment and people that provided positive signals during my differentiation. The master regulator allowing me to persist through the completion of this work and remain a functional researcher is my advisor, Dr. Shannon Carty. Shannon accepted me into her young lab as her first graduate student. During my Ph.D. she has orchestrated my development from a naïve scientist into a fairly experienced one capable of responding to challenges rapidly and effectively.

I am also incredibly thankful for the members of my committee meeting, Drs. Cheong-Hee Chang, Bethany B. Moore, Costas A. Lyssiotis, and Stephen CJ. Parker. I looked forward to my committee meetings, as they were filled with great supportive discussions that helped drive my work and my professional development. Outside of the committee meetings, each member continued to be available to support my development.

The Department of Computational Medicine and Bioinformatics (DCMB) helped me achieve one of my scientific dreams, becoming a proficient bioinformatics analyst. I am incredibly thankful to DCMB for not only offering the opportunity to pursue a master's in science with one's Ph.D. but also offering meaningful coursework and a welcoming, equitable learning environment. I also want to thank Drs. Stephen Guest, Christina Mitrea, and all the instructors and graduate teaching assistants; their passion for teaching and kindness made the challenging coursework an incredible experience.

I would like to thank the immunology program for its endless commitment to its students and our training. How to best train Ph.D. scientists is a complex process, but the program has managed a formula that continues to evolve to give us the best opportunities for development. I am also thankful for their commitment to building an inclusive and connected community of students. My time in the program has been wonderful, and I am grateful for the opportunities and support that have allowed me to grow during my time here.

It is well known that in the absence of $CD4^+$ T cell help, a $CD8^+$ T cell will become dysfunctional and fail to persist. There have been stellar members of the community who have greatly impacted my time as a graduate student. My cohort has been a stellar group of individuals, and I am thankful to have collaborated with almost all of them in some way through the years. I am grateful for the friendship of older students who helped me traverse graduate school.

Finally, I'd like my family and partner Dr. Rachel Harris for supporting my professional aspirations and dealing with my work tendencies.

Table of Contents

List of Figures

Abstract

$CD8^+$ T cells are a component of the immune system that are critical to eradicating intracellular pathogens and tumors, as well as providing long-lasting immune protection; however, not all immune responses elicit durable responses leading to loss of protection against infections and malignancy. Though $CD8^+$ T cells markedly upregulate translation and rapidly remodel their proteome during effector differentiation, little is understood about the role proteostasis plays in $CD8^+$ T cell immune responses. Sel1L is a critical component of the endoplasmic reticulum associated degradation (ERAD) complex, facilitating the recognition, retro-translocation of ER misfolded proteins and subsequent proteasomal degradation in the cytosol. Nothing is known about the role of ERAD in $CD8^+$ T cell responses.

First, we began by characterizing the experience of ER stress by utilizing *in vitro* models of T cell activation. Using orthogonal approaches leveraging microscopy, biochemistry and flow cytometry, we uncover that T cells experience transient ER stress *in vitro*. The ER stress is characterized by misfolded protein accumulation as well as induction of ER stress alleviating pathways such as the unfolded protein response (UPR) and ERAD. *In vivo* we used murine a model of acute viral infection, lymphocytic choriomeningitis virus Armstrong (LCMV). Utilizing this model, we find that LCMV specific T cells experience ER stress *in vivo* as well as inducing pathways that alleviate ER stress. These data demonstrate that T cell activation and differentiation is associated with transient ER stress and the induction of ER stress alleviating pathways.

Second, to determine how Sel1L/ERAD regulates antigen-specific effector $CD8^+$ T cell survival and function we generated mice with T cells reactive to LCMV that lack Sel1L/ERAD (Sel1LcKO-P14). At baseline Sel1LcKO-P14 cells are comparable to wild-type-P14, with no defects in activation or ER homeostasis. By transferring WT-P14 and Sel1LcKO-P14 in equivalent ratios into mice infected with LCMV, we find that Sel1L is necessary for T cell persistence as the Sel1LcKO-P14 fail to persist. Mechanistically, we find that Sel1LcKO-P14 have reduced oxidative metabolism (OXPHOS) a metabolic program necessary for optimal T cell persistence. To gain insight into how Sel1L regulates T cell metabolism we conducted *in vitro* studies and find that Sel1L loss is associated with reduction in c-Myc, a central regulator of T cell metabolism, and increased mitochondrial ER contact sites (MERCS).

Though the mechanism by which Sel1L regulates c-Myc and the role of MERCS in orchestrating T cell metabolism remain to be fully elucidated these results further demonstrate the connection between the ER and metabolism. Together these findings advance the understanding of pathways regulating T cell persistence. We present these findings in murine systems with correlates in human T cells, they will be significant for future studies aiming to improve the persistence of T cells.

Chapter 1 – Introduction

1.1 The logic of immunity

The immune system plays a vital role in protecting the host from foreign pathogens, cancerous cells, and homeostasis through the healing of wounds. Though cells of hematopoietic origin encompass the focus of "immune cells" many non-hematopoietic cells across the body play a role in initiating, coordinating, and resolving immune responses. The first challenge a pathogen faces is overcoming barrier tissues. At these sites, such as the airway, skin, and intestines, a tight epithelial layer prohibits the entry of foreign pathogen. Additionally, mucus, sweat, and acidity make for significant challenges to invading pathogens. In the event that a pathogen prevails over these barriers, it is met by an armament of germline encoded pathogen recognition receptors that directly recognize pathogen associated molecular patterns (i.e. viral RNA, viral DNA) and pattern recognition receptors that directly recognize danger associated molecular patterns (i.e. intracellular components in extracellular space such as histones). Though these receptors can recognize pathogens, they recognize broad patterns and are not specific to a given pathogen. T cell and B cell receptors are randomly generated in such a way to recognize non-self-protein and provide the specific recognition of antigen. The recognition of T cell receptors is restricted to major histocompatibility complexes (MHC) that present peptides. B cell receptors recognize soluble molecules. While T cell and B cell responses will not be until the latter part of the response myeloid cells such as macrophages and neutrophils serve as first responders eating away at pathogens and secreting inflammatory molecules. Natural Killer (NK) cells mediate the killing of pathogen

infected cells by secreting cytotoxic proteins, proteins that induce cell death in an infected/transformed cell expressing pathogen or danger associated molecular patterns. Later in the infection, $CD8^+$ T cells will orchestrate the killing of cells infected with intracellular pathogens through the specific recognition of pathogen derived proteins on host cell MHC class I. Importantly, after pathogen is cleared, a fraction of $CD8^+$ T cells will persist, referred to as memory $CD8^+$ T cells. These cells will protect the host from secondary infection by mounting a response that is faster and superior to the primary encounter, eliminating the pathogen before serious disease can occur. This principle of memory formation underlies the rationale of vaccines, where memory responses are generated by careful administration of vaccines sparing patients of risk of primary infection and still providing protection to pathogens. Unfortunately, immunity wanes over time, limiting protection. By understanding the processes that contribute to memory formation and persistence, superior vaccines can be generated.

1.2 Scope of the dissertation

The presented dissertation encompasses a mechanistic study that characterizes endoplasmic reticulum (ER) stress pathways in $CD8^+$ T cell fate and determines the consequences of loss of pathways limiting ER stress. The work is conducted in the context of *in vitro* activation of T cells as well as utilizing murine models of acute viral infection. In chapter 1, the molecular determinants of $CD8^+$ T cell fate will be introduced. The model system for studying T cell biology will be briefly introduced. How $CD8^+$ T cells differentiate during infection and known phenotypes, ontogeny and function will be discussed. I will also discuss how different cell intrinsic and extrinsic processes, such as metabolism and cytokines, orchestrate the fate of these cells. In doing so, I will introduce the dynamic regulation of protein synthesis during activation, the mechanisms of maintaining protein homeostasis, and highlight the consequences of failing to maintain

proteostasis in other cell types. Lastly, I will cover the proteostatic pathways central to the experimental work: the UPR and ERAD. In chapter 2, the methods utilized through the dissertation will be thoroughly discussed. Early in chapter 3 I will focus on characterizing proteostatic pathways during T cell activation in mice and humans. I will highlight the transient experience of proteostatic stress. To conclude the chapter, I will demonstrate the necessity of proteostatic pathways in maintaining $CD8^+$ T cell function. Finally, I will discuss the contributions and implications of this work to our understanding of T cell biology and therapeutic potential.

1.3 Lymphocytic choriomeningitis virus

Lymphocytic choriomeningitis virus (LCMV) is a member of the Arenaviridae family of RNA virus (1). The Arenaviridae family is subdivided into two groups according to antigenic properties. The tacaribe serocomplex composing viruses endogenous to the Americas such as the Guanarito, Latino, and Parana viruses. LCMV resides in the Lassa-lymphocytic choriomeningitis serocomplex. Though LCMV has been known to cause mild disease in humans, unlike its cousin Lassa virus, which is listed as a category A priority pathogen by the National Institute of Allergy and Infectious Diseases, LCMV is mostly known for its use as a laboratory model for studying immune responses to viral infection in mice.

A unique property of LCMV as a model system is that it is not lytic to the host mouse, thus the consequences of infection as they pertain to cell death and tissue damage are resultant of the immune response to virus and virus-infected cells. Furthermore, like other RNA viruses, it contains a small genome only 10.7 kilobases long. Of the 5 genes encoded in the viral genome, glycoprotein (GP), nucleoprotein (NP), polymerase (L), and Zinc ring (Z); GP and NP account for >98% of the antigen specific $CD8^+$ T cell response (2). Elegant studies utilizing truncated version of the LCMV genes revealed that in in the context of C57BL6 (B6) mice containing MHC $H2\text{-}D^b$

the major epitopes to be derived from GP gene product glycoprotein1 amino acids 33-41, GP gene product glycoprotein 2 amino acids 276-286, and nuclear protein gene product amino acids 396-404 (2-6). This knowledge allowed for the generation of peptides that are able to stimulate LCMV-specific $CD8^+$ T cells *ex vivo* in mechanistic studies.

Concurrently with these discoveries, different groups began to uncover biological insights that would converge into the discovery of memory T cells. An important study by the group of Mark M. Davis demonstrated that infection leads to the expansion specific T cell receptors (TCR) sequences, showing the expansion and preservation of specific T cell clones (7). Shortly after, the group revolutionized the study of T cell biology with the development of multimerized fluorescently labeled peptide-major histocompatibility complex MHC ligands, also known as MHC tetramers (8). MHC tetramers allowed for the identification of antigen specific T cells through flow cytometry, opening the doors for characterization and isolation of antigen specific cells longitudinally throughout infection. Utilizing MHC tetramers, Ahmed and colleagues were able to quantify specific responses to LCMV through time and asserted that $CD8^+$ T cells expanding during infection represented only antigen-specific, cells whereas before the convention was that ~ 95% of responding $CD8^+$ T cells were not antigen-specific (9).

1.4 Naïve T cell differentiation

Following their development in the thymus, $CD8^+$ T cells are endowed with a functional receptor that recognizes peptide sequences not found in the host in the context of their major histocompatibility complex. The diversity of T cell receptors gives the capacity for any given person or mouse to have numerous T cell clones that are reactive to pathogens that they have never seen. For a pathogen such as LCMV, the frequency of $CD8^+$ T cells reactive to model peptide GP33-41, also known as the "precursor frequency", is estimated to be approximately 100-200 cells

in a naïve mouse (10). In both mice and humans, thymic output of new T cells is diminished early in adulthood, meaning that naïve cells must be able to persist in a bioenergetically low demand state until they are needed (11).

During homeostasis, naïve T cells (TN) require two signals to be maintained: homeostatic cytokine interleukin (IL)-7 and contact with self MHC peptide complexes. Failure to engage in any of the homeostatic signals leads to loss of naïve T cells (12, 13). TN are maintained in a non-proliferative state and do not engage in the cell cycle, existing in the termed "G0" non-proliferating state of the cell cycle (for comprehensive review see Chapman et al.(14)). Additionally, TN cells maintain low metabolic, transcriptional, and translational rate together, these characteristics are referred to as "quiescence". Loss of naïve T cell quiescence without TCR activation and co-stimulation results in an inability of cells to survive (15-17).

TN cells are activated in secondary lymphoid organs (lymph nodes and the white pulp of spleen) by antigen presenting cells presenting their cognate peptide in the context of MHC. Activation results in exit of the quiescent state and leads to expansion of selected T cell clones. Relative to TN cells, activated cells have dramatic changes in transcription, metabolism, and protein synthesis. Both *in vitro* and *in vivo*, there approximately a 4-fold increase in protein synthesis that subsides after infection is cleared (18-24). Concurrently with changes in protein synthesis, T cells orchestrate remodeling of metabolic programs transitioning from oxidative phosphorylation to a glycolytic Warburg-like metabolic program (25). As cells transition from effector to memory there is a reacquisition of a quiescent phenotype of low protein synthesis, oxidative metabolism, and cell cycle arrest (18, 26-28).

1.5 Determinants of antigen specific CD8$^+$ T cell fate during infection

At the peak of the T cell response to acute viral infection such as LCMV-Armstrong (LCMV), antigen specific CD8$^+$ T cells can be found to have distinct persistence potential. The terminal effector (TE) subset, identified by KLGR1 expression and lack of IL-7 receptor alpha chain (CD127), contains limited potential to give rise to memory T cells (28). Memory precursor (MP) CD8$^+$ T cells are identified by expression of CD127 and lack of KLRG1 (29, 30). Adoptive transfer of memory precursors showed that these cells contained a preferential ability to give rise to memory CD8$^+$ T cells (29, 30). Though terminal effectors primarily die, they can contribute to the memory T cell pool though in a significantly reduced capacity (29-31).

1.5.1 *Transcription*

After stimulation of the T cell receptor, activation signals converge on various transcription factors including Nuclear Factor of Activated T cells (NFAT), Activator Protein-1 (AP-1) and Nuclear factor kappa-light-chain-enhancer of activated B cells (NF-kb) (32). Through these transcription factors, T cells acquire the transcriptional program required for their function. Microarray and RNA-sequencing have been employed to characterize the transcriptomes of T cells at different stages to help elucidate the mechanistic underpinning of their fate and function (30, 33).

At the transcriptional level, naïve, effector and memory CD8$^+$ contain distinct transcriptional programs (30, 34). Indeed, the transcriptional signature of cells through differentiation allowed for the identification of transcription factors both necessary and sufficient to orchestrate T cell fate. Specifically, cooperative activity of transcription factors T cell factor 1 (TCF-1), B cell lymphoma 6 (BCL-6), Eomesodermin (EOMES), Inhibitor of DNA Binding 3 (ID3), and Forkhead box protein O1 (FOXO1) driving memory formation and T-box expressed in

T cells (T-bet), B lymphocyte-induced maturation protein-1 (Blimp-1), DNA Binding Inhibitor 2 (ID2), Interferon Regulatory Factor 4 (IRF4) and Zearalenone biosynthesis protein 2 (ZEB2) driving terminal differentiation have shown to be necessary and sufficient to orchestrate each fate (35-43).

1.5.2 *Cytokines*

During infection $CD8^+$ T cells are exposed to a milieu of cytokines capable of signaling through cell surface receptors to orchestrate their fate, and this signal is classically referred to as signal 3. The most appreciated signal 3 cytokine is interleukin-2 (IL-2) originating from $CD4^+$ T cells. In recently activated $CD8^+$ T cells, the IL-2 high affinity receptor (CD25) is quickly expressed and provides necessary signaling for cells survival. In the absence of IL-2 from helper $CD4^+$ T cells, memory $CD8^+$ T cells fail to develop and function (44).

IL-7 and IL-15 are necessary but not sufficient for the persistence of $CD8^+$ T cells (29, 30). IL-7 signals through the IL-7 Receptor, a multimeric protein comprised of the IL-7 receptor alpha chain (CD127) and the common gamma chain (CD132). IL-15 signals through the multimeric receptor comprising IL15Ra (CD215), IL2Rb (CD122) and common gamma chain (CD132) (45, 46). These receptors induce key survival signaling such as the upregulation of key anti-apoptotic factor BCL-2 (46-49). IL-7 additionally has been implicated in supporting the metabolic program required for $CD8^+$ T cell persistence (50).

In conclusion, cytokines play a critical role in orchestrating $CD8^+$ T cell fate. The downstream pathways activated by cytokines are crucial for the function of cells. While the action of cytokines like IL-7 might not be sufficient to drive T cell fate, the pathways supported by cytokines play a crucial role in T cell persistence.

1.6 Metabolism

1.6.1 Naïve T cell metabolism

Before antigen encounter, T cells exist in a state of quiescence, defined as having low metabolism and remaining in a nonproliferative state of the cell cycle. Tonic TCR and IL-7 signaling are known to be necessary for T cell homeostasis. Specifically in the absence of IL-7 signaling, T cells lose the capacity to undergo oxidative phosphorylation (OXPHOS) and meet their bioenergetic needs even if excess nutrients are available (47, 51-53). Naïve T cells engage primarily OXPHOS to maintain their energy needs (26). Despite being called "quiescent" naïve T cells engage in a variety of process to maintain this state and require energy to traverse the vasculature as they survey secondary lymphoid organs, additionally active degradation and turnover of transcription factors, such as FOXO1, facilitates the exit from quiescence after activation (54, 55). Naïve T cell oxidative phosphorylation is driven primarily through glucose and fatty acids (56). Glutamine can make up for situations in which glucose is restricted and can contribute to OXPHOS in normal conditions (57, 58).

1.6.2 Activated T cell and memory T cell metabolism

As T cells become activated by antigen-presenting cells, the cell goes from a state of low metabolic need to a state of high energy expenditure that also requires components to support division and cytokine production. Early co-stimulation events through CD28 trigger the upregulation of glucose transporter GLUT1 via Ak strain transforming serine/threonine kinase (AKT) to support increased in anaerobic glycolysis (59-61). The increase in anaerobic glycolysis feeds the production of building blocks for other cellular process as well as driving optimal cytokine production (62). While OXPHOS is not the dominant metabolic program during the

period of T cell activation and clearance of pathogen, activation signals have primed the T cell for memory-forming potential. Additionally, CD28 and IL-7/15 cytokine signaling endows cells with fused mitochondria (63, 64), which are best able to support OXPHOS and allow for memory T cell formation. These findings highlight the careful orchestration of T cell activation and T cell metabolism.

Acquisition of memory fate is associated with a return to OXPHOS (26). The transition to OXPHOS also underlies the ability of cells to respond rapidly to antigen (65). However, unlike naïve cells, memory T cells utilize primarily fatty acid oxidation to drive OXPHOS (50, 65, 66). Again, signals from external cytokine play a critical role in coordinating these metabolic programs. IL-7 signaling drives the uptake of glycerol to facilitate triacyl-glycerol synthesis (50). Fatty acids from mobilized triglycerides as well as free fatty acids from other sources then contribute to oxidative phosphorylation (66). The mechanism underlying the metabolic advantage of fatty acid oxidation have remained elusive. In contrast in the setting of tumors, fatty acids, specifically very long chain fatty acids and oxidized fatty acids, have been demonstrated to have detrimental roles in T cell persistence, further underlying the importance of fatty acid metabolism in T cell persistence and memory formation (67, 68).

1.6.3 Mitochondrial dynamics in T cell metabolism

Various pathways have been implicated in the regulation of mitochondrial OXPHOS, with morphology being one of the most recognized. After activation, *in vitro* and *in vivo*, $CD8^+$ T cells robustly increase total mitochondrial mass, with memory T cells maintaining the highest amounts of mitochondrial content (69). There exists a strong correlation between mitochondrial metabolism and T cell function, and this is evident as reduction of mitochondrial mass is characteristic of T cell dysfunction in the setting of anti-tumor responses (69). Murine models of chronic viral

infection, such as LCMV Clone-13 (C13) demonstrate progressive dysfunction of antigen specific cells as well as impaired memory formation. Interestingly, $CD8^+$ T cells responding to chronic viral infections contain significantly increase mitochondrial content though dysfunctional relative to acute counterparts early in the infection (day 8) while there were no differences later in the chronic infection versus memory cells from acute setting (day 35) (70). These discrepancies in mitochondrial phenotype could be explained by context, as the tumor microenvironment versus lymphoid microenvironment likely differ. Bengsch et al (70) show that morphology of the mitochondria was associated with functionality. Indeed, elegant work has established that mitochondrial morphology is critical for maximizing the efficiency of the electron transport chain (ETC). Elongated mitochondrial networks, formed through fusion, increase the surface area of ETC compacting allowing for more OXPHOS (71). In $CD8^+$ T cells, memory formation is associated with the remodeling of mitochondria into fused networks with compacted cristae (63, 64). Signals downstream of CD28 have been shown to be mediating the compacting of mitochondrial cristae(64). In context of tumor responses, mitochondrial dysfunction was associated with reduced CD28 (72). How CD28 signaling directly regulates mitochondrial morphology, or whether rescuing CD28 by antagonizing CTLA-4, an inhibitory receptor that acts on CD28, promotes mitochondrial function through cristae remodeling have not been investigated.

1.6.4 Mitochondrial ER Contact Sites

While studies of T cell mitochondrial morphology have focused on regulation of the canonical fusion/fission proteins, emerging evidence has brought mitochondrial ER contact sites (MERCS) to the forefront of mechanism regulating T cell metabolism (73). Calcium flux from the ER into the mitochondria has been shown to drive the division of the inner mitochondrial membrane independently of canonical fission enzymes (74). The formation of MERCS has been

shown to occur with T cell differentiation as memory T cells have higher number of MERCS than naïve (75). Bantug et al. (75) demonstrate that the formation of these sites was associated with memory T cell OXPHOS, cytokine production and proliferation. A key limitation of this study is that MERCS are perturbed by inhibiting broad cellular process such as polymerization of actin, thus the perturbation of MERCS remains a challenge in their mechanistic study. Supplementation of T cells with lineoic acid was found to increase the formation of MERCS which was associated with the improvement of T cell persistence in setting of adoptive transfers into tumor burdened mice, enhanced OXPHOS and cytotoxicity (76). Various mechanisms of MERCS supporting T cell metabolism have been promoted. Bantug et al. (75) demonstrate that MERCS host various molecules important of T cell metabolism such as hexokinase-I (glucose metabolism) and the molecular target of rapamycin 2 (mTORC2)-AKT- Glycogen Synthase Kinase 3 Beta (GSK3B) (metabolic signaling). What signals from the ER and additional roles for the MERCS besides as a scaffold were not investigated by this group but these functions are likely to work in consort with the regulation of calcium signaling. T cells responding to tumors were found to have improved functionality when MERCS were promoted through overexpression of mitofusin 2 (MFN2) (77). Yang et al. (77) demonstrate that MFN2 interacts with ER-resident ATPase sarcoplasmic/endoplasmic reticulum Ca^{2+} transporting 2 (SERCA2) to drive calcium flux from the mitochondria into the ER, suggesting that ER to mitochondrial calcium flux in tumor infiltrating lymphocytes would require dampening. Calcium is required by several mitochondrial enzymes but its influx into the mitochondria must be regulated as it can have detrimental effects (78). Calcium efflux from the ER is a hallmark of T cell singling (79), in the future characterizing the association of MERCS with different calcium channels such as those associated with calcium flux after TCR stimulation can help bridge gaps in how TCR signaling instills metabolic reprograming.

1.7 Protein homeostasis

1.7.1 Protein synthesis and degradation:

Since the 1960s, it has been appreciated that activated T cells increase in size before proliferating (80). Modern proteomic approaches have allowed for the characterization of protein synthesis during activation. *In vitro* studies have demonstrated that T cells at 24 hours post activation synthesized around 800,000 proteins/min (19). Elegant studies combining genetic loss of function and inhibitors have characterized the signals regulating protein synthesis in T cells. Contrary to other cell types, MTORC1 was dispensable for the induction of protein synthesis after receiving mitogenic signals, only affecting cell cycle progression and metabolism of naïve T cells (20). TCR signaling through extracellular signal regulated kinase (ERK) is not the driving force of the increase in protein synthesis, as only ~10% of the proteome is impacted when ERK is inhibited in activated T cells (21). Of the reduced proteins, upon ERK inhibition, most aligned with markers of T cells activation such as CD25 and CD69 as well as key effector molecules such as Granzyme B and IFN-y. Finally, transcription factor c-Myc has been identified as master regulator of protein synthesis in activated T cells (22, 81). Loss of c-Myc results in a reduction of 50% of protein synthesis with cells then failing to survive. Mechanistically, c-Myc, downstream of TCR/CD28 and IL-2, is necessary for the upregulation of T cell metabolic programs that meet bioenergetic demand of T cell activation. It remains an open question whether co-stimulation licenses the expression of c-Myc rather than TCR.

The requirements for protein turnover in differentiating T cells are further exemplified by necessity of proteasomal degradation (82). Proteosome activity was both necessary and sufficient for $CD8^+$ T cell memory formation. Mechanistically, c-Myc degradation by the proteosome was necessary to drive the metabolic adaptation required for memory T cell formation. The effects of

protesome inhibition/activation on misfolded protein accumulation were not assessed nor were the activation of pathways regulating protein homeostasis.

1.7.2 Unfolded protein response

Accumulation of misfolded protein in the ER results in the activation of the unfolded protein response (UPR) (83). Under normal homeostatic conditions, basal molecular chaperones assist in the folding of newly synthesized protein, while protein disulfide isomerase assists in disulfide bond formation. Three major sensors are found in the ER that sense for misfolded protein, these are inositol-requiring enzyme 1 (IRE1), protein kinase R-like ER kinase (PERK) and activating transcription factor 6 (ATF6). Once these sensors recognize misfolded protein, they execute biochemical activity that result in the generation of distinct transcription factors that will coordinate the response to unfolded protein. IRE1 activation results in the splicing of XBP1 mRNA to generate spliced XBP1 (XBP1s). XBP1s will proceed to activate the transcription of chaperones, ER associated degradation components, as well as promoting increase in ER size (84). PERK activity through the eIF2a will induce the expression of ATF4. ATF4 will upregulate genes pertaining to redox homeostasis, apoptosis, amino acid metabolism and autophagy. CHOP C/EBP-Homologous Protein is also induced downstream of PERK/ATF4 and is known to execute a program sensitizing cells to apoptosis. ATF6 itself is cleaved by site 1 protease (S1P/S2P) to produce transcription factor ATF6 (p50). Importantly ATF6 transcriptionally activates XBP1 allowing for IRE1 branch to be executed (85). Together these factors coordinate a response to unfolded protein.

The role of the UPR in T cell biology has focused on the characterization of T cells lacking any of the main effector transcription factor of the UPR. The expression of XBP1 was found to be driven by IL-2 signaling while its splicing leading to activation into XBP1s was found to only

occur after TCR activation (86). How ATF6, the classical activator of XBP1 transcription, is regulated during T cell homeostasis or activation has not been explored nor its relationship to IL-2 signaling. The role of other common gamma chain cytokines in priming the unfolded protein response was not investigated. Utilizing the mouse model of acute viral infection LCMV, authors find that higher XBP1s activity was necessary and sufficient to drive terminal differentiation of antigen specific $CD8^+$ T cells. How XBP1s coordinates terminal T cell differentiation was not explored. Ma et al. (87) reported similar findings in the setting of tumors. Additionally, Ma et al. demonstrate that XBP1 is necessary for the upregulation of inhibitory receptors PD-1 and 2B4. Similarly, Song et al. (88), had demonstrated that XBP1 activity limited CD4 T cell metabolism and that its deletion improved $CD8^+$ T cell function in the context of tumors. Transcription factor CHOP has shown similar findings, being found to limit T cell function in the setting of tumors, however, by limiting the activity of Tbet (89). Taken together, these results demonstrate the activation of the unfolded protein response can have detrimental effects to T cell persistence and function.

1.8 Regulators of misfolded proteins

1.8.1 Oxidative Protein Folding

To rectify ER homeostasis, the unfolded protein response increases the expression of already present proteins that regulate protein folding, such as endoplasmic reticulum oxidoreductase 1 alpha (ERO1a) and protein disulfide isomerase (PDI). ERO1a is an oxyreductase that mediates the formation of disulfide bonds, key covalent bonds in cells that are necessary for folding of some proteins (90-92). Interestingly, ERO1a, despite having a role in maintaining protein homeostasis, can become overexpressed in setting of chronic ER stress leading to the generation and accumulation of reactive oxygen species (ROS), eventually inducing cell death (90,

92). In $CD8^+$ T cells, limiting ERO1a activity resolved mitochondrial dysfunction leading to alleviating T cell dysfunction both *in vitro* and *in vivo* (93). Complimentary studies targeting protein disulfide isomerase (PDI) have demonstrated similar findings, that over activity of this pathway can result in altered metabolism (94). Together, these results demonstrate that activity of a mechanism regulating protein folding can have detrimental effects to T cell survival and function. However, whether ERO1a or PDI activity was necessary for T cell function or persistence has not been studied. Furthermore, the extent to which these inhibitors limit enzyme function was not addressed in the studies. Additional studies are needed to determine the role of ERO1a and PDI in T cell function, as well as their relative contribution to maintaining ER homeostasis.

1.8.2 Biochemical mechanism of Endoplasmic Reticulum Associated Degradation

ER-associated degradation (ERAD) encompasses the processes responsible for the detection and degradation of misfolded proteins in the ER. During ERAD misfolded protein is identified in the ER, translocated to the cytoplasm across the ER membrane and then degraded by the ubiquitin proteosome system (UPS). Though various protein complexes engage in these activities, the Sel1L/Hrd1 ERAD complex is the most well defined and highly conserved. Several molecules have been identified as being recognized by Sel1L to deliver misfolded protein to ERAD such as ER degradation-enhancing alpha-mannosidase-like protein 1 (EDEM1), osteosarcoma-9 (OS-9), and glucose regulated protein 94 (GRP94) (95). Once complexed into Sel1L/HRD1, the retro-translocation from the ER lumen to the cytoplasm is putatively catalyzed by the Derlin-1/2 enzymes in conjunction with HRD1 which contain an ER membrane spanning pore (96). As the misfolded protein traverses the ERAD complex, ER resident E2 ligases ubiquitin conjugating enzyme E2 J1 and ubiquitin conjugating enzyme E2 G2 catalyzes the addition of the initial K48 ubiquitin marks to the misfolded protein (97). HRD1 in the pore structure created with

the derlins will then further polyubiquinate the misfolded protein (96). The ATPase valosin-containing protein (VCP) will utilize ATP to generate mechanical force to drive the complete translocation of the now misfolded protein into the cytoplasm. Delivery of the ubiquitinated misfolded to the proteosome is catalyzed by the chaperone BAG cochaperone 6 (BAG6) (98).

1.8.3 Physiological Roles of Sel1L/ERAD

Sel1L/ERAD is important for the viability or functionality of various cell types as evidenced by the lethality of systemic deletion (99) . For this reason, the study of Sel1L/ERAD has relied on cell type specific deletion of the gene through the use of tissue restricted cre recombinase or inducible deletions. Briefly, Cre is a site-specific recombinase that identifies sequences known as locus of X over P1 (loxp) and removes DNA segments between these sites. By genetically engineering mice with loxp sites around genes of interest and crossing them to mice expressing Cre restricted to a specific tissue, the progeny that contains both Cre and loxp will lose the gene of interest only in that tissue (for review on cre/lox system see (100)). Through the use of this system, the role of Sel1L and ERAD has been defined in a variety of cell types including: enterocytes, myocytes, cardiomyocytes, thyrocytes, hepatocytes, adipose tissue , pancreatic beta cells, neurons, podocytes, various immune cells and hematopoietic stem cells (reviewed here (101)). Though Sel1L/ERAD has a pivotal role in maintaining ER homeostasis, its loss manifest in various cellular and tissue phenotypes distinct from ER homeostasis. This variation could likely be attributed to cell type specific response to ER stress as well as the role of ERAD in selectively degrading certain proteins in a cell specific manner (102).

In both brown adipocytes and hepatic cells, loss of Sel1L/ERAD manifests in altered mitochondrial dynamics; however, brown adipocytes display enlarged mitochondria, while hepatocytes display more fragmented mitochondria (103, 104). Mechanistically, Sel1L limits the

protein levels of sigma non-opioid intracellular receptor 1 (SigmaR1) in brown adipocytes while mitochondrial membrane permeability is only impacted in the hepatocytes. Whether SigmaR1 is also dysregulated in hepatocytes was not evaluated. Though it appears SigmaR1 is also an Sel1L/ERAD substrate in kidney cells it is not a Se1L/ERAD target in T cells (unpublished data). Loss of Sel1L in hematopoietic stem cells (HSC) results in loss of quiescence due to hyperactivation of mTORC1 due to inability of these cells to degrade Ras homolog enriched in brain (Rheb) a negative regulator of mtorc1 activity (105, 106). Loss of Sel1L in non-transgenic T cells manifests in a loss of quiescence to that observed in HSCs however, T cell loss of quiescence in the absence of Sel1L was found to be independent of mtorc1 pathway and Sel1L loss did not affect Rheb levels (unpublished results). Therefore, the study of Sel1L/ERAD varies by cell type and is likely influenced significantly by cell state.

Chapter 2 – Methods

This chapter has been published:

Luis O. Correa-Medero, Shayna E. Jankowski, Hanna S. Hong, Nicholas D. Armas, Aditi I. Vijendra, Mack B. Reynolds, Garrett M. Fogo, Dominik Awad, Alexander T. Dils, Kantaro A. Inoki, Reid G. Williams, Annabelle M. Ye, Nadezhda Svezhova, Francisco Gomez-Rivera, Kathleen L. Collins, Mary X. O'Riordan, Thomas H. Sanderson, Costas A. Lyssiotis and Shannon A. Carty ER-associated degradation adapter Sel1L is required for $CD8^+$ T cell function and memory formation following acute viral infection. Cell Reports (2024) PMID: 38687642

2.1 Experimental models and subject participant details

2.1.1 Mice

C57BL/6J mice, and $CD4Cre^+$ mice were obtained from The Jackson Laboratory and bred at the University of Michigan. B6.SJL-Ptprca ($CD45.1^+$) mice were obtained from The Jackson Laboratory. Sel1L floxed mice(107) were a kind gift from Ling Qi, University of Virginia. All mice were backcrossed at least ten times to a C57BL/6J background. $Sel1L^{fl/fl}CD4^{+/}Cre$ were bred to P14(108, 109) mice to generate $Sel1L^{fl/fl}CD4Cre^+$ P14 mice. Control mice for experiments included age-matched P14 $Sel1L^{fl/fl}$, P14 $Sel1L^{+/+}CD4Cre^+$, P14 $Sel1L^{fl/fl}CD4Cre^-$ or C57BL/6J animals. All experiments were performed according to protocols approved by the Institutional Animal Care and Use Committee of the University of Michigan (PRO00009175; PRO00010912). Mice were bred and maintained in specific pathogen-free animal facility (22° C with 40% humidity) on a 12-hour dark/ 12-hour light cycle at the University of Michigan. Mice were used 6- to 10-week-old were used at start of experiments, both sexes are represented in the data and no sex differences were noted.

2.1.2 In vitro differentiation

Splenocytes from P14 mice, whose $CD8^+$ T cells are >85% $P14^+$, were cultured in T cell medium (10% FBS, 50uM 2-ME, 2mM L-glutamine/penicillin/streptomycin in IMDM) containing 100ng/ml gp33-41 (Anaspec, cat.# AS-61669, sequence: KAVYNFATC) and 100U/ml recombinant human IL-2 (PeproTech, cat.# 200-02) for 48hrs. After 48hrs of culture, cells were replated in T cell medium containing 100U/ml IL-2 an additional 24hrs. At 72hrs of incubation, $CD8^+$ P14 T cells were purified by negative selection using magnetic beads according to the manufacturer's instructions (Biolegend, cat.# 480008). Cells were then cultured for an additional 3 days in T cell medium supplemented with either recombinant IL-2 (100U/ml) or IL-15 (10ng/ml) (PeproTech, cat.# 210-15). Naïve $CD8^+$ T cells were purified from total splenocytes at the start of the experiment (Biolegend, cat.# 480044). For thapsigargin treatments, cells were cultured as above but were supplemented with 100uM thapsigargin for 2hrs or DMSO for vehicle controls. All cells were cultured in incubator maintained at 37° C with a humidified atmosphere containing 5% CO_2.

2.1.3 Infections and adoptive transfer

Mice were infected with $2x10^5$ pore-forming units (p.f.u.) LCMV-Armstrong intraperitoneally (i.p). For experiments on day 5 and day 8 p.i., spleen, lymph nodes and peripheral blood mononuclear cells (PBMCs) were isolated and single cell suspensions were obtained for flow cytometric or other downstream analysis. For longitudinal studies, PBMCs were collected at days 8, 15, 30 and 45 p.i. in a 4% sodium citrate solution. Peripheral blood mononuclear cells were then isolated utilizing a Ficoll-paque gradient (GE Healthcare, cat. # 45-001-749) and stained for flow cytometry. For adoptive co-transfer experiments, 1:1 mix of donor WT P14 (CD45.1/2) and Sel1LcKO P14 (CD45.2) cells was generated and transferred into $2.5x10^3$ cells of each donor was

co-transferred into congenically disparate mice sex-matched, 6-8 week old B6.SJL (CD45.1) mice. In select day 45 LCMV experiments, donor P14 cells were sorted to confirm lack of Cre escape via RT-PCR and data was excluded if deletion was <50%. For *Listeria monocytogenes* infections, mice were infected with 5.8-9.0×10^4 colony-forming units (CFU) *Listeria monocytogenes* that expresses the LCMV gp33 epitope (LM-gp33), as indicated and peripheral blood and spleens were collected on day 5p.i.. LM-gp33 was grown and bacterial loads were measured as previously described(110).

2.1.4 Human samples

Anonymized leukocytes isolated by apheresis were obtained from the New York Blood Center, and peripheral blood mononuclear cells (PBMCs) were isolated by Ficoll-Paque Plus (GE Healthcare, cat.# 17144002) centrifugation using SepMate tubes (Stemcell Technologies, cat.#85450) according to the manufacturer's protocol. $CD8^+$ lymphocytes were positively selected with Dynabeads according to the manufacturer's protocol (Invitrogen, cat.#11147D). Isolated $CD8^+$ cells were either rested in 10ng/ml human IL-7 (PeproTech, cat. # 200-07-10ug) for 3 days or activated using Dynabeads per manufacturer's protocol (Invitrogen, cat. #11131D;) in addition with 100 Units/ml human recombinant IL-2 in human T cell media (RPMI, Gibco, cat.# 11875093) supplemented with 50uM beta-mercaptoethanol (Sigma-Aldrich, cat.# M3148-250ML), 2mM L-glutamine/penicillin/streptomycin (Gibco, cat .#10378016), 10% FBS (Cytiva, cat.# SH3039603), and 1x non-essential amino acids (Gibco, cat.# 11140050). Cells were cultured for 3 days before staining and analyzed via flow cytometry. All samples were allocated the same way. Due to the deidentification processes we do not know age, sex ancestry, ethnicity nor socioeconomic status of the donors from which the samples used in this manuscript originated, which may limit the

generalizability. All cells were cultured in incubator maintained at 37° C with a humidified atmosphere containing 5% CO_2.

2.2 Method details

2.2.1 Flow cytometry and cell sorting

Single cell suspensions from indicated organs were isolated. Cells were washed in FACS buffer (PBS with 2% FBS) and stained with indicated antibodies or dyes. Intracellular staining was performed using a Cytofix/cytoperm kit (BD Biosciences, cat.# BDB554722) or a Foxp3/transcription factor staining buffer set (Invitrogen, cat.# 50-112-8857), according to manufacturer instructions. Live cell discrimination was performed using LIVE/DEAD Aqua stain (Invitrogen, cat.# L34965) according to the manufacturer's instructions. For apoptosis detection, cells were harvested, and after incubation with surface antibodies, cells were washed with Annexin Binding Buffer (Biolegend, cat.# 422201) and incubated with Annexin V (Biolegend, cat.# 640918) and 7AAD (Biolegend, cat.# 420403) for 20min at room temperature in the dark and immediately analyzed. For flow cytometric cell sorting, $CD8^+$ T cells were purified by negative selection magnetic cell sorting (Biolegend, cat.# 480008). Cells were sorted on FACS Aria. For flow cytometry experiments, data were acquired on BD Fortessa (BD Biosciences) and analyzed using FlowJo (version 10.6 or higher).

2.2.2 Intracellular cytokine detection

For experiments involving *ex vivo* stimulation, splenocytes from LCMV-infected animals at D8 p.i were stimulated with 100ng/ml gp33 peptide in the presence of Brefeldin A (BD, cat. #BDB555029) according to manufacturer instructions was added to cultures for 4-5 hours and then analyzed for intracellular cytokine staining. Boolean gating was used to generate table identifying

cells by their ability to produce any combination of cytokines (Granzyme B, IFNg TNFa,IL-2), degranulation maker CD107 or no cytokine production. Files were then imported into SPICE(111) displayed graphs were made using custom R scripts.

2.2.3 Extracellular flux analysis:

Seahorse assays were performed using a XF-96 Extracellular Flux Analyzer (Agilent). The day before the assay, sensor cartridges were incubated in dH_2O overnight then hydrated in XF calibrant (Agilent) for 1 hour in a non-CO_2 incubator at 37°C on the day of the assay. Following *in vitro* culture, cells were washed and resuspended in XF DMEM media. 2-2.5 $x10^5$ cells per well were seeded on poly-L-lysine-coated plates and allowed to equilibrate for 30 minutes in a non-CO_2 incubator at 37°C. Cartridges were loaded with 1-2μM oligomycin (O), carbonyl cyanide p-trifluoromethoxyphenylhydrazone (FCCP) (1 μM), and 1 μM rotenone/antimycin A (R/A). After the assay, measurements were normalized based on cell seeding density using CyQuant (Invitrogen). Spare respiratory capacity (metabolic fitness) was determined by subtracting basal OCR from maximal OCR measurements.

2.2.4 RNA sequencing and analysis

$5x10^4$ P14 cells per genotype were sorted from mice on day 8 p.i. of LCMV-Armstrong. After sort, cells were washed thoroughly in PBS followed by RNA extraction utilizing the RNA micro kit (Qiagen, cat. #74004) and removing contaminating genomic DNA utilizing DNase I treatment. Library prep and next-generation sequencing was carried out in the Advanced Genomics Core at the University of Michigan. Briefly, RNA was subjected to strand specific Poly-A selected library preparation followed by 151 bp paired-end sequencing according to the manufacturers protocol (Illumina NovaSeq). Bcl2fastq2 Conversion Software (Illumina) was used to generate de-

multiplexed Fastq files. The Fastqreads were trimmed using Cutadapt v2.3.(112) The reads were evaluated with FastQC v0.11.8 to determine quality of the data. Reads were mapped to the reference genome GRCm38 (ENSEMBL), using STAR v2.7.8a(113) and assigned count estimates to genes with RSEM v1.3.3.(114) Alignment options followed ENCODE standards for RNA-seq.(115) QC metrics from several different steps in the pipeline were aggregated by multiQC v1.7.(116) Differential gene expression was performed with DESEQ2. Log2Foldchange (WtvsKO), p-value and gene counts were then used in RNA-Enrich (117) software to determine differentially regulated pathways.

2.2.5 Immunoblotting:

RIPA buffer (Pierce, cat. #PI89900) supplemented with phosphatase and protease inhibitors (Thermo Scientific cat.# 1862495 and 1862209) was used to lyse cells, and protein concentrations were determined with BCA protein assay (Pierce, cat. #23227). Total protein lysate (10ug) or equivalent cell number lysates were separated by SDS-polyacrylamide gel electrophoresis (Invitrogen) followed by immunoblotting for K48-Ub (CST, cat.# 8081S), XBP1 (Novus Biologicals, cat.# NBP1-77681), ATF4 (CST, cat. #11815S), Sel1L (Abcam, cat. # ab78298), c-Myc (CST, cat. # 5605S), and Beta-actin (Sigma, cat. # A5441-.2ML). Using ImageJ software, bands were quantitated by obtaining mean gray value was for regions of interest encompassing band and lane background was then subtracted. All immunoblots are normalized to beta-actin before normalization to naive or WT.

2.2.6 Immunocytochemistry and confocal microscopy

Fixed cells were incubated in PBST (Phosphate Buffered Saline with 0.1% Triton X-100) containing 2% normal goat serum (Sigma-Aldrich, cat.# G9023) for 30 minutes at room

temperature, followed by labeling with anti-calreticulin (Invitrogen, cat.# PA3-900) diluted 1:50 in PBST. Cells were washed three times with PBST and then incubated in Hoechst diluted 1:1,000 and Alexa Fluor 647 (AF647) goat anti-rabbit (Invitrogen, cat.# A21246) diluted 1:300 in PBST. Labeling steps were carried out at room temperature for 1 hour. Cells were then washed, mounted with 90% glycerol diluted with PBS, and imaged by confocal microscopy. Images were acquired with a Leica SP8 confocal scan head mounted to a DMI 6000B CS microscope utilizing a 63X/1.4NA Oil immersion objective. Calreticulin-AF647 and Hoechst images were obtained sequentially by line using 630 nm excitation from a white-light laser paired with a hybrid detector to acquire calreticulin-AF647 at 662-700 nm, using time gated detection from 0.3 ns – 6.0 ns, followed by 405-nm diode laser excitation paired with a separate hybrid detector to detect Hoechst from 415-478 nm. Z-stacks were obtained to encompass the majority of the cell volume using a 299 nm step size, where each slice was acquired with a 59 nm pixel size using three-line averages at 400 hz scanning speed recording bi-directionally. All cell stages were imaged during each individual imaging session with the laser power and detector gain held constant during each session. LAS X (ver 3.7.4) was used to export the acquired confocal imaging data into TIF format as well as to generate maximum projections. Pipelines were created in CellProfiler (ver. 4.2.11)(118) to define the overall boundary of individual ER using maximum projections and to measure the total pixel intensity of calreticulin staining (IntegratedIntensity) at individual z-slices within these boundaries. Specifically, to generate the ER outlines using CellProfiler, cells in each maximum projection were first identified by segmenting nuclei into objects from the Hoechst channel using the IdentifyPrimaryObjects module. Global thresholding into three classes was performed using Otsu's method, with middle intensity pixels being assigned to the foreground. A lower bound of 0.05 was used for this thresholding. Clumped objects were both distinguished and

divided by Shape. Objects touching the edge of an image, as well as objects outside of a diameter range corresponding to a physical size of approximately 3.5 to 15 microns were discarded by this module. Holes within the identified objects were filled in, after both thresholding and declumping. With these segmented nuclei as seeds, a cell's ER was then segmented from the calreticulin channel with the IdentifySecondaryObjects module using the propagation method with thresholding by Otsu's method. ER objects touching the border of the image were discarded. The resulting ER objects were then saved as binary images that were then loaded into a second pipeline as primary objects via the IdentifyPrimaryObjects module. IntegratedIntensity measurements were then obtained from the calreticulin channel of each slice for each of the ER objects. The z-slice with the greatest IntegratedIntensity for a given cell was used for quantification. Annotated images of the corresponding slices were created by CellProfiler and manually reviewed to exclude any improperly segmented objects from the intensity analysis. To compare calreticulin staining intensities across different imaging sessions, normalized calreticulin staining intensity was calculated for each cell by dividing a given cell's IntegratedIntensity value by the average IntegratedIntensity value of the naïve $CD8^+$ T cells acquired during that imaging session.

2.2.7 RT-PCR

RNA was isolated from the indicated cell populations in RLT buffer supplemented with 10% 2-ME. Quantified RNA was subjected cDNA conversion through the SuperScript III first strand synthesis system (Invitrogen). RT-PCR of target genes was performed using primers listed in key recourses table. Relative expression was determined utilizing the $2^{-}\Delta\Delta ct$ method normalized toβ-actin unless viral RNA quantification. Viral RT-PCR and RNA relative quantification was carried out as described by McCausland et al.(119).

2.2.8 MERCS microscopy and analysis

T cells were plated in a poly-D-lysine-coated 384-well imaging-grade plates (Phenoplate, Perkin Elmer). After adhering by settling, cells were fixed with freshly prepared 4% paraformaldehyde (PFA) at RT for 15 min. Fixed wells were washed with PBS + 0.1% Triton X-100 (wash buffer). Wells were blocked with 5% BSA and 10% goat serum in wash buffer (block buffer) for 30 min at RT. A cocktail of anti-KDEL (ab176333; 1:500) and anti-TOM20 (ab56783; 1:500) primary antibodies was prepared in block buffer and incubated in each well for 16 hours at 4°C. Wells were washed with wash buffer and stained with AF594-conjugated anti-mouse IgG (A11005; 1:500) and AF488-conjugated anti-rabbit IgG (A11034; 1:500) secondary antibodies and DAPI (4′,6-diamidino-2-phenylindole) (1:1000) counterstain in block buffer for 30 min at RT. Wells were washed with PBS and immediately imaged at 60X magnification on a Cell Voyager 8000 automated confocal microscope (Yokogawa) or super resolution microscopy via Zeiss LSM 980 with Airyscan 2. During confocal image acquisition, maximum intensity projection (MIP) images were collected across 4 Z-planes spanning 4 μm and centered around a laser autofocus-defined focal plane for each analysis image. Using this automated method >100 cells were sampled per condition for each biological replicate. During Airyscan acquisition, images were collected across 9 Z-planes spanning 1.04 μm. Micrographs were deconvolved with Zeiss Zen software standard deconvolution. 3D rendering of Airyscan micrographs was achieved in Imaris image analysis software using consistent segmentation and surface rendering parameters between conditions. Mitochondria-ER contact sites (MERCS) were defined in Imaris software through thresholding and rendering colocalized regions between the TOM20 and KDEL stain. Representative images shown in this manuscript have uniformly scaled brightness and contrast within each experiment.

Open-source image analysis software CellProfiler was used for quantification of all micrographs. Image analysis was performed on raw images (MIP images from Yokogawa instrument software) using the University of Michigan Advanced Research Computing Great Lakes computing cluster. Automated single-cell analysis was achieved by segmentation of nuclear objects based on nuclear staining, DAPI, using the identify primary objects module, followed by propagation of the nuclear objects to the cellular periphery based on an empirically defined number of pixels roughly equal to the mean nuclear radius using the identify secondary objects module. Mitochondrial objects were defined by segmentation of TOM20 micrographs using two-class Otsu adaptive thresholding of the TOM20 stain in the identify primary objects module. Following object segmentation, the intensity of the KDEL stain in the total cellular and mitochondrial area was measured on a single-cell basis.

2.2.9 Mitochondrial morphology microscopy

At day 3 post activation, ~2-4x10^5 cells were seeded on poly-d-lysine coverslips and allowed to adhere for 4hrs at 37°C. Cells were fixed with 4% paraformaldehyde (ThermoFisher, 50980487) for 15 min at 37°C. Coverslips were incubated in blocking solution [5% goat serum (Sigma, G9023) and 0.3% Triton-X100 (Acros Organics, 215682500) in PBS] for 60 min. Coverslips were then incubated in primary antibody solution (1:1000 Mouse Anti-ATPB (Abcam, ab14730), 1% BSA (Sigma, A9647) and 0.3% Triton-X100 in PBS) at 4°C overnight. After primary incubation, coverslips were washed 3 × in PBS and incubated in secondary antibody solution (1:200 Anti-Mouse Alexa Fluor 488 (Invitrogen, A11029, 1% BSA (Sigma, A9647) and 0.3% Triton-X100 in PBS) for 60 min. Following secondary incubation, coverslips were washed 3 × with PBS and mounted on glass slides using Fluoroshield with DAPI (Sigma, F6057). Triplicate coverslips were used for each biological replicate. Coverslips was imaged using a Zeiss Axio Observer Z1 inverted

microscope with LED illumination. Image frames were selected using the DAPI signal to limit bias with 2-5 cells per frame. For each coverslip, 7-8 image z-stacks (0.24 μm slices) capturing the mitochondrial network were acquired at 63 × with oil immersion. Z-stacks were exported as individual image frames in TIFF format for post-processing. Analysis of 3D mitochondrial morphology was adapted from Fogo, Anzell et al.(120). Post-processing was performed in FIJI.(121) The following steps were performed using FIJI's batch processing feature. Background noise was removed using a rolling ball radius of 10 pixels. A median filter was then applied to each image with a radius of 2 pixels. Mitochondria were segmented using the Trainable Weka Segmentation plug-in.(122) The segmentation classifier model was trained using hand identified ATPB-positive mitochondria from processed images. Segmentation output images were converted to 8-bit binary images and the known scale was set. For the identification of mitochondrial objects in 3D, z-stacks were reconstructed using connected components labeling from the MorphoLibJ plug-in library.(123) Connected stacks were then imported into the 3D object manager (124), wherein size and shape measurements were acquired. Measures per mitochondrial object were averaged across the 20-24 images (triplicate coverslips) acquired per biological replicate. Image acquisition and post-processing were performed by personnel blinded to condition. 3D mitochondrial morphology was visualized using MeshLab software.(125)

2.2.10 RNA sequencing and analysis

$5x10^4$ P14 cells per genotype were sorted from mice on day 8 p.i. of LCMV-Armstrong. After sort, cells were washed thoroughly in PBS followed by RNA extraction utilizing the RNA micro kit (Qiagen, cat. #74004) and removing contaminating genomic DNA utilizing DNase I treatment. Library prep and next-generation sequencing was carried out in the Advanced Genomics Core at the University of Michigan. Briefly, RNA was subjected to strand specific Poly-A selected library

preparation followed by 151 bp paired-end sequencing according to the manufacturers protocol (Illumina NovaSeq). Bcl2fastq2 Conversion Software (Illumina) was used to generate de-multiplexed Fastq files. The Fastqreads were trimmed using Cutadapt v2.3.(112) The reads were evaluated with FastQC v0.11.8 to determine quality of the data. Reads were mapped to the reference genome GRCm38 (ENSEMBL), using STAR v2.7.8a(113) and assigned count estimates to genes with RSEM v1.3.3.(114) Alignment options followed ENCODE standards for RNA-seq.(115) QC metrics from several different steps in the pipeline were aggregated by multiQC v1.7.(116) Differential gene expression was performed with DESEQ2. Log2Foldchange (WtvsKO), p-value and gene counts were then used in RNA-Enrich (117) software to determine differentially regulated pathways.

2.2.11 Bioinformatic re-analysis of public data

For re-analysis of single cell transcriptomics from Kurd et al.(126), 10x Genomics CellRanger outputs for days 0-7 of LCMV-Armstrong were downloaded from gene expression omnibus GSE131847. Gene UMI tables were processed into scanpy(127) AnnData objects utilizing the scanpy.read_text() function. The dataset was filtered to keep genes identified in at least three cells. Cells containing at less than 200 genes, or more than 5% mitochondrial genes of total genes were removed. Total counts were normalized per cell using the function scanpy.pp.normalize_per_cell(), log transformed sc.pp.log1p(), and scaled scanpy.pp.scale( ). scanpy.pl.pca_variance_ratio was used to identify the first eight principal components as meaningful for identifying neighbors scanpy.pp.neighbors() and scanpy.tl.umap(). Single-cell gene set enrichment analysis was conducted utilizing the python implementation of decoupleR.(128) Gene Matrix file corresponding to murine Gene ontologies m5.go.v2023.1.Mm.symbols was downloaded from MSigDB.(129) Decoupler.run_ORA() was

used to generate pathway enrichment statistics. Data was exported and visualized using ggplot2 in R.

For analysis of Rieckmann et al.(130), processed and quantified data were downloaded from ProteomeXchange partner PRIDE (PXD004352) in Maxquant output format. Label free quantification of protein from "MaxLFQ" was then used for differential protein expression analysis.(131) Proteomes of $CD8^+$ T cell subsets at different activation states were then used to identify differentially expressed protein with parametric one-way ANOVA with Dunnett's multiple comparisons post-hoc test. For reanalysis of IL-2 proteomes, data was downloaded and reanalyzed on the immunological proteomics site(132) originating from Rollings et al(133).

For Tsao et al(134), Giles et al.(135) , Weber et al.(136), raw reads were downloaded from the Sequencing Read Archive (PRJNA791324,PRJNA744266, PRJNA692497) utilizing the SRATools fastqdump command. Data was processed using nf-core/rnaseq v3.12.0 (doi.org/10.5281/zenodo.1400710) of the nf-core collection of workflows.(137) Briefly, FASTQC was used to assess sequence quality. STAR(113) was used to align reads to reference transcriptome hg38. RSEM(114) was then used to estimate gene and isoform expression levels. RSEM counts were then imported into DESEQ2(138) for differential expression analysis. For Giles et al.(135), only data corresponding to $CD8^+$ T cells was processed. Gene Set Variation analysis was conducted utilizing GSVA R package(139) with Human biological pathways gene ontologies C5 and Hallmarks H. Turkeys' multiple comparison test was used to determine the significance in gene set score between $CD8^+$ T cell subsets. For Weber et al.(136), data was processed as above. DESEQ2 was used to identify differential expression between genes at day 15 undergoing continuous stimulation versus transiently rested cells. FGSEA(140) was used to perform gene set enrichment analysis using msigdb gene sets for gene ontology (C5) and hallmark (H). For Phillipp

et al.(141), raw counts were downloaded from GSE196463 and loaded into DESEQ2, and FGSEA was used as above.

For CHIP-seq data, raw reads were downloaded from the sequencing read archive utilizing the SRATTools fastqdump command. Data were processed using nf-core/CHIP-seq v2.0 (doi.org/10.5281/zenodo.3240506)(137).Briefly, FASTQ was uses to asses sequence quality. Alignment was done with Bowtie2(142), and peaks were identified using MACS2(143) (narrow peaks for IRF4(134). H3K27ac data was downloaded from repossessed compendium (GSE111902) originally published by Gray et al(144)

2.3 Quantification and statistical analysis

No statistical methods were used to predetermine sample size. Statistical tests used for each experiment are detailed in the figure legends and were calculated using Prism (version 10). Number (n) represents biological replicate, i.e., individual mouse or human. Error bars indicate standard deviation unless otherwise specified. To test for normality the following test were conducted Anderson-Darlin, Shapiro-Wilk, Kolmogorov-Smirnov as well as inspection of quantile quartile plots. Data corresponding to the co-transfer experiment in which WT and KO cells are in the same mouse, or the paired comparison of the same human T cells under different parallel conditions, paired two-tailed t-test were conducted. For statistical analysis of three or more normally distributed groups, one-way ANOVA was used, followed by Fisher's least significant difference to determine multiple comparisons. Comparisons of three or more groups that are normally distributed to a control group were conducted using one-way ANOVA followed by Dunnett's multiple comparison test. In comparisons of data with three or more groups that are sequentially tracked and are not normally distributed, Friedman's test with uncorrected Dunnett's multiple comparison test was used. For comparison of three or more groups that were not

sequentially tracked and are not normally distributed, the Kruskal-Wallis test was conducted with follow-up for multiple comparisons to a control group by Dunnett's multiple comparison test.

2.4 Materials

Table 1 Materials

REAGENT or RESOURCE	SOURCE	IDENTIFIER
Antibodies		
Beta-actin (Clone AC-15)	Sigma	cat. #A5441-.2ML; RRID:AB_476744
Calreticulin (Polyclonal)	Thermo Scientific	cat. #PA3900; RRID:AB_325990
XBP1s (Clone E9V3E)	Cell Signaling Technologies	cat. #40435S
c-Myc (Clone D84C12)	Cell Signaling Technologies	cat. #5605S RRID:AB_1903938
Opa1 (Clone D6U6N)	Cell Signaling Technologies	cat. #80471S; RRID:AB_2734117
Drp1 (Clone D6C7)	Cell Signaling Technologies	cat. #8570S; RRID:AB_10950498
phosphoDrp1(Ser616) (Polyclonal)	Cell Signaling Technologies	cat. #3455S; RRID:AB_2085352
K48-Ub (Clone D9D5)	Cell Signaling Technologies	cat. #8081S; RRID:AB_10859893
XBP1 (Polyclonal)	Novus Biologicals	cat. #NBP1- 77681; RRID:AB_11010815
ATF4 (Clone D4B8)	Cell Signaling Technologies	cat. #11815S; RRID:AB_2616025
Sel1L (Polyclonal)	Abcam	cat. #ab78298; RRID:AB_2285813
CHOP (Clone L63F7)	Cell Signaling Technologies	cat. # 2895T; RRID:AB_2089254
ATPB (Clone 3D5)	Abcam	cat. #ab14730; RRID:AB_301438
KDEL (Clone EPR12668)	Abcam	cat.# ab176333; RRID:AB_2819147
TOM20 (Clone 4F3)	Abcam	cat.# ab56783; RRID:AB_945896
CD44 AF700 (Clone IM7)	Biolegend	cat .# 103026; RRID:AB_493713
TCRb APC-Cy7 (Clone H57-597)	Biolegend	cat. # 109220; RRID:AB_893624
CD8a Pacific Blue (Clone 53-6.7)	Biolegend	cat. # 100725; RRID:AB_493425

CD127 PE-Cy7 (Clone A7R34)	Biolegend	cat. # 135014; RRID:AB_1937265
CD62L PE-Texas-Red (Clone MEL-14)	Biolegend	cat. # RM4317; RRID:AB_1479970
CD25 AF488 (Clone PC61)	Biolegend	cat. # 102017; RRID:AB_493334
CD69 APC (Clone H1.2F3)	Biolegned	cat. # 104514; RRID:AB_492843
CD45.1 PerCP-Cy5.5 (Clone A20)	eBiosciences	cat. # 45-0453-80; RRID:AB_925750
CD45.1 BV650 (Clone A20)	Biolegend	cat. # 110736; RRID:AB_2562564
CD45.1 AF700 (Clone A20)	Biolegend	cat. # 110724; RRID:AB_493733
CD45.2 PE (Clone 104)	Biolegend	cat. # 109808; RRID:AB_313445
CD45.2 Pacific Blue (Clone 104)	Biolegend	cat. # 109820; RRID:AB_492873
IFNg PerCP-Cy 5.5 (Clone XMG1.2)	Biolegend	cat. # 505822; RRID:AB_961361
TNFa BV421 (Clone MP6-XT22)	Fisher Scientific	cat. # BDB563387; RRID:AB_2925546
IL2 PE (Clone JES6-5H4)	Fisher Scientific	cat. # BDB554429; RRID:AB_398555
Granzyme B PE-Cy7 (Clone NGZB)	Fisher Scientific	cat. # 50-245-758; RRID:AB_10853338
CD107a FITC (Clone 1D4B)	Fisher Scientific	cat. # 121606; RRID:AB_572006
KLRG1 FITC (Clone 2F1)	Fisher Scientific	cat .# 50-990-3; RRID:AB_1311265
Ki-67 (Clone B56)	Fisher Scientific	cat. # BDB556026; RRID:AB_396302
TCF1 (Clone C63D9)	Cell Signaling Technologies	cat. # 14456S; RRID:AB_2798483
Goat anti-Mouse AF488 (Polyclonal)	Thermo Fisher Scientific	cat. # A-11029; RRID:AB_2534088
Goat anti-Mouse AF594 (Polyclonal)	Thermo Fisher Scientific	cat.# A-11005; RRID:AB_2534073
Goat anti-Rabbit 488 (Polyclonal)	Thermo Fisher Scientific	cat.# A-11034; RRID; AB_2576217
Bacterial and virus strains		
Listeria monocytogenes-gp33	Kaech et al.(145)	N/A
Lymphocytic choriomeningitis Virus - Armstrong strain	Rafi Ahmed	Grown by Wherry lab
Chemicals, peptides, and recombinant proteins		
Thapsigargin	Millipore-Sigma	cat.# T9033
2-Mercaptoethanol	Sigma-Aldrich	cat. # M3148-250ML

Ficoll-paque	GE Healthcare	cat.# 45-001-749
RIPA Buffer	Pierce	cat.# PI89900
Protease Inhibitor	Thermo Scientific	cat.# 1862495
Halt Phosphatase Inhibitor	Thermo Scientific	cat.# 1862209
gp33-41 (KAVYNFATC)	Anaspec	cat.# AS-61669
hIL-2	PeproTech	cat.# 200-02
mIL-15	PeproTech	cat.# 210-15
human IL-7	PeproTech	cat. # 200-07-10ug
BD Cytofix/cytoperm kit	BD Biosciences	cat.# BDB554722
Foxp3/transcription factor staining buffer	Invitrogen	cat.# 50-112-8857
Seahorse Mitostress kit	Agilent	cat. #103015-100
Critical commercial assays		
Proteostat	Enzo	cat.# ENZ-51023-KP002
DAPI	Sigma-Aldrich	cat. # D9542-1MG
ER Tracker	Thermo Scientific	cat .# E34250
gp33 $H2D^b$ Tetramer	NIH Tetramer Core	N/A
NP396 $H2D^b$ Tetramer	NIH Tetramer Core	N/A
tetramethylrhodamine methyl ester perchlorate (TMRM)	Thermo Fisher Scientific	cat.# T668
Mitotracker Green	Thermo Fisher Scientific	cat.#M7514
TaqMan Universal PCR Master Mix	Thermo Fisher Scientific	cat.# 4304437
Applied Biosystems POWER SYBR Green PCR Master Mix	Fisher Scientific	cat.# 43-676-59
Deposited data		
scRNA-seq: Mus musculus P14 $CD8^+$ T cells from LCMV-Armstrong infected mice	Kurd et al.(126)	GSE131847
Bulk-RNAseq: Mus musculus WT or Sel1LcKO P14 $CD8^+$ T cell from LCMV-Armstrong infected mice	This paper	GSE244315
Bulk-RNAseq: Human $CD8^+$ T cells	Giles et al.(135)	GSE179613
Bulk-RNAseq: Human T cells	Philipp et al.(141)	GSE196463
Bulk-RNAseq: Human GD2 CAR-T cells	Weber et al.(136)	GSE164950
Proteomics: Human $CD8^+$ T cells	Rieckmann et al.(130)	PXD004352
Proteomics: IL2 Withdrawal	Rollings et al.(133)	Processed data downloaded from http://immpres.co.uk(132) Raw data: PXD008112
Bulk-RNAseq: IRF4cKO	Tsao et al. (134)	GSE192389

IRF4 Chip-seq	Tsao et al. (134)	GSE192386
Experimental models: Organisms/strains		
C57BL/6J	The Jackson Laboratories	cat.# 000664; RRID:IMSR_JAX:000664
CD4Cre+	The Jackson Laboratories	cat.# 022071: IMSR_JAX:022071
B6.SJL-Ptprca (CD45.1+)	The Jackson Laboratories	cat.#002014; RRID:IMSR_JAX:002014
P14 mice	The Jackson Laboratories	cat.# 037394-JAX; RRID: MMRRC_037394-JAX
Sel1L fl/fl mice	Ling Qi lab(107)	N/A
C57BL/6J	The Jackson Laboratories	cat.# 000664; RRID:IMSR_JAX:000664
Oligonucleotides		
RT-PCR Primer: LCMV-GP Forward (5'GCAACTGCTGTG TTCCCGAAAC)	McCausland et al(119)	N/A
RT-PCR Primer: LCMV-GP Reverse (5'CATTCACCTGGACTTTGTCAGACTC)	McCausland et al(119)	N/A
RT-PCR Primer: Mouse-16s Forward (5'CCGCAAGGGAAAGATGAAAGAC)	Quiros et al(146)	N/A
RT-PCR Primer: Mouse-16s Reverse (5'TCGTTTGGTTTCGGGGTTTC)	Quiros et al(146)	N/A
RT-PCR Primer: Mouse-Sel1L Forward (5'TGAATCACACCAAAGCCCTG)	Liu et al(147)	N/A
RT-PCR Primer: Mouse-Sel1L Reverse (5'GCGTAGAGAAAGCCAAGACC)	Liu et al(147)	N/A
RT-PCR: TaqMan assay-Sel1L-Mm01326442	N/A	cat.#433118
RT-PCR: TaqMan assay ActB-Mm00607939	N.A	cat.# 4331182
Software and algorithms		
FlowJo 10.10	BD	RRID:SCR_008520
Prism 10.0	GraphPad	RRID:SCR_002798
deseq2 1.38.3	Love et al.(138)	RRID:SCR_015687
Tximport 1.26.1	Sonesson et al.(148)	RRID:SCR_016752
r-base 4.2.3	The R foundation	https://www.r-project.org/
python 3.11.3		
FASTQC 0.11.9	N/A	https://www.bioinformatics.babraham.ac.uk/projects/fastqc/:RRID:SCR_014583

Rsem 1.3.1	Li et al.(114)	10.1186/1471-2105-12-323:RRID:SCR_013027
STAR 2.7.10a	Dobin et al.(113)	10.1093/bioinformatics/bts635:RRID:SCR_004463
RNA-Enrich 1	Lee et al.(117)	RID:SCR_004463
Cutadapt 3.4	Marcel et al.(112)	RRID:SCR_011841
multiQC 1.14	Ewels et al.(116)	10.1093/bioinformatics/btw354:RRID:SCR_014982
scanpy 1.9.1	Wolf et al.(127)	https://doi.org/10.1186/s13059-017-1382-0:RRID:SCR_018139
Decoupler 1.1	Badia et al.(128)	N/A
SRATools 2.8.2	NCBI	https://hpc.nih.gov/apps/sratoolkit.html:
GSVA 1.46	Hezelman et al.(139)	RRID:SCR_021058
Perseus 2.0.10.0	Tyanova et al.(149)	RRID:SCR_015753
fgsea 1.24	Korotkevich et al.(140)	RRID:SCR_020938
Tidyverse 2.0	Wickham et al.(150)	RRID:SCR_019186
Conda 4.12.0	Anaconda	RRID:SCR_018317
nf-core/rnas-seq 3.12.0	Ewels et al.(137)	RRID:SCR_024135
Zeiss Zen	Zeis	RRID:SCR_013672
Imaris	Oxford Instruments	RRID:SCR_007370
CellProfiler	Stirling et al.(118)	RRID:SCR_007358
SPICE v6	Roederer et al.(111)	RRID:SCR_016603
Bowtie 2 v	Langmead et al.((142))	RRID:SCR_016368
MACS2 2.2.7.1	Zhang et al.(143)	RRID:SCR_013291
Integrative Genomics Viewer (IGV)	Thorvaldsdóttir et al.(151)	RRID:SCR_011793
Other		
BD Fortessa	BD	N/A
XF-96 Extracellular Flux Analyzer	Agilent	N/A
Nova-seq	Illumina	N/A
SepMate tubes	Stemcell Technologies	cat. #85450
Cyquant	Invitrogen	cat. #C7026
CD8+ lymphocytes isolation kit	Invitrogen	cat. #11147D
ECL Film	Fisher Scientific	cat. # 45-001-508
Femto ECL Substrate	Fisher Scientific	cat. # PI34095
ECL Substrate	Fisher Scientific	cat. # PI32209
Tris Glycine Transfer buffer	Fisher Scientific	cat. # LC3675
Tris glycine Running buffer	Thermo Scientific	cat. #LC26754
Tris buffered saline	Bio-Rad	cat. # 1706435

Brain Heart Infusion Agar	Sigma-Aldrich	cat. # 70138
Brain Heart Infusion Broth	Sigma-Aldrich	cat. # 53286
Mojosort™ Mouse CD8 T Cell Isolation Kit	Biolegend	cat. # 480008
Brefeldin A	Beckton Dickson	cat. #BDB555029
LIVE/DEAD Aqua	Invitrogen	cat. # L34965
Annexin Binding Buffer	Biolegend	cat. # 422201
Annexin V	Biolegend	cat. # 640918
7AAD	Biolegend	cat. # 420403
RPMI	Gibco	cat. # 11875093
L-glutamine/penicillin/streptomycin	Gibco	cat. #10378016
Non-essential amino acids	Gibco	cat. # 11140050
CD3/28 Dynabeads	Invitrogen	cat. #11131D
Fetal Bovine Serum	Thermo Fisher Scientific	cat. # SH3039603

Chapter 3 - ER-Associated Degradation Adapter Sel1L Is Required for CD8$^+$ T Cell Function and Memory Formation Following Acute Viral Infection

This chapter has been published:

Luis O. Correa-Medero, Shayna E. Jankowski, Hanna S. Hong, Nicholas D. Armas, Aditi I. Vijendra, Mack B. Reynolds, Garrett M. Fogo, Dominik Awad, Alexander T. Dils, Kantaro A. Inoki, Reid G. Williams, Annabelle M. Ye, Nadezhda Svezhova, Francisco Gomez-Rivera, Kathleen L. Collins, Mary X. O'Riordan, Thomas H. Sanderson, Costas A. Lyssiotis and Shannon A. Carty. ER-associated degradation adapter Sel1L is required for CD8$^+$ T cell function and memory formation following acute viral infection. Cell Reports (2024) PMID: 38687642

3.1 Abstract

The maintenance of antigen-specific CD8$^+$ T cells underlies the efficacy of vaccines and immunotherapies. Pathways contributing to CD8$^+$ T cell loss are not completely understood. Uncovering the pathways underlying the limited persistence of CD8$^+$ T cells would be of significant benefit for developing novel strategies of promoting T cell persistence. Here, we demonstrate murine CD8$^+$ T cells experience endoplasmic reticulum (ER) stress following activation and the ER-associated degradation (ERAD) adapter Sel1L is induced in activated CD8$^+$ T cells. Sel1L loss limits CD8$^+$ T cell function and memory formation following acute viral infection. Mechanistically, Sel1L is required for optimal bioenergetics and c-Myc expression. Finally, we demonstrate that human CD8$^+$ T cells experience ER stress upon activation and that ER stress is negatively associated with improved T cell functionality in T cell- redirecting therapies. Together these results demonstrate that ER stress and ERAD are important regulators of T cell function and persistence.

3.2 Introduction

Following T cell receptor (TCR)-mediated recognition of cognate antigen, naïve $CD8^+$ T cells are activated, undergo rapid clonal expansion, and acquire effector function, including cytokine and cytotoxic molecule production, to eliminate intracellular pathogens and tumors (9, 152, 153). After the peak of expansion, the majority of the responding $CD8^+$ T cells become terminally differentiated and undergo cell death following antigen clearance, however a small fraction of antigen-specific cells persists as memory $CD8^+$ T cells providing long-lived immune protection by rapidly responding upon antigen re-challenge (154, 155) .

As a consequence of TCR-mediated activation, antigen-specific $CD8^+$ T cells undergo dramatic transcriptional, epigenetic, metabolic and proteomic changes that endow proper function and differentiation (81, 156, 157). Initial work demonstrated that though naïve murine $CD8^+$ T cells had relatively low protein synthesis, antigen-specific $CD8^+$ T cells experience the greatest levels of translation at day 5 post-acute viral infection, followed by a significant reduction by day 8 post-infection (18). In both human and murine T cells, sophisticated proteomic studies corroborated the transition from low basal translation in naïve cells to a marked increase in protein synthesis in activated cells (19-24). Translation is the most error-prone step in gene expression with ~10-30% of all newly synthesized proteins being ubiquitinated and targeted for degradation (158, 159), thus the question arises how cells handle this increase in misfolded protein. Both elevated demand for protein folding and increases in misfolded proteins have been shown to trigger endoplasmic reticulum (ER) stress, whose resolution or failure to resolve have important consequences in cell fate and survival across various cell types (83, 160).

Several studies have started to dissect how maintenance of protein homeostasis and ER stress may regulate $CD8^+$ T cell fate and function. The reduction of proteasome activity early in

$CD8^+$ T cell differentiation promoted terminal differentiation, whereas enhanced proteasomal activity led to the promotion of memory characteristics in $CD8^+$ T cells (82), raising the question if ER stress resulting from accumulated misfolded proteins following proteasomal inhibition blocks $CD8^+$ T cell memory formation. Two pathways known to mediate clearance of misfolded protein and thus alleviate ER stress are the unfolded protein response (UPR) and endoplasmic reticulum-associated degradation (ERAD) pathways. Several groups have studied the role of the UPR pathways in $CD8^+$ T cell differentiation and in multiple settings found that UPR activation is associated with terminal differentiation and T cell dysfunction, while deletion of UPR components enhanced T cell function (86, 87, 89). However, very little is known about the role of ERAD in $CD8^+$ T cell fate and function.

Sel1L acts as an adaptor of the ERAD complex, recognizing misfolded proteins in the ER and recruiting them to be translocated to the cytosol for proteasomal degradation (161). Sel1L also binds and stabilizes Hrd1, the E3 ubiquitin ligase of the ERAD complex.(107) In various cell types, ERAD has been shown to be critical in maintaining ER homeostasis by selectively degrading misfolded protein, loss of this function then results in disrupted homeostasis manifesting in cell death, altered differentiation and mitochondrial dysfunction (103, 106, 107, 147, 162-168). ERAD via Hrd1 deletion is known to regulate $CD4^+$ T cell differentiation, survival, and cytokine production *in vitro* and *in vivo* (169, 170). We and others have demonstrated that Sel1L is necessary for naïve T cell homeostasis (171, 172). How $CD8^+$ T cells manage stresses associated with activation and the role of Sel1L/ERAD are unknown.

We sought to understand the role of ER stress in $CD8^+$ T cell function and persistence following an acute viral infection. Utilizing *in vitro* and *in vivo* models of antigen-specific $CD8^+$ T cell differentiation, we found that T cell activation is associated with a transient induction of ER

stress, UPR signaling and Sel1L expression. Loss of Sel1L, a critical ERAD component, resulted in impaired effector molecule production and memory formation of antigen-specific $CD8^+$ T cells following acute viral infection in a cell-intrinsic manner. Mechanistically, we found that Sel1L/ERAD was required for antigen-specific $CD8^+$ T cell oxidative metabolism, mitochondrial fusion and c-Myc expression, which are important for $CD8^+$ T memory. Furthermore, we found that ER stress is upregulated following activation of human $CD8^+$ T cells and is associated with terminal differentiation, while alleviation of ER stress is associated with improved $CD8^+$ T cell persistence and function in T cell immunotherapies. Our findings demonstrate a critical role of Sel1L/ERAD in promoting $CD8^+$ T cell effector function and persistence.

3.3 Results

3.3.1 Activated $CD8^+$ T cells experience ER stress

As human and murine $CD8^+$ T cells are activated, they quickly upregulate protein synthesis, increase total protein content and remodel their proteome (18, 20-22, 133). However, it is unclear if this rapid increase in translation induces ER stress. To answer this question, we serially characterized readouts of ER stress in $CD8^+$ T cells using a well-characterized model of *in vitro* differentiation (26, 173). In this system, splenocytes from wild-type (WT) T cell receptor (TCR) transgenic mice, which have $CD8^+$ T cells expressing the TCR transgene recognizing the lymphocytic choriomeningitis virus (LCMV) epitope glycoprotein (gp) 33-41 (P14 cells), are activated with LCMV gp33-41 peptide in the presence of IL-2 for three days, and then isolated activated P14 $CD8^+$ T cells (T_{ACT}) were differentiated into IL-2 'effector' cells (IL-2 T_E) or IL-15 'memory' cells (IL-15 T_M) for an additional 3 days (**Figure 3-1A**). Since an increase in ER size has been correlated with ER stress (174, 175), we used immunofluorescent staining for calreticulin, an ER-resident chaperone (176), to quantitate ER size in $CD8^+$ T cells over the course of

differentiation. Confocal microscopy demonstrated an increase in calreticulin in T_{ACT} cells relative to naïve cells (**Figure 3-1B**), which is consistent with other reports that TCR activation increases ER size in T cells (177). However, an increase in ER size could also correlate with increased translation, thus we examined other ER stress measures. When misfolded proteins accumulate in the cell, they form protein aggresomes (178), which can be detected by the fluorescent dye PROTEOSTAT. To measure proteome quality over the course of differentiation, we measured the cellular levels of misfolded protein aggregates using PROTEOSTAT by flow cytometry and lysine 48-linked ubiquitination (K48-Ub), which is sufficient to target damaged or misfolded proteins for proteasomal degradation (179), by immunoblotting. Activation of P14 cells was associated with a significant increase in misfolded protein in T_{ACT} cells that partially resolved over time (**Figure 3-1C**). We found that T_{ACT} cells consistently contained the highest amount of K48-Ub compared to naïve T cells, IL-2 T_E or IL-15 T_M cells (**Figure 3-1D**).

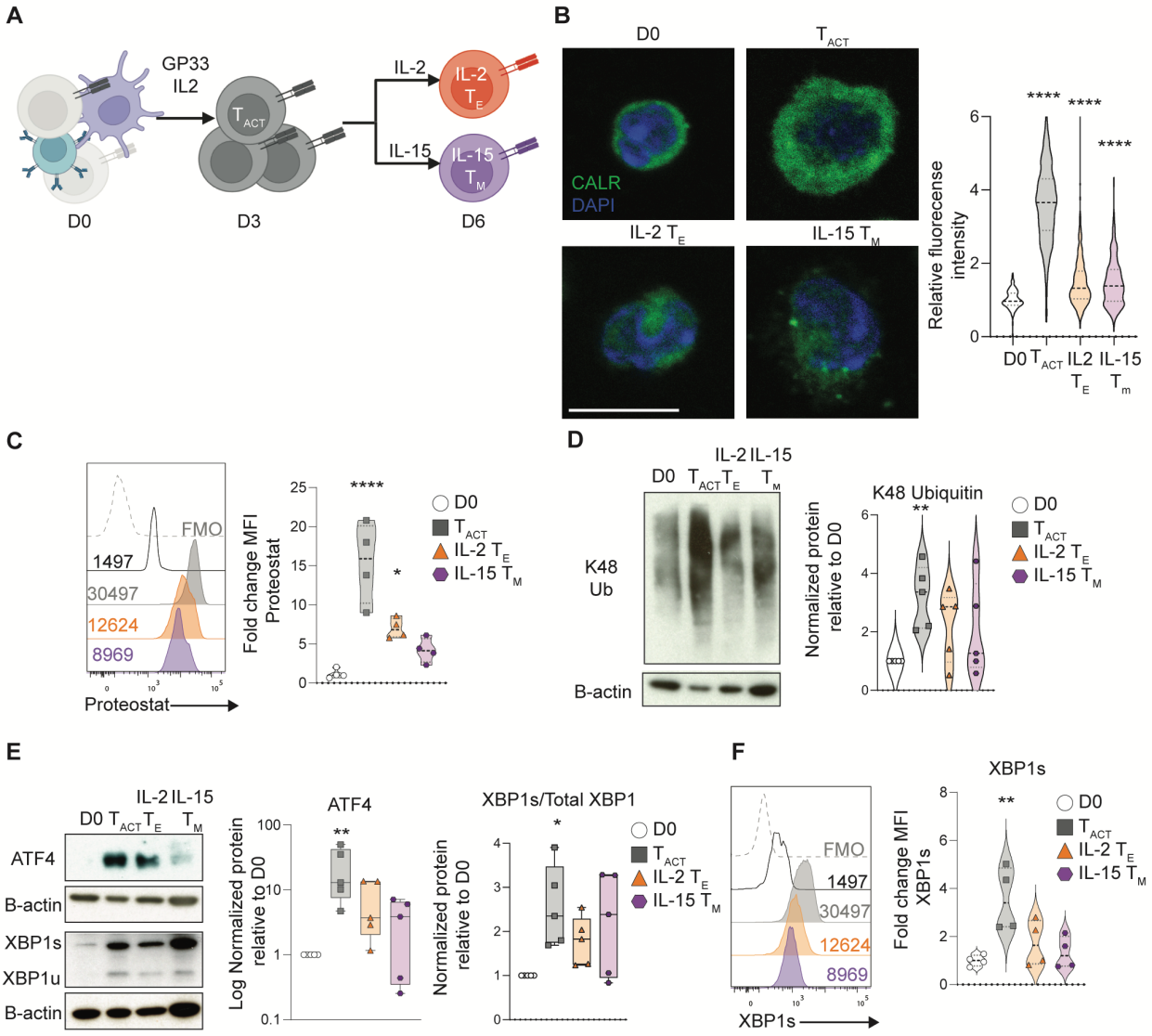

Figure 3-1: T cell activation induces ER stress *in vitro*.

(A) Experimental schema: splenocytes from wild-type (WT) P14 transgenic mice were activated *in vitro* with LCMV gp33-41 peptide in the presence of IL-2 for three days (T_{ACT}), then incubated with either IL-2 to generate IL-2 'effector' cells (IL-2 T_E) or IL-15 to generate IL-15 'memory' cells (IL-15 T_M). Created with BioRender.com. **(B)** *Left*, confocal microscopy and associated quantification of calreticulin (CALR) in *in vitro* naïve (D0), T_{ACT} (D3), IL-2 T_E and IL-15 T_M P14 cells, with scale bar representing 10uM. **(C)** *Left*, representative histograms of PROTEOSTAT in *in vitro* naïve (D0), T_{ACT}, IL-2 T_E and IL-15 T_M. *Right*, fold change in median fluorescence intensity (MFI) of PROTEOSTAT normalized to naïve. **(D)** *Left*, representative immunoblot of K48-Ub in serially collected *in vitro* naïve, T_{ACT}, IL-2 T_E and IL-15 T_M P14 cells. *Right*, densitometry quantification of the K48-Ub immunoblot bands in indicated conditions. **(E)** *Left*, representative immunoblot of ATF4 and XBP1 (spliced/unspliced) in serially collected *in vitro* naïve, T_{ACT}, IL-2 T_E and IL-15 T_M P14 cells. *Right*, densitometry quantification of the immunoblot bands. **(F)** *Left*, representative histograms of XBP1s in *in vitro* naïve, T_{ACT}, IL-2 T_E and IL-15 T_M. *Right*, fold change in MFI of XBP1s normalized to naïve. Data representative of naïve n=276, T_{ACT}= 376, IL-2 T_E n= 882, IL-15 T_M n =751 (B) n=4 (C, F) n=5 (D, E). All immunoblot data are normalized B-actin, then to naïve. *p<0.05, **p<0.01, one-way ANOVA with uncorrected Fisher's least significant difference (B-F).

The increase in ER size, protein aggresomes and K48-Ub levels following $CD8^+$ T cell activation suggest an increase in ER stress. In the setting of increased ER stress, the highly conserved UPR pathway is activated to either restore homeostatic balance or trigger apoptosis if cellular stress is unable to be relieved (160). The UPR employs three distinct ER-bound proteins [inositol-requiring enzyme 1a (IRE1a), activating transcription factor 6 (ATF6), and PKR-like ER kinase (PERK)] that sense unfolded protein in the ER and activate distinct transcriptional programs to resolve stress or execute apoptosis (160). We performed western blots for representative members of the UPR pathway. PERK activity can be measured by the induction of activating transcription factor 4 (ATF4) expression and IRE1a activity can be measured by XBP1 splicing (85, 180). As predicted and in agreement with previous findings (86, 93), the transition from naïve to T_{ACT} was associated with increased ATF4 expression and spliced XBP1 (XBP1s)/unspliced XBP1 ratio (**Figure 3-1E**). XBP1s induction was orthogonally validated by intracellular flow cytometry (**Figure 3-1F**). Together these data suggest that $CD8^+$ T cells experience ER stress and UPR induction after activation *in vitro*.

3.3.2 Antigen-specific $CD8^+$ T cells experience dynamic ER stress in vivo.

We next tested whether differentiating $CD8^+$ T cells experience dynamic ER stress *in vivo*. Araki and colleagues (18) demonstrated that translation is highest in antigen-specific $CD8^+$ T cells at day 5 following LCMV-Armstrong acute viral infection. Based on these data, we hypothesized that antigen-specific $CD8^+$ T cells would have the highest levels of ER stress at this timepoint. Reanalysis of a single cell atlas consisting of antigen-specific $CD8^+$ T cells responding to LCMV-Armstrong over time (126) corroborated that hallmark signature for UPR was enriched at days 4-5 post-infection (p.i) (**Figure 3-2A**) suggesting that virus-specific $CD8^+$ T cells may experience dynamic ER stress during the course of early activation and differentiation *in vivo*.

To confirm experimentally the transient ER stress experienced by antigen-specific $CD8^+$ T cells, wild-type (WT) mice were infected with LCMV-Armstrong asynchronously. ER stress markers were measured in LCMV-specific $CD8^+$ T cells at days 5 and 8 p.i. and compared to naïve $CD8^+$ T cells from uninfected mice. While naïve cells contained the lowest amount of protein aggresomes, gp33-specific $CD8^+$ T cells on day 5 p.i. had an 2-fold increase in PROTEOSTAT staining that is reduced to 1.5-fold by day 8 p.i. relative to uninfected naïve cells (**Figure 3-2B**), suggesting that misfolded proteins peak in viral-specific $CD8^+$ T cells around day 5 p.i.. To examine changes in ER size, we used ER Tracker, a flow cytometric reagent that measures a volumetric readout of ER size which may serve as a surrogate readout for ER stress (174, 181). Antigen-specific $CD8^+$ T cells on day 5 p.i. had a 4-fold increase ER volume compared to naïve cells, which subsequently subsided to baseline by day 8 p.i. (**Figure 3-2C**).

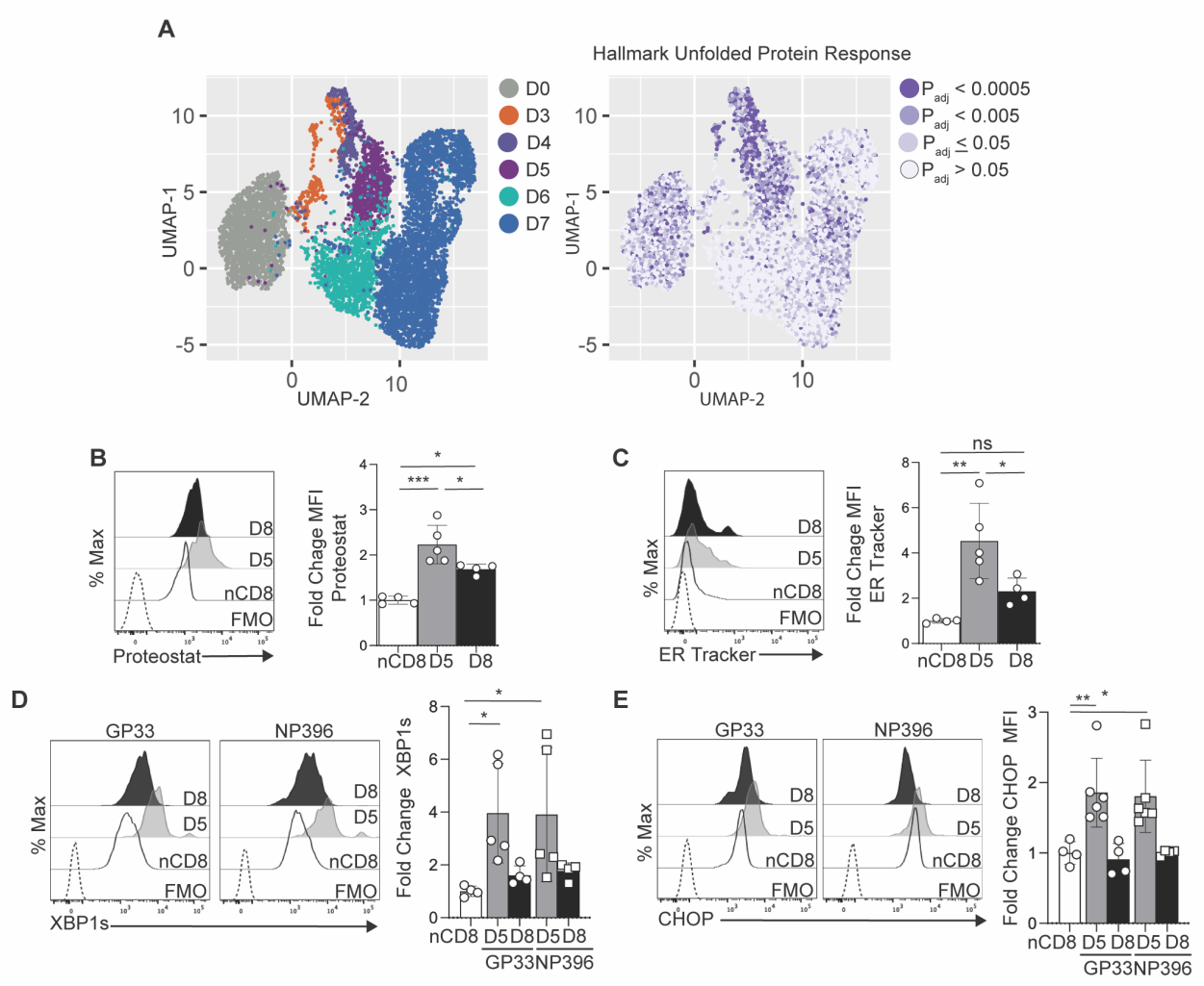

Figure 3-2: Antigen-specific CD8$^+$ T cells experience dynamic ER stress during an acute viral infection in vivo.

(A) *Left*, UMAP projection of P14 cells responding to LCMV infection (GSE131847) determined by Scanpy. Each dot corresponds to one individual cell colored by day of infection. *Right*, enrichment (adjusted p-values) of gene module "Hallmark Unfolded Protein Response" determined by Fisher's exact test (decouplr) and used to color UMAP plots. **(B-C)** *Left*, representative histograms of PROTEOSTAT **(B)** or ER Tracker **(C)** in gp33$^+$CD44$^+$CD8$^+$ TCRb$^+$ splenocytes isolated on indicated days p.i. LCMV compared to naïve CD8$^+$ T cells from uninfected mice. *Right*, fold change in MFI of PROTEOSTAT or ER Tracker normalized to uninfected naïve CD8$^+$ T cells. **D-E)** *Left*, representative histograms of intracellular XBP1s (D) and intracellular CHOP (E) in gp33$^+$ or NP396$^+$CD44$^+$CD8$^+$ TCRb$^+$ splenocytes. *Right*, fold change in MFI of XBP1s (D) or CHOP (E) in gp33$^+$ or NP396$^+$ normalized to uninfected naïve CD8$^+$ T cells. Fluorescence minus one (FMO) depicted as negative control in histograms. Data are representative of n=4-6, 2 independent experiments. *p<0.05, **p<0.01, ***p<0.001; one-way ANOVA with Dunnett's multiple comparison test.

Since UPR pathways are activated in response to ER stress (160), we measured intracellular expression of two UPR transcription factors, the PERK target CHOP and the IRE1a

target XBP1s in LCMV-specific CD8$^+$ T cells. Tetramers against immunodominant peptides gp33-41 and nucleoprotein (NP) 396-404 were used to generalize findings beyond one reactive population. Consistent with our prior data and others (86, 93), expression of UPR factors peaked in LCMV-specific CD8$^+$ T cells on day 5 compared to uninfected naïve cells and returned to baseline levels by day 8 in both LCMV-specific populations (**Figure 3-2D-E**). Together, our data demonstrate that activated CD8$^+$ T cells experience dynamic ER stress during differentiation following an acute viral infection.

3.3.3 Sel1L is upregulated in activated CD8$^+$ T cells

Dynamic ER stress experienced by antigen-specific CD8$^+$ T cells suggest that pathways regulating ER stress responses will be critical to CD8$^+$ T cell differentiation and function. Elegant work has demonstrated that UPR activity diminishes T cell function and persistence suggesting that enhanced ER stress is detrimental (87-89, 93). Similarly, the proteosome activity enhances CD8$^+$ T cell persistence while loss of proteosome function limits persistence and memory formation (82, 182). Sel1L, a critical component of ERAD, has been demonstrated to be indispensable for maintaining ER homeostasis and survival in other cell types (106, 107, 147, 162, 163, 167, 183). However, nothing is known about the cell-intrinsic role of Sel1L/ERAD in activated CD8$^+$ T cells, thus we sought to elucidate its role in CD8$^+$ T cell fate. First, we examined Sel1L protein expression and found it increased significantly following activation and was maintained in both IL-2 T_E and IL-15 T_M during *in vitro* differentiation (**Figure 3-3A**). In a similar fashion, Sel1L protein expression was upregulated in gp33$^+$ and NP396$^+$ CD8$^+$ T cells on day 8 p.i. relative to naïve cells from uninfected controls (**Figure 3-3B**). Together, these data demonstrate that Sel1L is induced in CD8$^+$ T cells after antigen encounter.

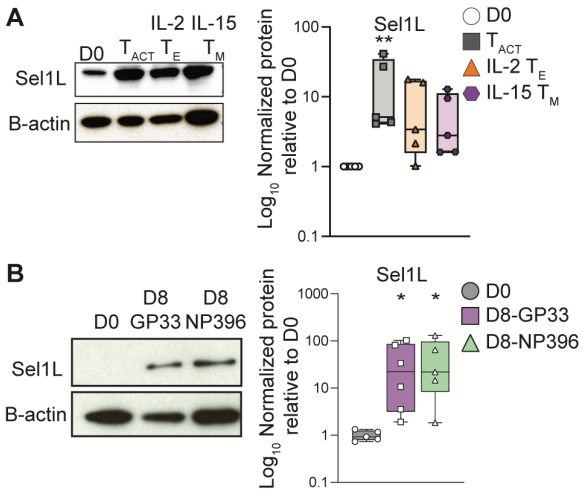

Figure 3-3: Sel1L is induced in antigen-experienced cells.

(A) Left, representative immunoblot of Sel1L and B-actin in serially collected *in vitro* naïve, T_{ACT}, IL-2 TE cells and IL-15 TM cells (10ug lysates). Right, densitometry quantification of the immunoblot band normalized to B-actin. **(B)** Left, representative immunoblot of uninfected naïve $CD8^+$ T cells and $gp33^+$ and $NP396^+$ $CD8^+$ T cells ($2x10^5$ cells) from mice on day 8 (D8) LCMV. Right, densitometry quantification of the immunoblot band normalized to B-actin. Data are representative of n=5-6 from 2 independent experiments. *p<0.05, **p<0.01. Friedman test with Dunnett's multiple comparisons test (A), Kruskal-Wallis test with Dunnett's multiple comparisons test (B).

3.3.4 Possible mechanism regulating Sel1L expression in $CD8^+$ T cells

To investigate the signals regulating Sel1L expression, we treated naïve, T_{ACT}, IL-2 T_E cells and IL-15 T_M cells with 100nM thapsigargin to induce ER stress. Interestingly, none of the T cell subsets experienced significant changes in Sel1L expression upon thapsigargin exposure **(Figure 3-4A)**. From our *in vitro* model, we noted that conditions containing TCR stimulation and cytokine resulted in increased Sel1L. To test the role of IL-2 in regulating Sel1L expression, we reanalyzed a proteomics data set of D6 IL-2 maintained or withdrawn from IL-2 for 24 hours. Importantly, withdrawal did not impact the viability over 24 hours (133) . Removal of IL-2 resulted in reduced expression of Sel1L **(Figure 3-4B)**. However, we were not able to find evidence of IL-2 mediating transcription factors STAT3/STAT5 binding to the Sel1L locus in T cells (data not shown). This suggested a possible indirect mechanism of IL-2-mediated regulation through non-

STAT transcription factors downstream of other IL-2 activated kinases (184). It is well known that TCR activation results in the induction of transcription factors to orchestrate the activation of genes required for effector fate and function. IRF4 is a well-studied transcription factor induced after TCR activation (185) whose expression is possibly regulated by common gamma chain cytokine (IL-2, IL-4, IL-7, IL-15) stimulation (185-187). We looked for IRF4 binding of Sel1L locus through reanalysis of ChIP-seq data of *in vitro* activated IL-2 T_E (134) and integration with histone 3 lysine 27 acetylation CHIP-seq to identify cis-regulatory elements (188). IRF4 indeed did bind to the Sel1L transcriptional start site and is marked by H3K27ac in naive, effector, and memory T cells, denoting that IRF4 is binding a functional enhancer region across T cell states **(Figure 3-4C)**. To further corroborate the role of IRF4 in regulating Sel1L expression, we reanalyzed RNA-seq of D6 effector T cells lacking IRF4 (134) and found that IRF4 deficient cells have reduced engagement of the unfolded protein response and significantly reduced Sel1L RNA expression (**Figure 3-4D**). Together, these results suggest that TCR and IL-2, through an IRF4 axis, cooperate to maintain Sel1L expression in T cells.

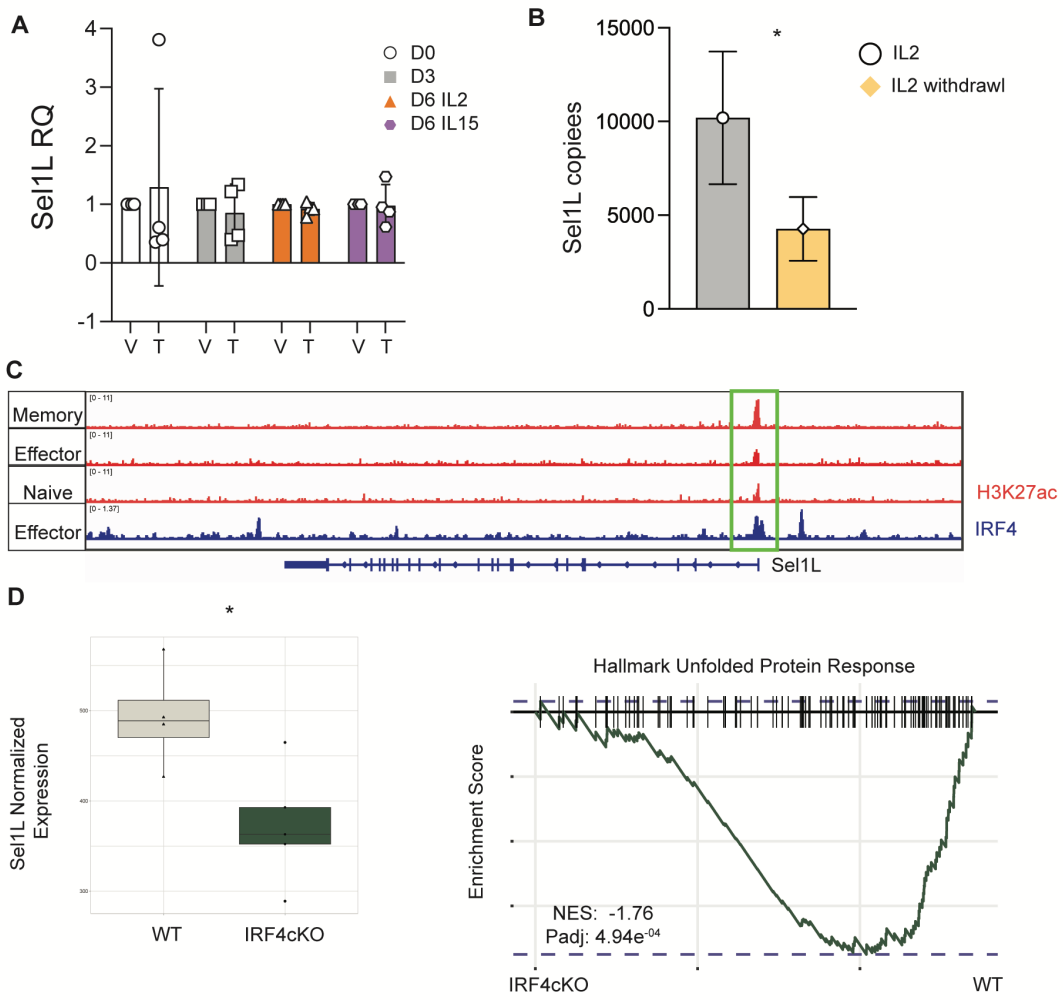

Figure 3-4: Regulation of Sel1L transcription in CD8$^+$ T cells

(A) Sel1L mRNA induction with vehicle or thapsigargin treatment under indicated conditions. **(B)** Sel1L protein copy number in IL-2 T_E cells maintained in or withdrawn from IL-2 for 24hrs. **(C)** IRF4 ChIP in effector T cells at Sel1L locus with reference H3K27ac. **(D)** Left, normalized Sel1L RNA expression in WT and IRF4cKO T cells; right, gene set enrichment analysis of UPR hallmarks in WT and IRF4cKO T cells.

3.3.5 Sel1L/ERAD is required for optimal CD8$^+$ T cell effector function

Recently we demonstrated that Ag-specific responses to *Listeria monocytogenes* (LM) were impaired in Sel1L conditional knockout (Sel1L$^{fl/fl}$CD4Cre; Sel1LcKO) mice (171); we now sought to investigate if Sel1LcKO mice impairment to acute bacterial infection was generalizable to viral infection. Utilizing the LCMV-Armstrong experimental system, we find that Sel1LcKO

mice experience equivalent viral LCMV burden at day 8 p.i. as measured by RNA levels (119) (**Figure 3-5A**). At memory timepoints, Sel1LcKO mice have reduced formation of LCMV-specific CD8$^+$ T cells (**Figure 3-5B**). To assess memory function, equal numbers of gp33$^+$ CD8$^+$ T cells from WT or Sel1LcKO mice previously infected with LCMV were transferred into congenic hosts. Host mice were subsequently infected with *Listeria monocytogenes* engineered to express the LCMV epitope gp33 (LM-gp33). Five days after LM-gp33 infection, we noted a decreased frequency of transferred Sel1LcKO gp33$^+$ cells in the peripheral blood mononuclear cells (PBMCs) and spleen relative to WT controls (**Figure 3-5C-D**). Measurements of liver *Listeria* bacterial burden on day 5 p.i. demonstrated increased bacterial load in the mice which received Sel1LcKO memory cells compared to those that received WT memory cells (**Figure 3-5E**). These data support a cell-intrinsic role for Sel1L in memory CD8$^+$ T cell protective function; however, deriving conclusions on Sel1L's role in CD8$^+$ T cell-mediated immunity in this system is confounded by the severe lymphopenia and lack of Sel1L expression in both CD4$^+$ and CD8$^+$ T cells in the Sel1LcKO mice.(171)

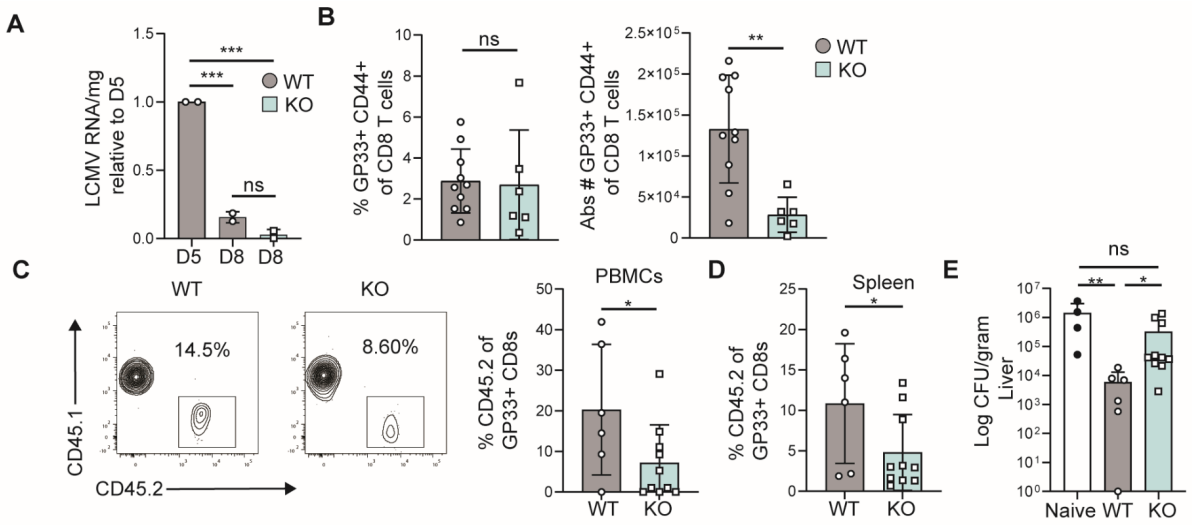

Figure 3-5: Sel1L is required for T cell function.

WT and Sel1LcKO mice were infected with LCMV-Armstrong and organs isolated at indicated timepoint. For memory recall experiments, equal numbers of WT or Sel1LcKO gp33$^+$ CD8$^+$ T cells (>day 40 p.i.) were adoptively

transferred into B6.SJL (CD45.1) mice, which were infected with *Listeria monocytogenes* expressing gp33 (LM-gp33) the following day. **(A)** Relative comparison of LCMV glycoprotein (GP)-encoding RNA/mg kidney tissue in WT day 5 post-LCMV (positive control), WT day 8 post-LCMV and Sel1LcKO day 8 post-LCMV. **(B)** Frequency (left) and absolute number (right) of $gp33^+$ $CD44^+$ $CD8^+$ T cells among splenocytes from LCMV-infected WT and Sel1LcKO mice at day 45 p.i. **(C)** Left, Representative flow cytometric analysis of donor CD45.2 on $gp33^+$ $CD44^+$ $CD8^+$ T cells among PBMCs from LM-gp33 infected mice at D5 p.i. Right, bar graph of frequency of donor $CD45.2^+$ cells among $gp33^+$ $CD44^+$ $CD8^+$ T cells. **(D)** Frequency of donor $gp33^+$ $CD44^+$ $CD8^+$ T cells among splenocytes from B6.SJL hosts on day 5 p.i. LM-gp33. **(E)** Bacterial load (colony forming units, cfu) per gram of liver on day 5 p.i. LM-gp33 of congenic hosts that received no T cells (naïve), or either WT or Sel1LcKO $gp33^+$ memory $CD8^+$ T cells. Data representative of 4/genotype, 2 independent experiments (A), 10/WT, 6/KO, 2 independent experiment (B-D). ns $p>0.05$; * $p<0.05$; ** $p<0.01$; *** $p<0.001$; one-way ANOVA with Šídák's multiple comparisons test (A), unpaired t-test (B), unpaired one-tailed t-test (C-D), one-way ANOVA with Kruskal-Wallis test (E).

Thus to interrogate the cell-intrinsic role of Sel1L, we generated Sel1LcKO mice that express the transgenic P14 TCR (Sel1LcKO P14). At baseline, Sel1LcKO P14 mice had comparable frequencies and absolute numbers of peripheral T cell populations as WT P14 littermates (**Figure 3-6A**), as well as similar expression of naïve markers CD62L and CD127 (**Figure 3-6B**). Sel1LcKO P14 cells did not have detectable ER stress as measured by ER size, PROTEOSTAT, CHOP and XBP1s expression compared to WT P14 cells (**Figure 3-6C**). Following *in vitro* activation with cognate peptide in the presence of splenic antigen presenting cells, Sel1LcKO P14 cells upregulated TCR activation markers CD25 and CD69 at a similar frequency and to similar levels as WT P14 cells (**Figure 3-6D**) indicating no alterations in early TCR signaling or activation. Together these data suggest that Sel1L deficiency does not alter T cell homeostasis or TCR activation in Sel1LcKO mice expressing a fixed TCR.

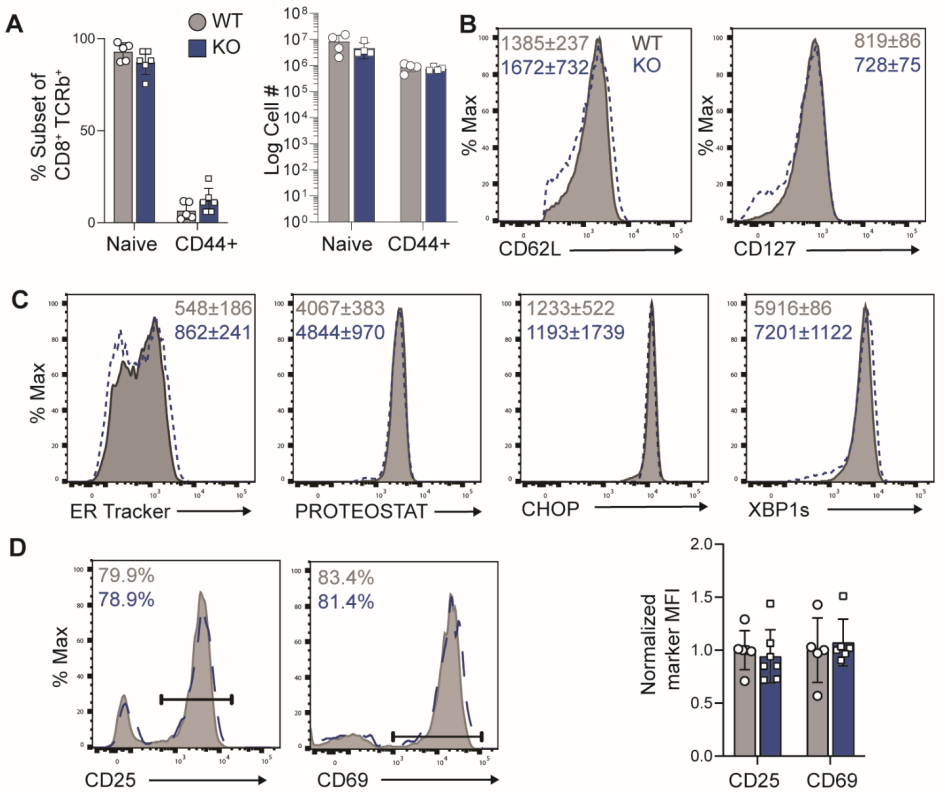

Figure 3-6: Loss of Sel1L does not alter P14 CD8$^+$ T cell homeostasis, proteostasis nor activation.

Characterization of peripheral T cell subsets in Sel1LcKO P14 mice (blue) and littermate controls (WT P14, grey) aged 6-10 weeks. **(A)** *Left*, Frequency, right, absolute number of naïve (CD44$^-$ CD62L$^+$) and CD44^{hi} populations among CD8$^+$ T cells isolated from the spleens of WT P14 and Sel1LcKO P14 mice. **(B)** CD62L and CD127 surface expression on naïve CD8$^+$ T cells from WT P14 (grey filled histogram) and Sel1LcKO P14 (blue dashed histogram) mice; inset, normalized MFI ± S.D. of CD62L and CD127. **(C)** Representative histograms of ER Tracker, PROTEOST, CHOP and XBP1s staining in naïve CD8 T cells from WT P14 or Sel1LcKO P14 mice; inset, MFI ± S.D. **(D)** *Left*, histogram of CD25 and CD69 upregulation on CD8$^+$ T cells from WT P14 and Sel1LcKO P14 mice 16hrs after activation *in vitro* with frequency positive, normalized to WT; inset, Frequency CD25$^+$ or CD69$^+$. *Right*, normalized MFI among marker + cells. n=4-7/genotype 3 independent experiments (A-C), n=6-7/genotype 3 independent experiments (D). ns p>0.05. Unpaired t-test (A-D).

To determine the cell-intrinsic role of Sel1L/ERAD in CD8$^+$ T cell function, we transferred congenically disparate WT P14 and Sel1LcKO P14 cells mixed in a 1:1 ratio into congenic recipient B6.SJL mice that were subsequently infected with LCMV-Armstrong. Eight days p.i., stimulation of splenocytes with gp33-41 was performed to assess effector molecule expression. Intracellular staining revealed a significant decrease in cytokine double (IFNγ^+,TNFα^+) as well as polyfunctional producers (i.e. production of multiple cytokine) in Sel1LcKO P14 (**Figure 3-7A);**

importantly polyfunctional $CD8^+$ T cells have been associated with superior control of viral infections.(189, 190) Loss of double polyfunctional cells appeared to primarily be driven by lack of TNFα-expressing cells as the frequency of IFNγ-expressing cells was not significantly altered. However, on a per cell basis, cytokine-producing cells had both lower IFNγ and TNFα expression. To examine global effector molecule co-expression, we performed SPICE analysis(111) on the stimulated WT and Sel1L-deficient P14 cells and found that WT cells consistently were more able to co-express 4-5 effector molecules than Sel1LcKO cells (**Figure 3-7B**). Together these data demonstrate that Sel1L/ERAD is essential for optimal $CD8^+$ T cell function in a cell-intrinsic manner.

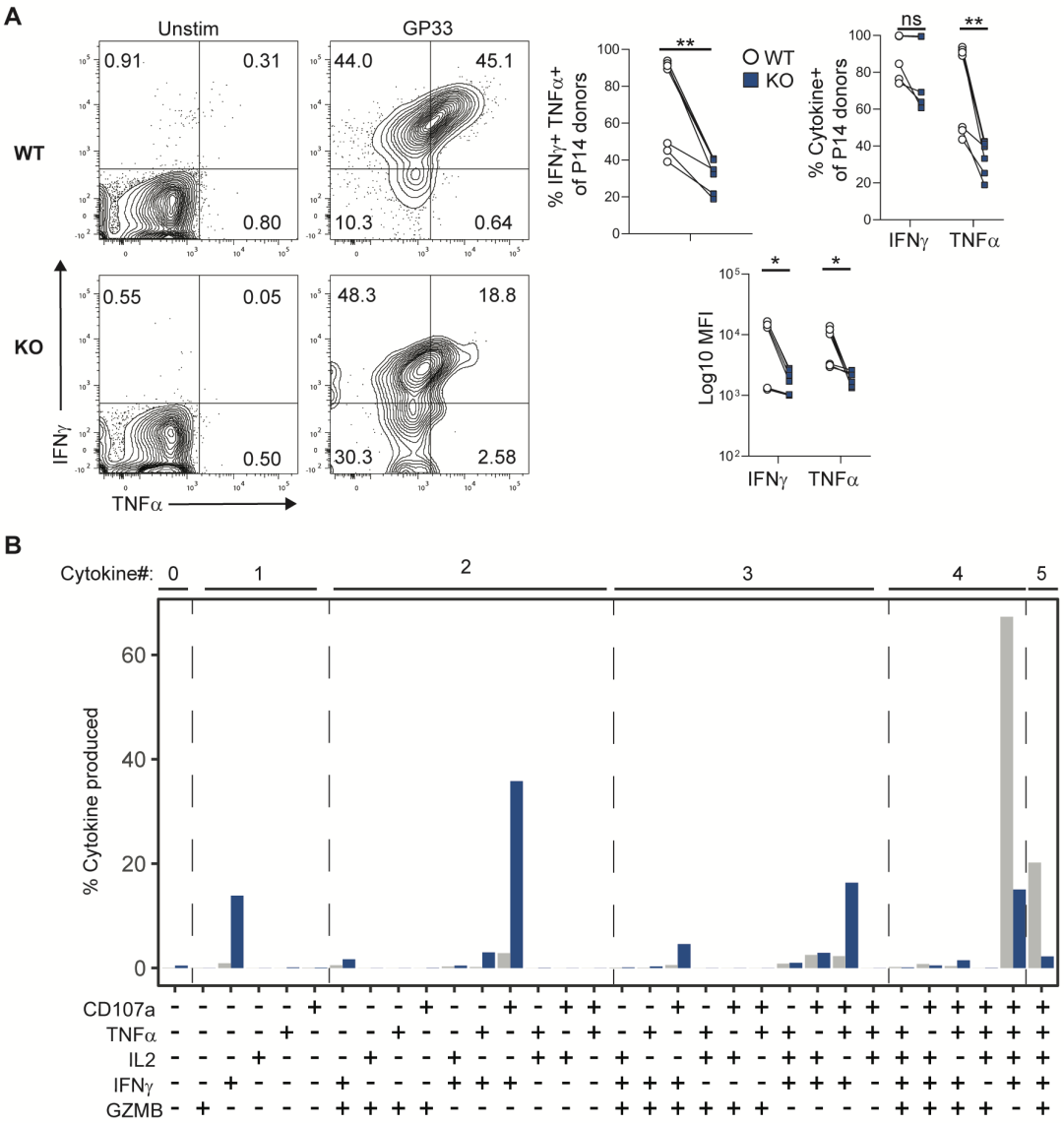

Figure 3-7: Sel1L/ERAD is required for optimal CD8$^+$ T cell effector function.

Peripheral blood lymphocytes from Sel1LcKO P14 (CD45.2) and WT P14 (CD45.1/2) mice were mixed to generate a 1:1 mix of donor P14 cells, which was subsequently transferred into B6.SJL (CD45.1) mice. These mice were infected with LCMV-Armstrong the following day. At day 8 p.i., splenocytes were stimulated ex vivo with gp33 peptide. **(A)** Representative plots of intracellular TNFα and IFNγ expression (left) and frequencies (top right) of indicated cell populations in donor P14 cells, as well as MFI of indicated cytokine among cytokine+ populations (bottom right). **(B)** Cytokine co-expression in ex vivo restimulated WT or KO P14 cells at day 8 p.i. Dashed lines separate columns by number of cytokines produced. Representative of n=8/genotype, 2 independent experiments. *p<0.05, **p<0.01, ***p<0.001, paired t-test.

3.3.6 Sel1L/ERAD is required for CD8$^+$ T cell survival and memory formation

Resolution of ER stress is critical for cell survival, loss of Sel1L in other cell types has been associated with cell death and dysfunction. Limited T cell persistence is a barrier to more

efficacious immunotherapeutics; however, pathways contributing to limited T cell persistence are not fully understood. The transient ER stress as well as the selective induction of Sel1L in antigen-experienced cells suggested that Sel1L/ERAD would be necessary for persistence of antigen-specific $CD8^+$ T cells during acute viral infections. We co-transferred equal numbers of congenically distinct WT P14 and Sel1LcKO P14 into B6.SJL mice and subsequently infected them with LCMV-Armstrong. At day 5 p.i., Sel1LcKO P14 donor cells moderately out-competed WT P14 donors (**Figure 3-8A**) with no alteration in differentiation nor apoptosis (**Figure 3-8B-C**). Sel1LcKO P14 donor cells had significantly reduced CD25 expression (**Figure 3-8D**). Examination of UPR activation revealed no differences in Sel1LcKO P14 relative to transferred WT P14 cells (**Figure 3-8E-F**). Together these data demonstrate that Sel1L/ERAD was not required for initial T cell expansion nor the maintenance of protein homeostasis at day 5 p.i.. In contrast, by day 8 p.i., the Sel1LcKO P14 population had reduced frequency in the spleen, lymph nodes, and blood compared to the WT P14 population (**Figure 3-9A**), suggesting that Sel1L was required for later stages of antigen-specific $CD8^+$ T cell survival and expansion. To determine whether this alteration in frequency was due to decreased proliferation or increased cell death, we performed Ki67 staining and 7-AAD/Annexin V staining. Despite being found at slightly higher frequencies than WT at day 5 p.i. (**Figure 3-8A**), Sel1LcKO P14 expressed marginally lower levels of the proliferation marker Ki67 compared to WT on day 8 p.i. (**Figure 3-9B**). Apoptosis as measured by Annexin V and 7-AAD staining suggest that Sel1LcKO P14 die at a greater rate than WT P14 cells at day 8 p.i. (**Figure 3-9C**). Though both proliferation and apoptosis were statistically significantly altered in the setting of Sel1L loss, the magnitude of apoptosis differences exceeded the minor difference in proliferation, suggesting that Sel1L is necessary primarily to

safeguard virus-specific CD8$^+$ T cells from apoptosis at the peak of expansion following an acute viral infection.

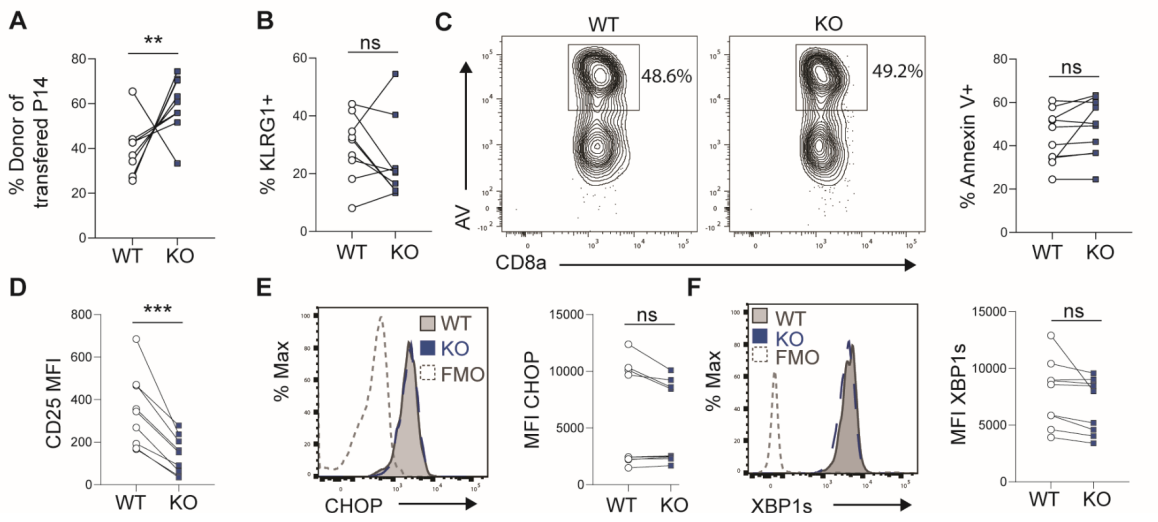

Figure 3-8: Sel1L is not required for initial expansion or homeostasis of antigen-specific CD8$^+$ T cells.

Sel1LcKO P14 (CD45.2) and WT P14 (CD45.1/2) cells were mixed 1:1 and adoptively co-transferred into B6.SJL (CD45.1) mice, which were infected with LCMV-Armstrong the following day. Flow cytometric analysis of donor P14 cells isolated from host spleens was performed on day 5 p.i. (**A)** Frequency of donor P14 of transferred cells at day 5 p.i. **(B)** Frequency of donor P14 cells expressing KLRG1. **(C)** *Left*, representative flow cytometry of Annexin V (AV) expression on donor WT or Sel1LcKO P14 cells. *Righ*t, frequency of Annexin V$^+$ of donor P14. **(D)** MFI of CD25 on donor P14 cells. **(E-F)** *Left*, representative histogram of intracellular CHOP (E) or XBP1s (E) expression in donor P14 cells; *Right*, MFI of CHOP and XBP1s expression in donor P14 cells. n=9/genotype 2 independent experiments (A-B); n=10/genotype, 2 independent experiments (C); n=9/genotype 2 independent experiments (D-F); ns $p>0.05$; ** $p<0.01$, paired t-test.

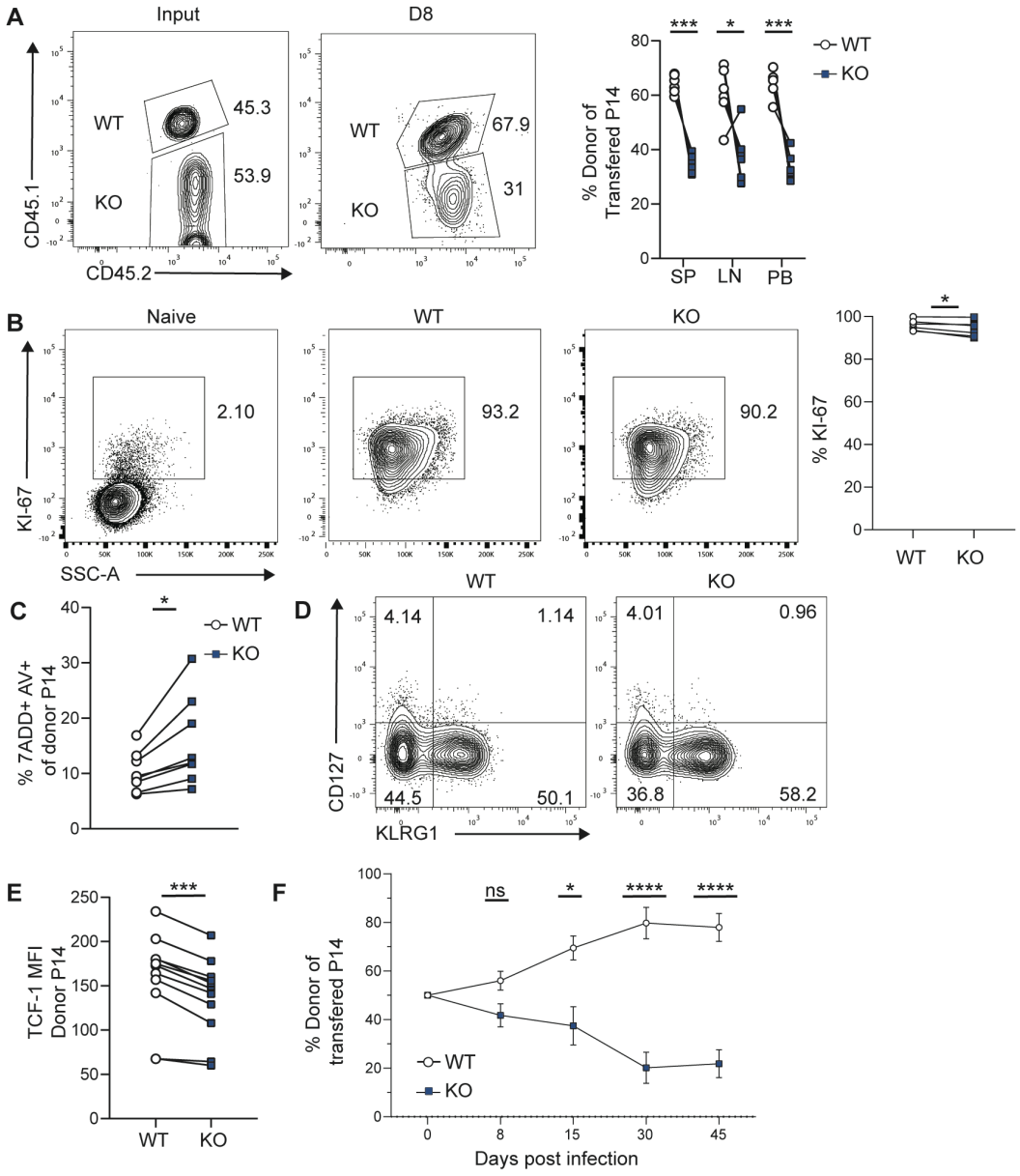

Figure 3-9 Sel1L/ERAD is required for CD8$^+$ T cell survival and memory formation.

Sel1LcKO P14 (CD45.2) and WT P14 (CD45.1/2) cells were mixed 1:1 and adoptively co-transferred into B6.SJL (CD45.1) mice, which were infected with LCMV-Armstrong the following day. Flow cytometric analysis of donor P14 cells was performed on day 8 (D8; A-E) and peripheral blood mononuclear cells (PBMCs) serially collected (F). **(A)** *Left*, representative flow cytometric analysis of donor P14 input; *center*, at D8 p.i.. *Right*, Donor frequencies of indicated genotypes in spleen (SP), lymph nodes (LN) and peripheral blood (PB). **(B)** *Left*, representative flow cytometric analysis of Ki67 in naïve CD8$^+$ T cells as negative control and donor P14. *Right*, Frequency of Ki67$^+$ population in donor P14 cells. **(C)** Frequency of 7AAD$^+$Annexin V (AV)$^+$ populations among donor P14. **(D)** Representative flow cytometric analysis of CD127 and KLRG1 expression on donor P14 cells. E) MFI of TCF-1 in donor P14 populations. F) Frequency of indicated genotypes among donor P14 cells in PBMCs at indicated time points ± S.E.M.. Data are representative of n=6/genotype, 2 independent experiments (A-B); n=8/genotype, 2 independent experiments (C); n=5-9, 2-3 independent experiments (D); n=11, 3 independent experiments (E); n=12, 3 independent experiments (F). Non-significant (ns) p> 0.05, *p<0.05, **p<0.01, ***p<0.001, paired t-test.

During acute viral responses, $CD8^+$ T cell differentiate into heterogenous cell states with different memory potential, which can be identified by different cell surface proteins and different canonical transcription factors. Phenotypically, terminal effector (TE) cells express high surface expression of killer cell lectin-like receptor G1 (KLRG1) and low expression of the interleukin-7 receptor α (IL7ra; CD127) whereas memory precursor (MP) cells express high levels of CD127 and low KLRG1.(28-30) MP cells primarily seed the memory T cell pool and TE cells have a significantly reduced capacity to contribute to the long-lived memory T cell pool.(30) Phenotypically, Sel1LcKO P14 cells had similar TE and MP populations as WT (**Figure 3-9D**). However, Sel1LcKO P14 demonstrated significantly reduced expression of transcription factor TCF1 (**Figure 3-9E**), known to be required for $CD8^+$ T cell memory formation and stemness.(40, 191, 192) To determine the necessity of Sel1L/ERAD in long term persistence of viral-specific $CD8^+$ T cells, we longitudinally tracked co-transferred Sel1LcKO and WT P14 cells in the peripheral blood of congenic hosts following LCMV. We observed a steady decrease in the persistence of Sel1LcKO P14 compared to WT over time (**Figure 3-9F**). Despite the lack of persistence, Sel1LcKO P14 cells had similar frequencies of central memory (T_{CM}) and effector memory (T_{EM}) subsets (193-195) as WT P14 cells (**Figure 3-10A**). Importantly, we noticed variation in the rates of Sel1LcKO P14 persistence in recipient mice at memory timepoints despite deriving from the same donor. Thus, we sorted donor cells at day 45 p.i. to confirm continued Sel1L deletion. We found that that Sel1LcKO P14 cells that persisted at the highest levels no longer had complete Sel1L deletion (**Figure 3-10B**), suggesting that they expanded from a small population that had initially escaped Cre recombinase deletion. These data point to a strong selection pressure to maintain Sel1L expression to promote $CD8^+$ T cell survival. Together, these

data demonstrate that Sel1L/ERAD is essential for CD8$^+$ T cell persistence in a cell-intrinsic manner following an acute viral infection.

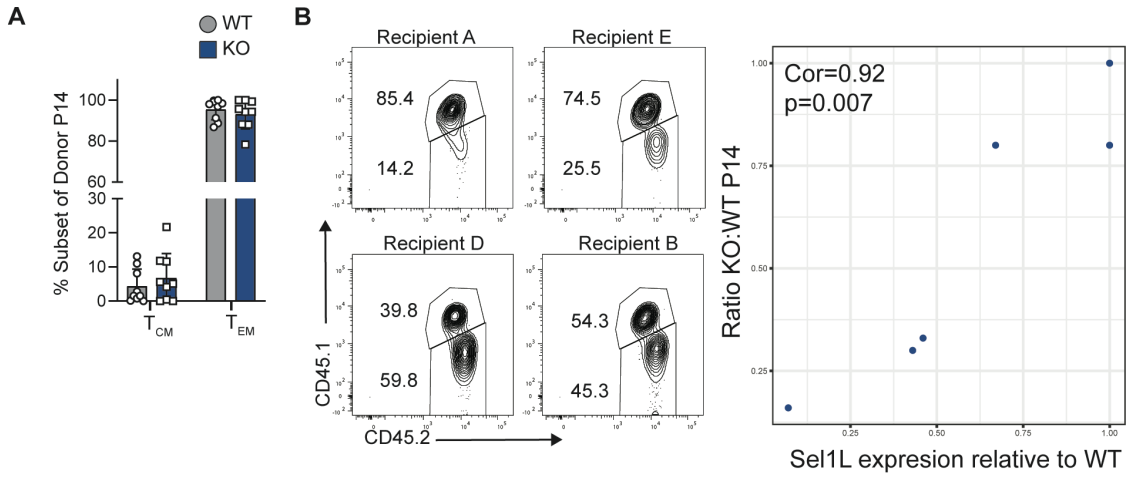

Figure 3-10:Characterization of WT and Sel1LcKO memory P14 cells

Sel1LcKO P14 (CD45.2) and WT P14 (CD45.1/2) cells were mixed 1:1 and adoptively co-transferred into B6.SJL (CD45.1) mice, which were infected with LCMV-Armstrong the next day. Flow cytometric analysis of donor P14 cells isolated from host spleens was performed on day 45 p.i. and cells were sorted to measure Sel1L deletion. **(A)** Frequency of donor P14 memory CD8$^+$ T cell subsets TCM (CD62L$^+$ CD44$^+$) or TEM (CD62L$^-$ CD44$^+$) at day 45 p.i.. **(B)** Left, representative flow cytometric analysis of donor WT and KO P14 cells day 45 p.i. from same donors co-transferred into different recipients; Right, Expression of Sel1L in sorted Sel1LcKO P14 relative to WT P14 cells versus ratio of KO to WT among donor P14 in recipient spleen at day 45p.i.. Data representative n= 9 donor pairs, 2 independent experiments (A) of 6 donor pairs, 2 independent experiments (B); ns p>0.05, paired t-test.(A) Pearson correlation (B)

3.3.7 Sel1L regulates CD8$^+$ T cell metabolism

To gain insights into the mechanism whereby Sel1L regulates CD8$^+$ T cell persistence, we performed RNA-seq analysis on Sel1LcKO P14 and WT P14 at day 8 post-LCMV infection. Pathway analysis (117) of WT P14 and Sel1LcKO P14 transcriptomes demonstrated Sel1LcKO P14 cells contained a decrease in terms corresponding to protein synthesis, such as the ribosome and rRNA binding, and an increase in terms corresponding to the ER, Golgi apparatus, response to hydrogen peroxide and fatty acid metabolism; known pathways to be upregulated in cells experiencing ER stress (**Figure 3-11A**).(90, 117) Pathways corresponding to the regulation of apoptosis were also enriched in Sel1LcKO P14 corroborating our previous data. Expression of

cytokines Gzmb, IFNγ, and IL2 were not altered suggesting that cytokine production defect observed above is primarily due to translational defects and not transcription (**Figure 3-12A**). Furthermore, immune signature analysis demonstrated that the Sel1LcKO P14 transcriptome was enriched in terms corresponding to terminal differentiation and T cell exhaustion while being depleted in terms corresponding to memory formation (**Figure 3-12B**), which corresponds to the data demonstrating lower TCF1 expression and lack of persistence in Sel1L-deficient P14 cells. Additionally, most altered pathways were related to cellular metabolism with terms corresponding to oxidative phosphorylation such as "respiratory chain complex IV," "oxidative phosphorylation," "NADH dehydrogenase activity" and "mitochondrial respiratory chain complex I" being significantly depleted in Sel1LcKO P14 cells compared to WT (**Figure 3-11A**).

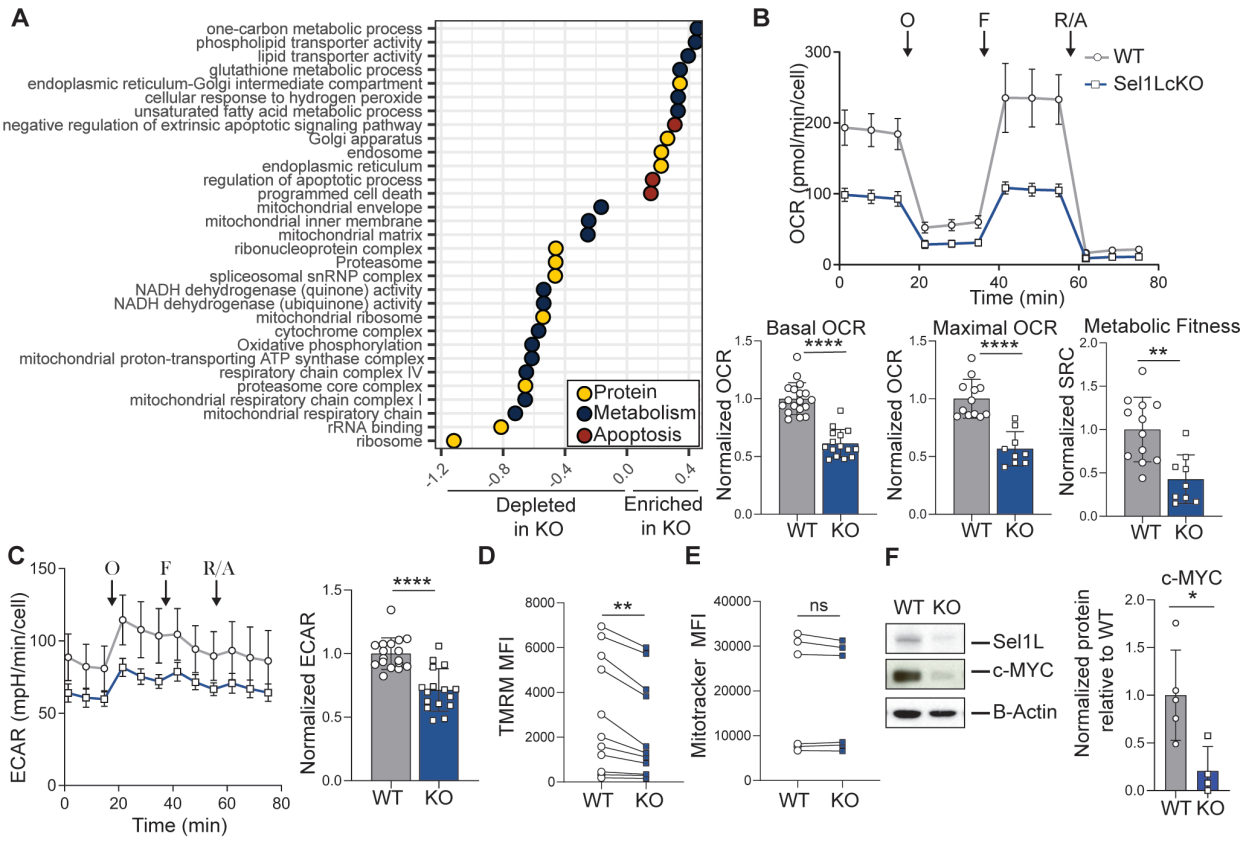

Figure 3-11: Sel1L/ERAD regulates CD8⁺ T cell metabolism.

(A) Pathway analysis of pathways significantly altered (FDR<0.05) in Sel1LcKO P14 relative to WT P14 transcriptome at D8 p.i.. **(B)** Extracellular flux analysis of activated Sel1LcKO P14 and WT P14 cells to assess OXPHOS activity including basal oxygen consumption rate (OCR), maximal OCR and metabolic fitness as measured by spare respiratory capacity (SRC). **(C)** Extracellular flux analysis of activated Sel1LcKO P14 and WT P14 quantifying basal extracellular acidification rate (ECAR). **(D-E)** MFI of TMRM (D) or Mitotracker Green (E) in Sel1LcKO P14 and WT P14 cells at D8 p.i.. **(F)** Left, representative immunoblot of Sel1L, cMyc and B-Actin in WT and KO $CD8^+$ T_{ACT} and right, densitometry quantification of the c-Myc immunoblot bands in indicated conditions normalized to B-actin, then to WT. Data are representative of n=3/genotype, 1 independent experiment (A), n=3/genotype; 3 independent experiments (B-C); n=7/genotype, 2 independent experiments (D); n=12/genotype 3 independent experiments (E); n=5/WT, 4/KO, 2 independent experiments (F). ns $p>0.05$, *$p<0.05$, **$p<0.01$, ****$p<0.0001$, unpaired t-test (B-C, F), paired t-test (D-E).

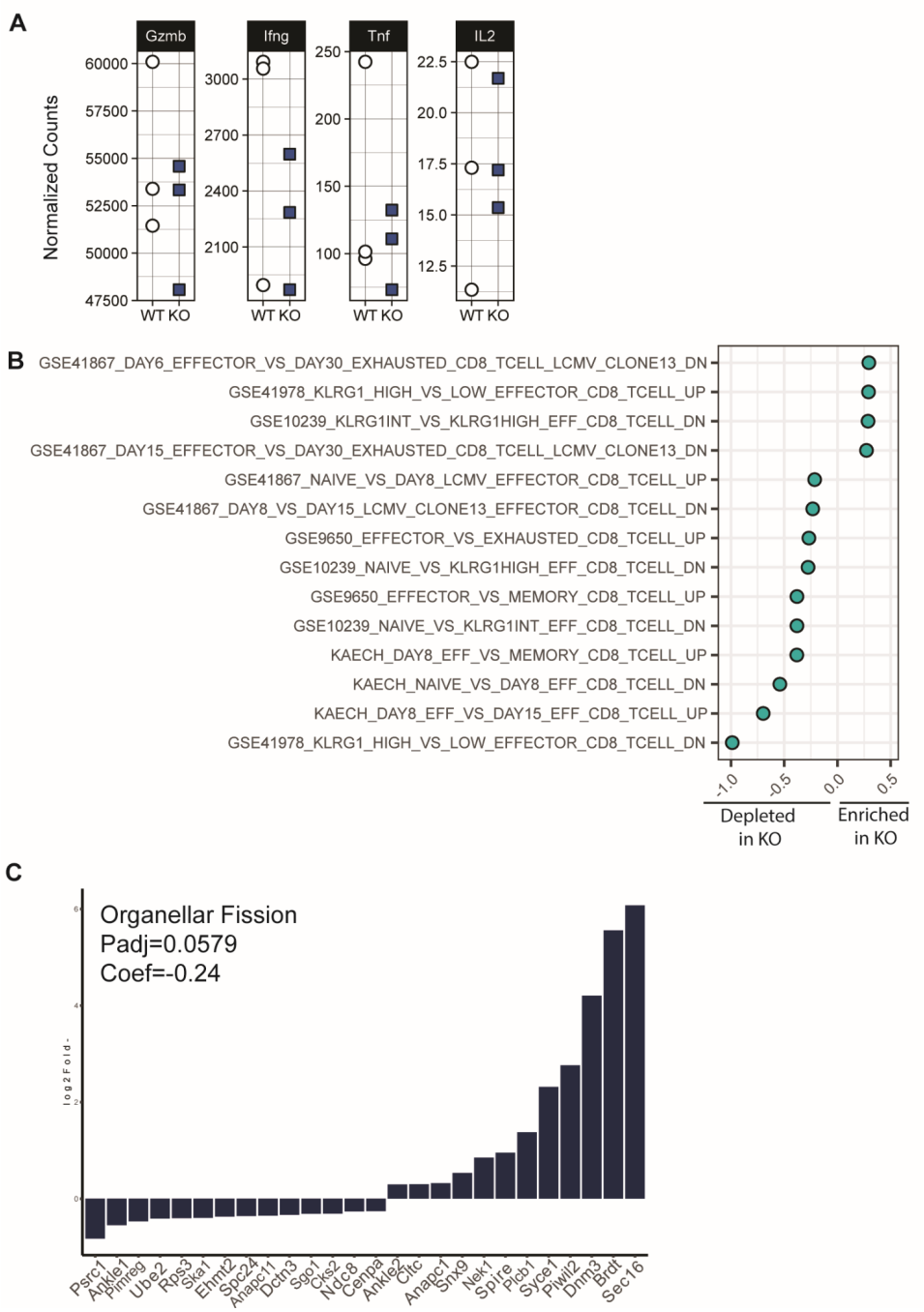

Figure 3-12: Gene expression and immune signatures from Sel1L-deficient LCMV-specific CD8$^+$ T cells.

Sel1LcKO P14 (CD45.2) and WT P14 (CD45.1/2) mice were mixed 1:1 and adoptively co-transferred into B6.SJL (CD45.1) mice, which were infected with LCMV-Armstrong the following day. RNA-seq analysis of donor P14 cells isolated from host spleens was performed on day 8 p.i.. **(A)** Normalized counts from RNA-seq transcriptome of donor P14 for *Gzmb*, *Ifng*, *Tnf* and *IL2* in donor WT and Sel1LcKO P14 cells at day 8 p.i.. **(B)** Immune signatures transcriptionally enriched or depleted in donor Sel1LcKO P14 compared to WT P14 cells at day 8 post LCMV. **(C)** Bar graph of gene expression changes KO/WT compromising Gene Ontology: Organellar Fission.

Since oxidative phosphorylation (OXPHOS) is known to play a critical role in $CD8^+$ T cell persistence and memory (26), we focused on determining if Sel1L regulates $CD8^+$ T cell metabolism. Previous work in brown adipocytes demonstrated that Sel1L deletion impaired mitochondrial oxidative phosphorylation by altering mitochondria morphology and accumulation (103). To interrogate the role of Sel1L in $CD8^+$ T cell metabolism, we profiled activated WT and Sel1LcKO P14 cells using extracellular flux analysis. Consistent with our RNA-Seq data, Sel1L loss impaired OXPHOS with decreased basal and maximal oxygen consumption rate (**Figure 3-11B**) compared to WT. Sel1L was also required to maintain spare respiratory capacity, also known as metabolic fitness, a measurement that reflects the reserved energy in cell to respond to stress. Importantly, spare respiratory capacity has been linked to the ability of $CD8^+$ T cells to persist long-term *in vivo* (26). In addition, activated Sel1LcKO P14 cells also had reduced glycolysis as measured by extracellular acidification rate (**Figure 3-11C**). To correlate theses finding *in vivo*, we examined WT and Sel1LcKO P14 cells directly *ex vivo* on day 8 p.i. using cationic dye tetramethylrhodamine methyl ester perchlorate (TMRM) to determine the relative mitochondrial membrane potential of the transferred cells. Reduced mitochondrial membrane potential suggest Sel1L-deficient P14 cells have reduced OXPHOS capacity while maintaining similar amounts of mitochondria as measured by Mitotracker green (**Figure 3-11D-E**). Overall, these results demonstrate that Sel1L is required for optimal $CD8^+$ T cell bioenergetic capacity.

Mitochondrial morphology is a critical regulator of a cell's capacity to undergo oxidative phosphorylation (71, 196). In $CD8^+$ T cells, mitochondrial fusion has been demonstrated as a key checkpoint promoting T cell persistence (63). We investigated the role of Sel1L in regulating mitochondrial morphology in T cells. In contrast to previous data in adipocytes, in which the loss of Sel1L resulted in increased mitochondrial fusion (103), confocal microscopy of *in vitro*

activated Sel1LcKO P14 revealed altered mitochondrial morphology with reduced mitochondrial volume, surface area, and length compared to WT (**Figure 3-13A**), consistent with increased mitochondrial fission. Mitochondrial fusion and fission is a tightly regulated process in association with mitochondrial-endoplasmic reticulum contact sites (MERCS) (73, 197). There was no apparent difference in expression of the mitochondrial morphology regulators Drp1 and Opa1 (**Figure 3-13B**) (63, 198, 199), thus we investigated MERCS formation. Super resolution microscopy for ER (KDEL) and mitochondria (TOM20) of WT and Se1lLcKO T_{ACT} cells revealed an increase in ER-associated mitochondria (**Figure 3-13C**), consistent with increased MERCS formation in the absence of Sel1L. Future investigation is required to elucidate the direct molecular mechanism by which Sel1L regulates mitochondrial morphology and MERCS formation and determine the extent to which these changes are required to maintain cellular metabolism.

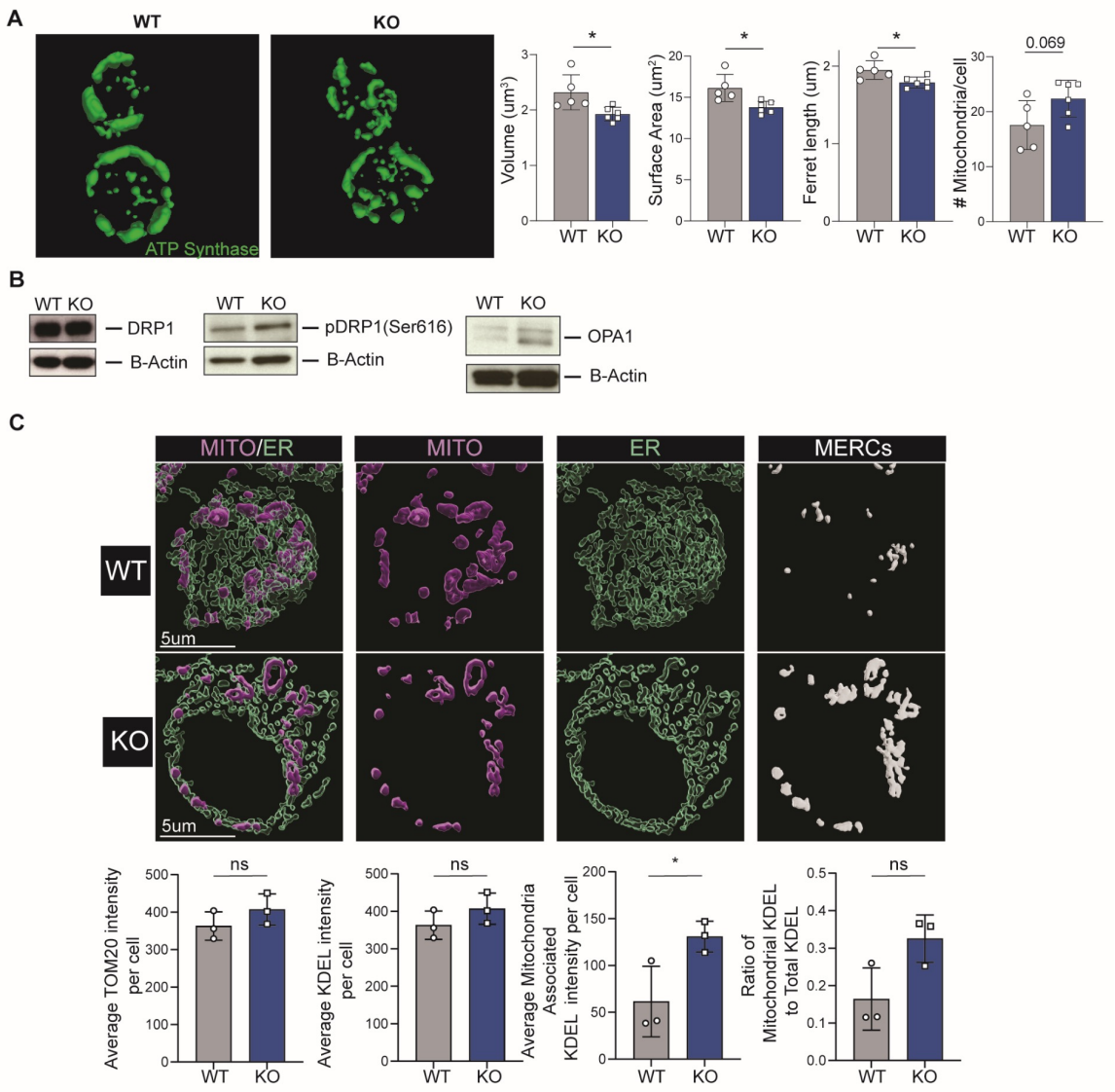

Figure 3-13: CD8⁺ T cell mitochondrial morphology is maintained in a Sel1L-dependent manner.

WT P14 and Sel1LcKO P14 splenocytes were activated *in vitro* with LCMV gp33-41 peptide in the presence of IL-2 for three days (T_{ACT}) and isolated CD8⁺ T cells were evaluated for protein expression or microscopic analysis. **(A)** *Left*, mitochondrial morphology in WT and Sel1LcKO T_{ACT}. Mitochondria stained with ATP synthase (ATP5b). *Right*, quantitative assessment of mitochondrial morphology volume, surface area ferret length and mitochondrial number per cell. **(B)** Representative Western blots of DRP1, phospho-DRP1 (pDRP1 Ser616) and OPA1 in WT and Sel1LcKO T_{ACT}. **(C)** *Top*, representative three-dimensional render of representative confocal fluorescence micrographs from WT and Sel1LcKO T_{ACT} subjected to immunofluorescence labeling of TOM20 (mitochondria) and KDEL (ER). Mitochondrial ER contact sites (MERCS) represent colocalized regions between mitochondria and ER. *Bottom*, quantification of TOM20 intensity, KDEL intensity, Mitochondria-associated KDEL, and Mitochondrial enrichment of KDEL. Data representative of n=5/genotype, 2 independent experiments (A), n>3/genotype 2-3 independent experiments (D), n=3/genotype, 1 independent experiment. ns $p>0.05$; * $p<0.05$; unpaired t-test (A-C)

Given the critical role of c-Myc in orchestrating T cell metabolism (56, 200), we also investigated if c-Myc expression was altered. Following activation with antigen, Sel1LcKO P14 cells expressed significantly less c-Myc protein compared to WT P14 cells (**Figure 3-11F**). Together these data suggest a possible mechanism by which Sel1L maintains sufficient T cell bioenergetics; however, further investigation will be needed to evaluate relative contributions of these findings.

3.3.8 ER stress in human T cells

Uncovering novel pathways regulating T cell persistence can provide valuable insight into the immunotherapy development and may increase the likelihood of therapeutic benefit for patients (201). After antigen clearance, a minority of T cells persist and acquire memory phenotype in both mice and humans (202). Memory T cell subsets have distinct capacities for protection against re-infection, severe disease, and therapeutic efficacy (203-205). Specifically, T stem-cell memory (T_{SCM}) cells are considered the least differentiated and contain the largest potential for memory response and generating effector progeny (206, 207). Central memory (T_{CM}), retain similar properties as T_{SCM} cells but contain reduced stem-like properties. Effector memory T (T_{EM}) cells behave more as committed progenitor cells, undergoing terminal differentiation after antigen re-encounter (208) and T_{EM} cells that re-express CD45RA (TEMRA) cells represent a subset that is most differentiated and has acquired full effector function. Finally, $PD1^+$ $CD39^+$ are putative exhausted T cells that could represent alternate differentiation lineage (209-211). We sought to determine if human $CD8^+$ T cell differentiation states were associated with enhancement of gene signatures corresponding to ER stress. Utilizing a published transcriptional dataset of human T cell subsets from healthy donors (135), we conducted gene set variation analysis and found that terms corresponding to ER stress increased with terminal T cell differentiation (**Figure 14A**).

Given our findings demonstrating that murine T cell activation resulted in induction of ER stress pathways, we asked if human $CD8^+$ T cells underwent a similar process. Indeed, reanalysis of proteomic data of resting and activated human $CD8^+$ T cell subsets (130) reveals a significant upregulation of proteostatic proteins protein disulfide isomerase (PDIA6), PKR-like ER kinase (PERK), ER stress induced chaperone BiP and ER oxidoreductase-1-like (ERO1L) across all subsets after activation (**Figure 14B**). Interestingly, Sel1L RNA expressions was only increased in TEMRA cells relative to naïve (**Figure 15A**). While Sel1L protein levels were stable across resting subsets, T cell activation increased expression of Sel1L protein (**Figure 15B**). Previous work in other cell types has shown that ERAD gene expression is induced by XBP1 activity (84, 212, 213), surprisingly there is only a subset-specific correlation of Sel1L expression with XBP1 in human T cells suggesting the possibility that other transcription factors may control Sel1L expression in T cells (**Figure 15C**). Next, we sought to corroborate that T cell activation resulted in the accumulation of misfolded protein. Activation of $CD8^+$ T cells from healthy human donors revealed that activated $CD8^+$ T cells accumulate misfolded protein relative to resting, unstimulated cells (**Figure 14C**). Additionally, activated $CD8^+$ T cells upregulated ER stress marker XBP1s relative to rested cells (**Figure 14C**).

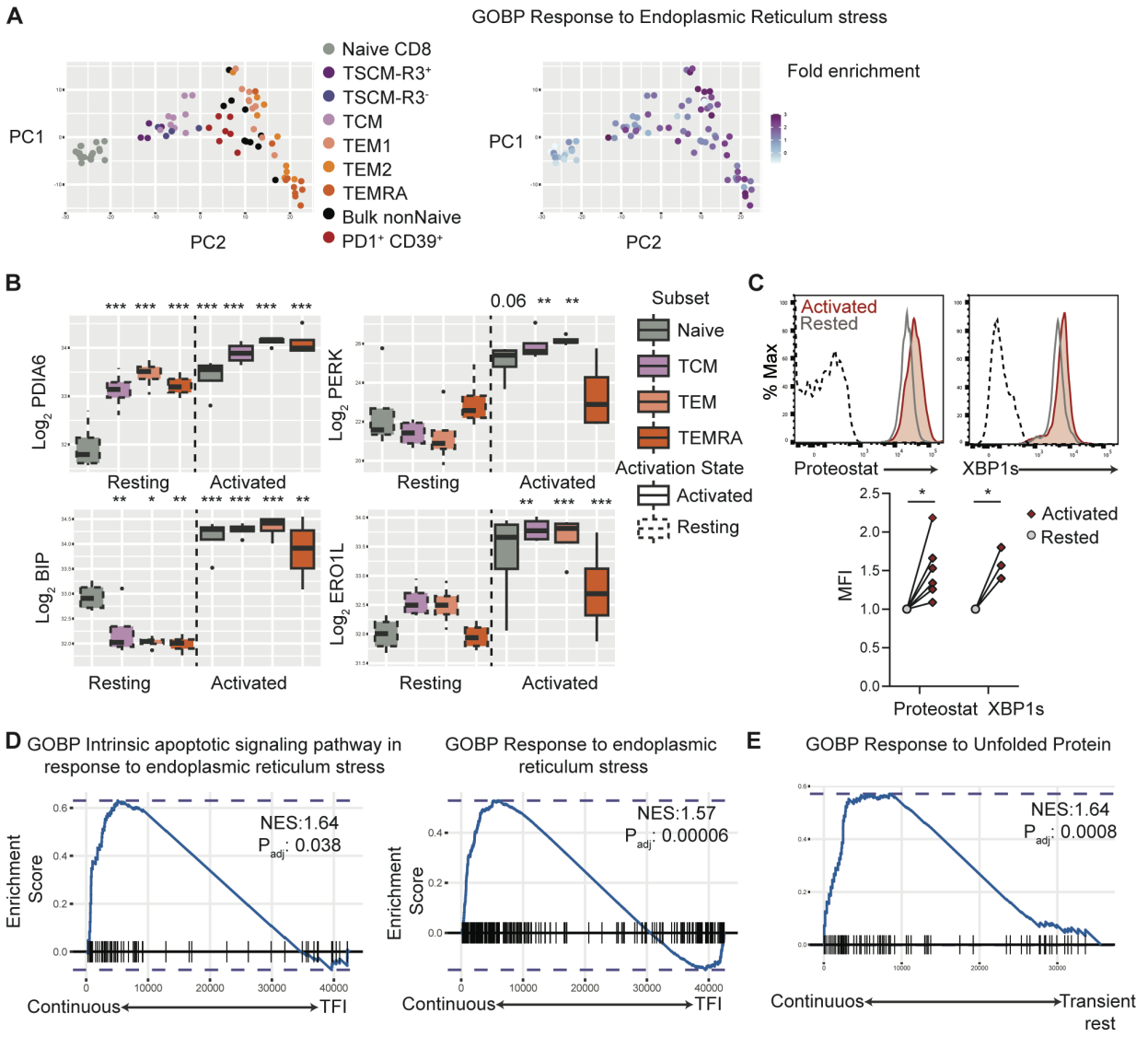

Figure 3-14: Human CD8⁺ T cells experience of endoplasmic reticulum stress is associated with terminal differentiation and reduced persistence.

(A) *Left*, Primary component analysis (PCA) of human CD8⁺ T cell transcriptomes from peripheral blood of healthy donors from GSE179613. *Right*, PCA from left colored by fold enrichment of genetic signature (GSVA) "GOBP Response to Endoplasmic Reticulum stress" relative to naïve cells. **(B)** Log2 intensity of representative ER stress markers PDIA6, PERK, BIP, and ERO1L in indicated subset and activation state from human CD8⁺ T cell proteomes from PXD004352. **(C)** Representative flow cytometry histograms (*top*) of Proteostat and XBP1s MFI *(bottom)* of Proteostat and XBP1s in CD8⁺ CD3⁺ cells from healthy human donors 3 days after activation with CD3/CD28 dynabeads + IL2 or rested in IL-7. **(D)** Leading edge plots of GSEA of human T cells undergoing continuously stimulation from bispecific CD3xCD19 (AMG 562) T cells versus cells that experienced a treatment free interval (TFI) at day 15 from GSE196463. **(E)** Leading edge plots of GSEA of continuously stimulated GD2 CAR-T cells versus transiently rested cells at day 15 from GSE164950. n=7-11/subset (A), n=4/subset (B), n = 6 Proteostat, n = 3 XBP1s (C). 2-3 independent experiments. n = 3/group (D), n= 3/group. ns p>0.05, *p<0.05, **p<0.01, ***p<0.001, ****p<0.0001, unpaired t-test (B), paired t-test (C).

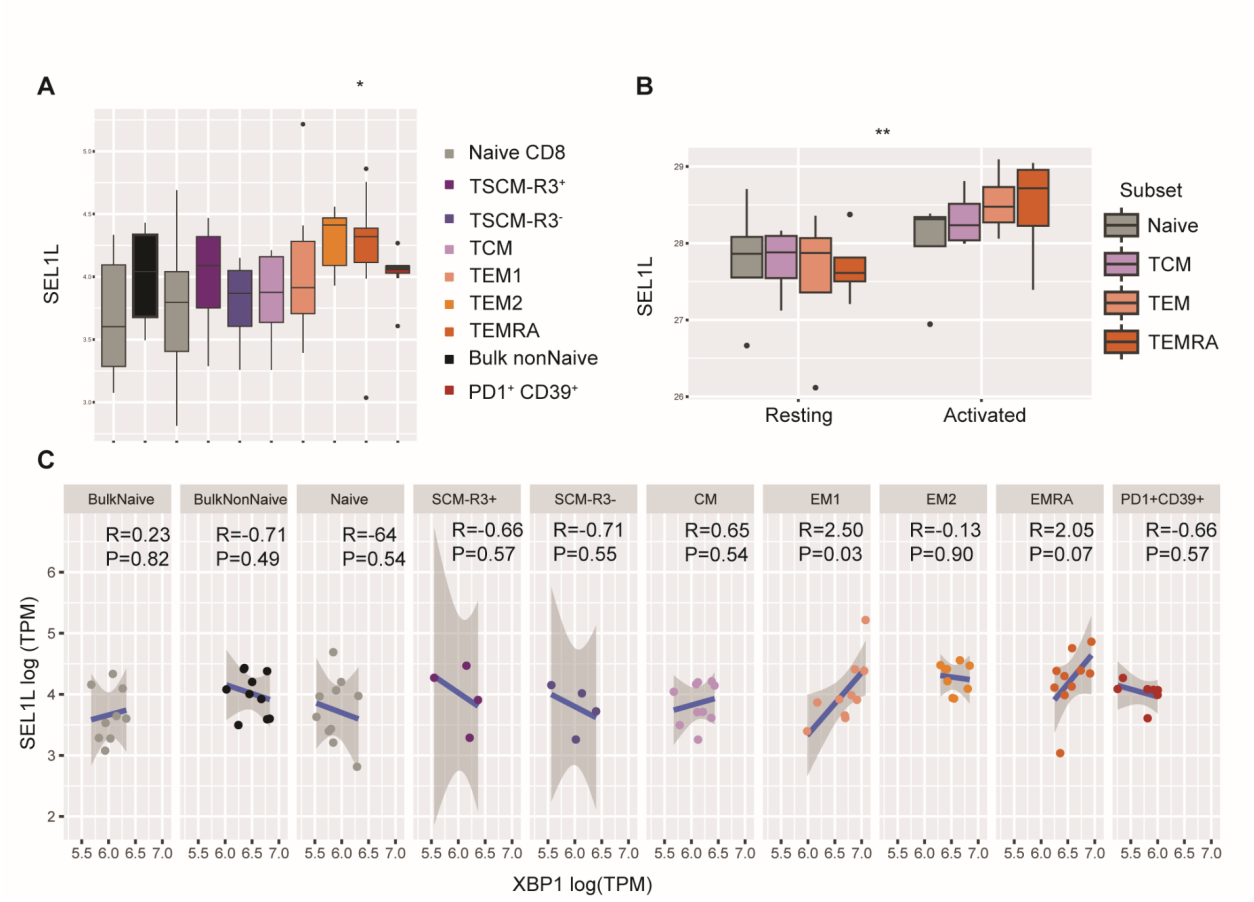

Figure 3-15: Sel1L expression in human CD8$^+$ T cells.

(A) Normalized counts of Sel1L from corresponding transcriptomes of human CD8$^+$ T cells subsets from GSE179613. **(B)** Log2 intensity of Sel1L protein from corresponding human CD8$^+$ T cell subsets from PXD004352. **(C)** Correlation of XBP1 and Sel1L normalized counts per human CD8$^+$ T cell subset from GSE179613.

To investigate the role of ER stress in T cell-based immunotherapies, we examined the relationship of ER stress pathways and T cell fitness in this setting. In the last decade, bispecific antibodies and chimeric antigen receptor T (CAR-T) cell therapy have been approved to treat and potentially cure relapsed/refractory B cell malignancies (214, 215). However, lack of persistence and T cell exhaustion remain roadblocks to optimizing clinical responses for more patients. Bispecific antibodies contain two antibody variable regions, one that includes anti-CD3, tethered by a linker to a tumor-specific antigen, such as anti-CD19. In a study identifying mechanisms of exhaustion in T cells responding to the anti-CD3 x anti-CD19 therapy AMG562 (141), the authors

find that treatment free intervals (TFI) ameliorate T cell exhaustion and improves T cell persistence, cytotoxic function, and metabolic profile compared to continuous exposure to AMG562. Reanalysis of transcriptomic data of the responding T cells demonstrated that continuous stimulation resulted in enhanced ER stress compared to cells that experienced TFIs (**Figure 14D**). In a separate data set, CAR-T cells were found to have improved functionality after undergoing rest from CAR stimulation (136). We posited that reversal of ER stress could be associated with improved CAR-T cell function; indeed we find that CAR-T cell reinvigoration was associated with reversal of transcriptional signatures corresponding to "Response to Unfolded Protein" (**Figure 14E**). Together these data demonstrate that ER stress is induced during human T cell activation and is associated with terminal differentiation, while the reversal of ER stress is associated with improved T cell persistence and function in two T cell-based immunotherapeutic modalities. Future studies are needed to determine causality and elucidate whether modulating ER stress could be sufficient to improve T cell persistence and function in therapeutic settings.

3.4 Discussion

Understanding fundamental molecular pathways that regulate $CD8^+$ T cell function and fate are critical to improving T cell-mediated responses to viral infections and cancer, as well as identifying novel targets to improve immunotherapies. $CD8^+$ T cell proteome remodeling is known to be dynamically regulated following acute viral infection, with significant amounts of new protein synthesis occurring; however, the experience of ER stress nor the cell-intrinsic role of Sel1L/ERAD play in $CD8^+$ T cell fate following viral infection have not been explored. Herein we demonstrate that viral-specific murine $CD8^+$ T cells experience transient ER stress during acute viral infection and identify Sel1L/ERAD as necessary for effector function, optimal metabolism, and $CD8^+$ T cell persistence after viral infection. Furthermore, we find that primary human $CD8^+$

T cells experience ER stress following activation and that ER stress is negatively associated with function and persistence in T cell-based immunotherapies.

Thus far, studies of ER stress pathways in T cells have focused primarily on the role of the UPR pathway. Acute bacterial and viral infection were shown to activate the IRE1/XBP1 pathway in $CD8^+$ T cells *in vivo* with overexpression of XBP1s promoting terminally differentiated $KLRG1^+$ cells (86). Both XBP1s and CHOP have been found to have detrimental roles in $CD8^+$ T cell persistence in tumor models suggesting that signals derived from ER stress limit T cell persistence (87, 89). Protein misfolding and ER stress were not directly studied. It is also apparent that, in situations of chronic misfolded protein, enzymes responsible for clearing misfolded protein can have detrimental effects for cell survival as evidenced by chemical inhibition of endoplasmic reticulum oxidoreductase 1 alpha (ERO1a) and protein disulfide isomerase (PDI), an ER chaperone that that promotes protein folding and stability (216), in murine T cells enhances cell survival even in settings of chronic ER stress (93, 94). However, orthogonal genetic studies are required to ensure the validity of these findings as inhibitors of these enzymes have low selectivity and potential of target effects.(217) The role of proteostatic enzymes and their maladaptation seems to be context-dependent as Fernandez-Alfara et al. (218) elegantly demonstrate that that loss of CPEB4, an enzyme required for ER stress adaptation, lead to exacerbated UPR activation and limited T cell persistence and function.

The ERAD pathway mediates the clearance of misfolded protein. In various cell types, including hematopoietic stem cells and $CD4^+$ T cells, ERAD has been shown to be required for cellular homeostasis (105, 107, 147, 162-167) with the ERAD adaptor Sel1L is ubiquitously expressed across various tissues.(103, 105-107, 147, 162-168, 171, 183) ERAD loss has cell- and stage-specific implications for cellular function and/or survival (101), as well as cell-specific

targets (102). In T cells, deletion of the ERAD ubiquitin ligase Hrd1 in mature conventional T cells mediated by CD4Cre deletion results in severe lymphopenia with loss of both $CD4^+$ and $CD8^+$ T cells (219). We and others have reported similar findings utilizing CD4cre-mediated deletion of Sel1L during homeostasis (171, 172). In contrast, Hrd1 deletion in only $CD4^+$ regulatory T cells (Tregs) induced ER stress that limited their stability and immunosuppressive function without impairing survival (170). In this study, we find that Sel1L protein expression is induced in primary murine $CD8^+$ T cells after TCR-mediated activation *in vitro* and *in vivo*. This upregulation coincides with an increase in ER stress indicators *in vitro* such as K48-ubiquitin and protein aggresome formation, as well as upregulation of the UPR factors ATF4 and XBP1s. These data suggest that T cell activation results in ER stress requiring the upregulation of Sel1L along with UPR pathways to maintain ER homeostasis.

Limited persistence of $CD8^+$ T cells is intrinsically correlated with the reduced capacity to perform oxidative metabolism (26, 63, 66, 220). We demonstrate that Sel1L is required for activated $CD8^+$ T cells to maintain OXPHOS. Several other pathways involved in relieving ER stress have been implicated in OXPHOS regulation in T cells. For instance, proteasomal inhibition results in reduced OXPHOS, while attenuated UPR signaling through loss of transcriptional effectors XBP1 or PERK, restores OXPHOS in T cells (82, 88, 93). Together these results suggest disrupted ER homeostasis as a possible mechanism for maintaining OXPHOS in T cells, though no unifying molecular mechanisms has been identified.

It is well established that mitochondrial dynamics are critical for oxidative metabolism (63, 64, 71, 72). Our data show that Sel1L loss alters mitochondrial morphology leading to an increase in smaller (ie, more fissed) mitochondria and increased MERCS formation. Multiple lines of evidence link chronic ER stress to mitochondrial fission and increased mitochondrial-ER contacts

(73, 221). Though we did not identify protein expression differences in the mitochondrial morphology regulators phospho/total Drp1, or Opa1, intriguingly we did note an increase in MERCS formation in the setting of Sel1L loss. ER tubules have been shown to mediate mitochondrial fission through physical constriction of mitochondrial membranes (222) raising an intriguing possibly if increased MERCS formation is responsible for the mitochondrial fission noted. However, MERCS also serve a wide variety of other cellular functions, including calcium homeostasis and lipid exchange (73, 76, 197). Mitochondrial-ER interplay has been increasingly recognized to play key roles in T cell fate and function (75-77). Thus additional work to define exactly how ERAD regulates MERCS formation and immunometabolic functions will critical to understand how ER homeostasis pathways regulate T cell metabolism.

In our studies, we also noted c-Myc expression was significantly lower in the setting of Sel1L deficiency. c-Myc is essential for T cell metabolism after activation (56, 200, 223) and promotes $CD8^+$ T cell persistence (224, 225). In T cells, TCR signaling is known to regulate Myc transcription and c-Myc protein levels (200, 226, 227), while IL-2 signaling is required to maintain c-Myc protein levels (200). Given that CD25 expression (the high-affinity IL-2 receptor) was significantly reduced in Sel1-deficient P14 cells on day 5 p.i. *in vivo*, these observations suggest a possible model whereby Sel1L/ERAD maintains CD25 and c-Myc expression to support the bioenergetic demands of T persistence.

In human $CD8^+$ T cells, we demonstrate that they experience ER stress following TCR-mediated activation, as evidenced by increased protein aggresomes and XBP1s expression. Furthermore, bioinformatic analyses of healthy human donor transcriptomes and proteomes correlate ER stress and UPR activation with terminal differentiation and activation. In recent years, T cell-redirecting immunotherapies, such as CAR-T and bispecific antibodies, are revolutionizing

therapies for patients with relapsed/refractory multiple myeloma, B-cell lymphomas and leukemias (214, 228, 229) and may provide an effective therapy for some autoimmune diseases (230). In murine models of adoptive cellular therapy for solid tumors, mitigating ER stress in T cells improves anti-tumor responses (87-89, 94). Given that exhaustion and lack of persistence is one of the major hurdles needed to further improve T cell-redirecting therapies (231), we posited that ER stress may play a role in limiting efficacy of these therapeutic T cells targeted to hematologic malignancies. Analysis of two publicly available datasets examining approaches to improve CAR-T and bispecific antibody function and persistence found an association between downregulated ER stress pathways and improved persistence/function. These data raise the possibility that ER stress may limit the persistence and/or function of therapeutic T cells; however, this observation could be a correlative rather than causative. Mechanistic studies are needed to delineate the role ER stress plays in limiting T cell-redirecting therapies and if therapeutically alleviating ER stress can improve clinical outcomes.

Maintenance of ER homeostasis is a shared biological necessity across cell types but the outcomes of ER stress responses vary widely by cell-type and biological context. Collectively, our data identify Sel1L/ERAD as an important regulator of $CD8^+$ T cell function and persistence following acute viral infection and highlight the interplay of Sel1L/ERAD and metabolism in maintaining T cell immunity. Future studies are needed to determine if ERAD and other ER stress pathways are targetable pathways to modulate T cell immunity and improve T cell-based immunotherapies.

3.4.1 Limitations of study:

While we identified that Sel1L/ERAD was required for optimal cellular metabolism, it remains unclear the exact molecular mechanism that underlies this bioenergetic insufficiency. We

noted several dysregulated pathways including altered mitochondrial dynamics, altered MERCs and lower c-Myc expression. How Sel1L/ERAD loss directly or indirectly contributes to these findings and the extent to which each contributes to loss of optimal metabolism remains unclear.

Additional limitations are that we noted a fraction of Sel1LcKO cells undergo Cre escape *in vivo* following acute viral infection. This heterogeneity may have led to less significant *in vivo* results than if we had used a Cre reporter system as we were measuring bulk population marked by tetramer positivity or peptide reactivity for the *in vivo* experiments.

Additionally, our bioinformatic analysis of re-directed human T cells, while intriguing and informative, is limited by the intrinsic correlative nature of such analyses. It is possible that the increased ER stress signatures noted are a result of the repeated antigen receptor stimulation and do not play a causal role in T cell exhaustion or function in T cell immunotherapies.

Chapter 4 – Discussion

4.1 Summary of results:

At the start of this thesis research, we had the objective of uncovering the status of protein homeostasis through $CD8^+$ T cell differentiation. This included the characterization of pathways responsible for maintaining protein homeostasis. Data discussed in this dissertation illuminates protein homeostasis under normal T cell differentiation and how dysfunction in processes contributing to homeostasis are sufficient to drive T cell dysfunction. In chapter 3, it is demonstrated that protein homeostasis is transiently perturbed under normal differentiation. While other studies had shown a detrimental role for transcription factors of the unfolded protein response in tumors, no study had implicated these factors as being transiently induced under "normal" acute conditions. Additionally, we characterize the necessity of Sel1L/ERAD in T cell persistence and function during acute viral infection. Sel1L/ERAD ensure adequate T cell metabolism though various mechanism are possible, MERCS and c-MYC, and likely work in consort (**Figure 4-1**).

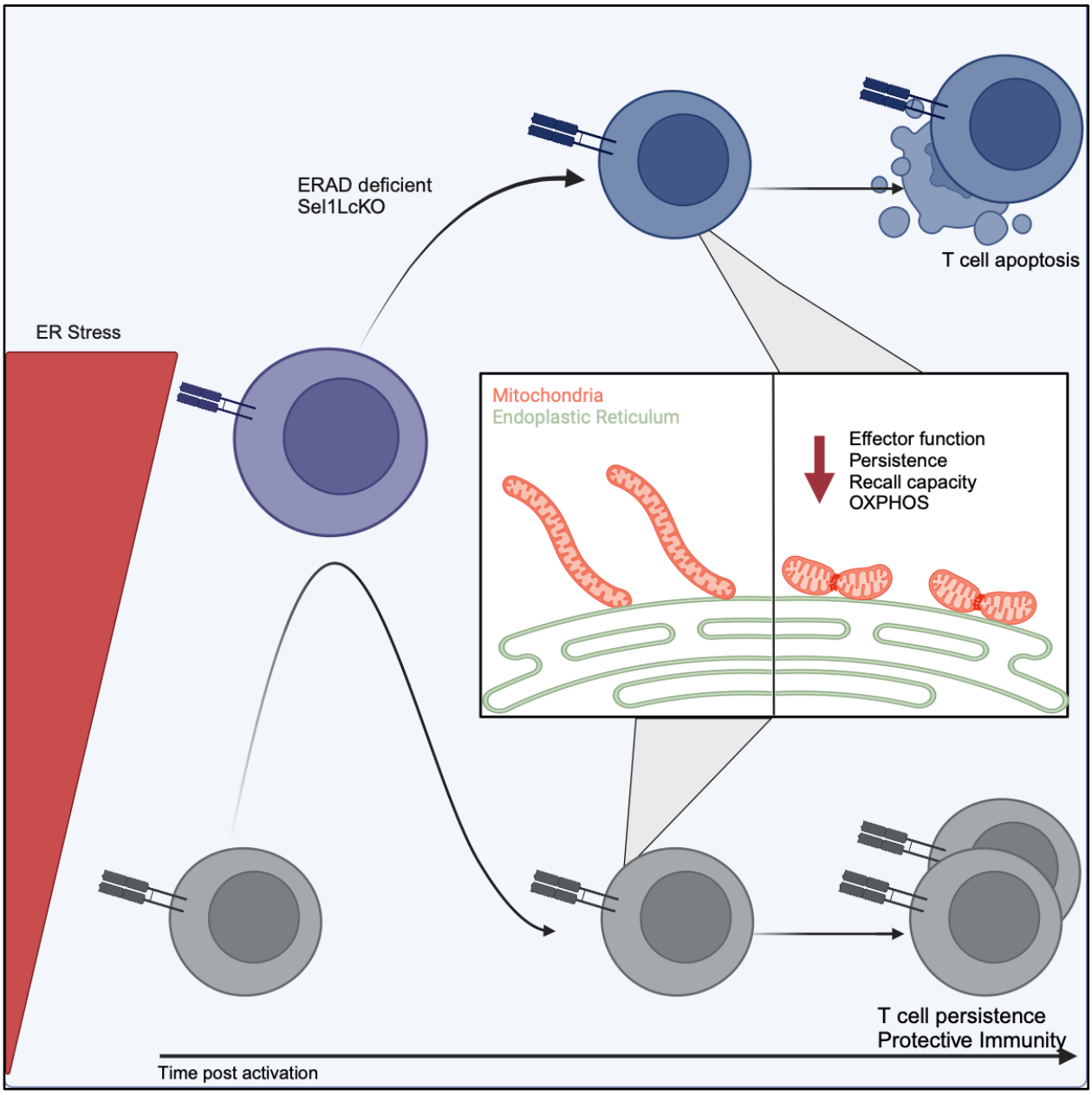

Figure 4-1: Summary diagram of results presented in chapter 3.

The diagram depicts a T cell after activation. As it goes through expansion, it experiences ER stress. After antigen clearance, the T cell returns to naïve-like ER stress levels associated with the formation of elongated mitochondrial networks. The top of the graph shows the fate of ERAD-deficient Sel1LcKO, who fail to adopt the metabolic programs and mitochondrial morphology associated with memory formation and primarily die by apoptosis. Inset highlights deficiencies of Sel1LcKO $CD8^+$ T cell while portraying increased contact between the mitochondria and ER.

4.2 Discussion: Mechanism of Sel1L-mediated regulation of T cell mitochondrial metabolism: Unanswered questions

A question brought on by the investigation conducted in chapter 3 concerns the mechanisms by which Sel1L regulates mitochondrial metabolism. In chapter one, it had been discussed how Sel1L regulates mitochondrial metabolism through distinct mechanisms in hepatocytes and brown adipose tissue. The mechanism of mitochondria dysfunction in brown adipocytes was driven by altered ER mitochondrial contacts mediated through SigmaR1 while hepatocytes had altered redox balance measured in part by dyes CellRox and Mitosox. $CD8^+$ T cells lacking Sel1L, neither displayed altered SigmaR1expression nor redox balance as measured by flow cytometric dyes CellRox and Mitosox. Towards addressing the potential mechanism, Sel1LcKO-P14 cells were differentiated in glucose-containing or galactose-containing media. Galactose-containing media drives T cells into a metabolic circuit that relies on glutamine-mediated OXPHOS (62, 220). Interestingly, Sel1LcKO-P14 cells did not succumb under these conditions suggesting that OXPHOS, at least in terms required for cell survival, was engaged adequately (data not shown). Though additional studies are required to corroborate these findings, the data suggest that the metabolic deficiency observed in Sel1LcKO-P14 is perhaps limited to an inability to metabolize glucose and contribute to OXPHOS rather than OXPHOS itself. Metabolic flux analysis could be conducted to catalog the fate of glucose and its relative utilization in Sel1LcKO-P14.

Mitochondrial dysfunction in the absence of Sel1L/ERAD is also associated with dysregulated mitochondrial ER contacts (103). Briefly, the ER and mitochondria become physically associated and exchange metabolites, signaling molecules and even enzymes (see Wu et al. (232)) Evaluation of these contacts has been difficult as they are primarily observable by

microscopy, a technique that is not as easily amenable to heterogenous populations nor scarce cell number like $CD8^+$ T cells.

Recently several groups have begun characterizing Mitochondrial Endoplasmic Reticulum Contact Sites (MERCS) in T cell biology. Supplementation of T cells with lineoleic acid was found to enhances OXPHOS and was associated with the formation of MERCS, while reshaping the lipid landscape of the T cells (76). Relative to naïve cells, memory T cells form more MERCS and appear to be required for the enhanced recall response carried out by memory cells (73, 75). GRP75, a prototypical factor regulating the anchoring of ER and mitochondria was found to be required for enhanced metabolic capacity of memory cells and the maintenance of ER-mito contacts (75). In $CD8^+$ T cells responding to tumors, it was found that mitofusion2, a protein known to regulate fusion of mitochondria was required for ER-mito contacts and that loss of these contacts limited T cell function (77). Mechanistically, it was found that Mfn2-mediated formation of MERCS assisted in alleviating ER calcium load by recruiting SERCA2 calcium channel to pump calcium ions out of the mitochondria. Bantug et al. (75) find that MERCs serve as a scaffold for Mtorc2 to relive AKT inhibition of GSK3B. Elevated GSK3B is then associated with enhanced metabolism by driving glucose import into mitochondria through stabilized glucose importer HK-I. Taken together these findings demonstrate a dynamic role for the MERCS in supplying and removing metabolites from the mitochondria while acting as signaling hubs in T cells. Our results as presented in chapter 3, where we see an increase in MERCS being associated with reduced metabolism, suggest that over-accumulation MERCS could be detrimental in T cell metabolism. In the future, it would be of a benefit to understand the kinetics of MERCS formation as well as the composition of MERCS throughout T cell differentiation. How Sel1L interfaces within MERCS is an open question. Given its role Sel1L, would not be hypothesized to localize with

MERCS but it is a study we did not yet undertake. Furthermore, Sel1L's role could lie in the regulation of protein associated with MERCS or disruption of cellular process that then limit MERCS accumulation. Two likely mechanisms can be investigated building off the previous work characterizing MERCS as signaling hubs and sites of metabolite transfer. First, given that MERCS are signaling hubs, that GSK3B localizes to them and that cMyc a target of GSK3B is lost in Sel1LcKO, I would hypothesize that MERCS enhance the degradation of c-Myc by promoting the activity of GSK3B. Second, given that MERCS mediate the transfer of key metabolites such as calcium, I would hypothesize that the mitochondria in the absence of Sel1L is being drained of key metabolites such as calcium.

4.3 Role of protein homeostasis in memory T cell recall responses

As part of our investigation in chapter 3, we conducted experiments transferring memory T cells lacking Sel1L/ERAD and found them unable to confer protective immunity. The data however are complicated by the use of Sel1LcKO mice who experience severe lymphopenia, possibly impacting the development of the memory T cells. A possible objective of future investigation would be to identify pathways contributing to memory T cell responses. I would hypothesize that upregulation of proteostatic pathways underlie superior recall responses by memory T cells and their progeny. It is well known that the effector progeny of memory cells is greater in magnitude and can persist to a greater degree after infection (233). Enhanced bioenergetics has been characterized as a mechanism underlying recall capacity of memory T cells (65). Given our work demonstrating that $CD8^+$ T cells experience ER stress during activation, examining proteostatic pathways and ER homeostasis in comparison to primary responding cells would give significant insight into capacity of these cells types. To adequately study the role of Sel1L/ERAD in recall responses, the tamoxifen inducible cre recombinase

under the control of estrogen receptor promoter can be employed to temporally delete Sel1L/ERAD and follow the homeostasis of memory cells. Additionally, deletion before infection could allow for the investigation into the role of proteostatic pathways in mediating the superior recall capacity of memory T cells.

4.4 Potential directions for elucidating proteostatic control of T cell fate:

Our data convincingly demonstrate the role of Sel1L/ERAD in regulating $CD8^+$ T cell persistence, and our study of Sel1LcKO-P14 $CD8^+$ T cells has revealed interesting stage-specific, effector but not naïve stage, regulation of T cell memory. It is thus apparent that unbiased screens would help shape our understanding of factors regulating protein homeostasis in T cells. Pooled CRISPR screens, a method that allows for the deletion of individual genes in individual cells in a pooled matter coupled with flow cytometric readouts of protein aggregates, misfolded protein, or UPR activation, could help decipher the pathways regulating proteostasis (234). We had observed that naïve T cells but not D3 T_{ACT} experience apoptosis after exposure to ER stress inducers. One could couple this phenomenon to uncover genes and processes that afford resistance to ER stress induced apoptosis. Care must be taken to ascertain ER stress induced apoptosis rather than general resistance to apoptosis.

In data from Chapter 3, it was observed that *in vitro* differentiated IL-2 T_E and IL-15 T_M have distinct proteostasis capacities, with IL-15 T_M having fewer protein aggregates and reduced activation of the UPR. These data suggest that cytokines can impact and regulate protein homeostasis, but careful study is required as these cytokines can impact proliferation and rates of protein translation. Furthermore, during immune responses, inflammatory cytokines such as TNFα, interferons and IL-6 and "anti-inflammatory" cytokines such as IL-10 and TGFB act on

the T cell to regulate fate and function. How these and other cytokines contribute to proteostasis and, thus, cell fate are unknown and serve as interesting areas of exploration.

One of the more significant remaining questions is whether the specific degradation of some factor by Sel1L/ERAD accounts for the role of Sel1L/ERAD in T cells or if the role of Sel1L/ERAD lies simply in dealing with misfolded protein. Towards answering these questions, conducting unbiased proteomics will identify the differential abundance of proteins in T cells lacking Sel1L versus WT. Additionally, the laboratory is actively engaging in the assessment of other proteostatic mechanisms in Sel1LcKO T cells to determine if they are hyperactivated and lead to the observed phenotypes. Finally, an alternative hypothesis is that from the perspective of protein homeostasis, T cells are resilient to loss of Sel1L/ERAD but cannot compensate for its role in metabolism. Data in chapter 3 demonstrate that Sel1L is required to maintain c-Myc expression in T cells. As discussed in chapter 1, it is well appreciated that c-Myc is necessary for T cell activation and survival. Proteasomal degradation, constitutes the major mode of c-Myc regulation. If the mechanism by which Sel1L regulates c-Myc occurs in the absence of other proteostatic pathways (i.e., proteasome from Sel1LKO is not hyperactivated and degrading c-Myc), the latter hypothesis would remain supported.

4.5 Future direction: Protein homeostasis during chronic antigen stimulation

Data from this thesis illuminate T cell differentiation as being associated with the experience of transient proteostatic stress and misfolded protein accumulation. Increased protein synthesis through T cell differentiation is closely associated with the experience of ER stress based on our data. We lacked the timing to address the role of chronic stimulation and the effects of inflammatory cytokines on ER homeostasis.

A strain of LCMV, Clone 13 (C13), has the unique property of inducting a chronic viral infection, where the virus persists indefinitely in the host (235). In the C13 experimental system, antigen specific $CD8^+$ T cells acquire a state of hyporesponsiveness and fail to form memory cells. The hyporesponsive state is acquired early on. Evidence of altered phenotype and functionality are noted as early as day 8 post infection (p.i.). In our work, we demonstrate that, *in vivo*, the experience of ER stress is experienced by the T cells responding to antigen. Given this paradigm, where ER stress and the mechanism of alleviating it are tied to TCR signaling, it is of interest to investigate proteostatic pathways in T cells in an environment where they are being chronically stimulated.

Data from other groups demonstrates that $CD8^+$ T cells at day 8 p.i. of LCMV-C13 infection have the highest levels of protein synthesis rates relative to acute counterparts (135). Reanalysis of bulk RNA-seq and single cell RNA-seq from these timepoints could be useful in assessing the activation of the unfolded protein in the antigen-specific response from the chronic infection relative to that of the acute response. It has been extensively reported that transcription factors of the UPR could drive the exhaustion of T cells (86-89). Transcriptional studies of exhausted T cells responding to tumors and chronic viral infection have shown that there are similarities (236). Interestingly, isolation of tumor infiltrating lymphocytes (TILs) from B16-F10 melanoma model revealed that TILs have significant accumulation of protein aggregates 10-fold relative to naïve cells measured utilizing PROTEOSTAT dye (data not shown). In our studies in the acute viral infection setting, effector cells on day 5 p.i. encountered only a two-fold increase. Future head-to-head studies are needed to adequately assess this comparison. Within the TILs however, we did observe an increase in misfolded protein aggregates in more terminally differentiated subset ($TIM3^{hi}$ $CD44^+$) cells relative to progenitor like cells ($TIM3^{low}$ $CD44^+$) cells suggesting that accumulation of misfolded protein is associated with terminal differentiation (data not shown). Future mechanistic studies would be needed to address whether this increase is driving terminal differentiation. Characterization of ER stress in these cells is needed to clarify the discordant data where we observed reduced transcriptional signatures of UPR in the exhausted cells (data not shown) but see significant amounts of PROTEOSTAT. Given previous work demonstrating increased activity of UPR factors (87-89),

it is possible that post-transcriptional regulation of UPR is at play. Our previous data demonstrated that TCR stimulation drove the upregulation of the UPR/ERAD in the acute setting. One could hypothesize that the acquisition of a hyporesponsive state, like that of exhausted T cells, results in an inability to induce factors of the UPR/ERAD. Data presented in chapter 3, where TCR/IL2 promote upregulation of UPR/ERAD in acute setting supports the possible mechanism where hyporesponsiveness in chronic setting limits adaptive UPR/ERAD leading to the accumulation of misfolded protein and subsequent cell death.

4.6 Future Directions: Getting RIDD of memory T cells

I was interested in investigating the role of the UPR pathways in T cells that might differ from other cell types. IRE1 is one of the key branches of the UPR (83). Previous work has focused on the role of XBP1s, transcription factor induced by IRE1 in the role of coordinating T cell exhaustion programs (87). XBP1s is sufficient to drive the expression of inhibitory receptors in exhausted cells and its loss is associate with gaining T cell functionality (87). As an enzyme IRE1 has other activities that are understudied in T cell biology. Specifically, IRE1 is able to oligomerize and then mediate the degradation of several mRNAs to regulate cell fate and function (237). Degradation of RNAs is limited to those containing a motif CUGA as well as a corresponding secondary structure. The experience of ER stress causes oligomerization of IRE1 and the activation of its RNAase function. Though elegant studies have characterized the targets of Regulated IRE1a Dependent Decay (RIDD), they are limited to the transcriptome of the subject cell type (i.e embryonic kidney cells) which would miss transcripts restricted to immune cells. Thus I had the objective of identifying mechanism of IRE1 control of T cell fate. My hypothesis was that RIDD limits T cell memory through the degradation of RNAs necessary for memory formation.

To begin to probe the activity of RIDD in $CD8^+$ T cell differentiation I looked at the expression of canonical RIDD targets (fermt3, rnf213, irf7, dgat2) at day 5 and day 8 post

LCMV-Armstrong infection. All four were downregulated at day 5, timepoint which cells would be experiencing the highest levels of ER stress (data not shown). Le Thomas et al. (238) developed software that brought together algorithms in RNA motif finding and folding to identify IRE1 targets, gRIDD. I utilized the gRIDD software on transcripts found in $CD8^+$ T cells at day 8 of LCMV-Armstrong and observed several factors associated with T cell memory formation containing IRE1 motifs with predicted folding probabilities similar to that of XBP1 (data not shown). Together these data suggest that IRE1 RNAse function might be a critical regulator of T cell memory formation in addition to XBP1s. Given that T cells experiences transient ER stress the effects of IRE1 on memory potential are likely restricted to context of enhanced and persistent ER stress. A difficulty in undertaking this study would be the generation of a system that allows for the disruption of IRE RNAse while preserving XBP1s activity.

4.7 Modulation of ERAD and protein homeostasis as therapeutic strategy to improve T cell function

My thesis research has defined for the first time the dynamic ER stress that virus-specific $CD8^+$ T cells experience as they respond to an acute viral infection and identified Sel1L/ERAD as a novel regulator of $CD8^+$ T cell function and persistence. Several key questions remain to be addressed before targeting ER stress for therapeutic development.

Is ER stress, as naturally experienced during differentiation, detrimental to T cell responses? The work in this thesis and others (89, 93, 218) has established that T cells experience ER stress. To demonstrate ER stress's detrimental role, we have relied on genetic models lacking key proteostatic pathway possibly generating supraphysiologic alterations. This raises the question as to whether evolution has shaped the T cell response to be resilient to a threshold of ER stress

that is not naturally surpassed. It could also be that the loss of T cells resulting from excess ER stress impacts the pool of antigen-specific cells and then the memory T cell pool. To test these hypotheses, methods of alleviating ER stress in T cells must be devised. Overexpression of Sel1L has proven difficult in other cell types (239). Other strategies have focused on the systemic administration of chemical chaperones, which could have effects on T cell responses through other cell types; for example, XBP1, a product of the UPR, is required for dendritic cell development and differentiation (240). Systemic attenuation of ER stress is thus likely to limit T cell priming from dendritic cells, resulting in diminished response. A limitation of the presented work is thus an inability to demonstrate the sufficiency of alleviating ER stress to improve T cell functionality and persistence.

Are there contexts where T cells experience high levels of ER stress? Previous sections of the thesis highlight this possibility in the context of chronic stimulation. With advances in cellular engineering for therapeutic potential, T cells are routinely processed to be administered as living drugs. Through these engineering processes, cells are expanded and forced to express chimeric antigen receptors to drive their functionality by the use of lentiviral overexpression. It is well appreciated that the manufacturing process limits the viability and stem-like properties of the T cell (201, 241). Thus, one could hypothesize, based on our work, that ER stress resulting from T cell engineering limits viability and stemness, leading to limited production and/or therapeutic efficacy. Various agents approved by the FDA are known to act to reduce ER stress; these include 4-Phenylpyruvate (242) and bromocriptine (243), among others. The incorporation of these agents into manufacturing processes will require significant preclinical and clinical development. Thus, characterizing the ER stress response during therapeutic T cell engineering and manufacturing could allow for the improvement of these therapeutics.

4.8 Critical appraisal and concluding remarks

Though this work refers to ERAD as the processes mediated by Sel1L and its complexes, there exist other forms of ERAD independent of Sel1L. Delineating how other forms ERAD are orchestrated and their contribution to T cell biology will be important. Subsequently, improved systems for identifying alterations to protein homeostasis such as reagents for measuring misfolded protein are necessary. Current approaches such as PROTEOSTAT only detect misfolded protein aggregates, leaving out the nuances of misfolded protein. Additionally, our work tested necessity of the ERAD pathway, but due technical constraints it has been difficult to demonstrate the sufficiency of the pathway in orchestrating T cell fate. The phenomena of Cre escape though supporting the role of necessity for T cell persistence occluded mechanistic work by dampening the effect of Sel1L loss. In future experiments reporter systems for Cre deletion could be used to ensure recovery of pure populations and to best uncover biological pathways altered by loss of Sel1L in T cells.

Approaches to improving T cell functionality remain limited. Here, we utilized murine models of viral infection and *in vitro* and bioinformatic human T cell studies to investigate protein homeostasis, specifically ER stress in T cells. Our goals were to characterize proteostatic pathways in $CD8^+$ T cells and to determine the necessity of Sel1/ERAD in T cell fate. We hope that the continuation of this work will shed insights into how protein homeostasis can regulate T cell metabolism and possible approaches to improving T cell functionality. Upon re-analysis of public data sets of T cell responses, it was noted that ER stress and associated gene sets were often significant but underreported in the literature. It is likely that ER stress and associated pathways remained underreported due to a lack of literature supporting ER stress as a relevant pathway in T cell biology. This work could ignite further investigation into different pathways that regulate T

cell proteostasis and subsequent studies of intervention to modulate protein homeostasis and, subsequently, T cell fate.

Bibliography

1. Gonzalez JP, Emonet S, de Lamballerie X, and Charrel R. Arenaviruses. *Curr Top Microbiol Immunol.* 2007;315:253-88.
2. Riviere Y, Southern PJ, Ahmed R, and Oldstone MB. Biology of cloned cytotoxic T lymphocytes specific for lymphocytic choriomeningitis virus. V. Recognition is restricted to gene products encoded by the viral S RNA segment. *J Immunol.* 1986;136(1):304-7.
3. Oldstone MB, Whitton JL, Lewicki H, and Tishon A. Fine dissection of a nine amino acid glycoprotein epitope, a major determinant recognized by lymphocytic choriomeningitis virus-specific class I-restricted H-2Db cytotoxic T lymphocytes. *J Exp Med.* 1988;168(2):559-70.
4. Klavinskis LS, Whitton JL, Joly E, and Oldstone MB. Vaccination and protection from a lethal viral infection: identification, incorporation, and use of a cytotoxic T lymphocyte glycoprotein epitope. *Virology.* 1990;178(2):393-400.
5. Whitton JL, Southern PJ, and Oldstone MB. Analyses of the cytotoxic T lymphocyte responses to glycoprotein and nucleoprotein components of lymphocytic choriomeningitis virus. *Virology.* 1988;162(2):321-7.
6. Whitton JL, Tishon A, Lewicki H, Gebhard J, Cook T, Salvato M, et al. Molecular analyses of a five-amino-acid cytotoxic T-lymphocyte (CTL) epitope: an immunodominant region which induces nonreciprocal CTL cross-reactivity. *J Virol.* 1989;63(10):4303-10.
7. McHeyzer-Williams MG, and Davis MM. Antigen-specific development of primary and memory T cells in vivo. *Science.* 1995;268(5207):106-11.
8. Altman JD, Moss PA, Goulder PJ, Barouch DH, McHeyzer-Williams MG, Bell JI, et al. Phenotypic analysis of antigen-specific T lymphocytes. *Science.* 1996;274(5284):94-6.
9. Murali-Krishna K, Altman JD, Suresh M, Sourdive DJ, Zajac AJ, Miller JD, et al. Counting antigen-specific CD8 T cells: a reevaluation of bystander activation during viral infection. *Immunity.* 1998;8(2):177-87.
10. Blattman JN, Antia R, Sourdive DJ, Wang X, Kaech SM, Murali-Krishna K, et al. Estimating the precursor frequency of naive antigen-specific CD8 T cells. *J Exp Med.* 2002;195(5):657-64.
11. Chapman NM, Boothby MR, and Chi H. Metabolic coordination of T cell quiescence and activation. *Nat Rev Immunol.* 2020;20(1):55-70.
12. Kieper WC, Burghardt JT, and Surh CD. A role for TCR affinity in regulating naive T cell homeostasis. *J Immunol.* 2004;172(1):40-4.
13. Moses CT, Thorstenson KM, Jameson SC, and Khoruts A. Competition for self ligands restrains homeostatic proliferation of naive CD4 T cells. *Proc Natl Acad Sci U S A.* 2003;100(3):1185-90.
14. Chapman NM, and Chi H. Hallmarks of T-cell Exit from Quiescence. *Cancer Immunol Res.* 2018;6(5):502-8.

15. Berger M, Krebs P, Crozat K, Li X, Croker BA, Siggs OM, et al. An Slfn2 mutation causes lymphoid and myeloid immunodeficiency due to loss of immune cell quiescence. *Nat Immunol.* 2010;11(4):335-43.
16. Yang K, Neale G, Green DR, He W, and Chi H. The tumor suppressor Tsc1 enforces quiescence of naive T cells to promote immune homeostasis and function. *Nat Immunol.* 2011;12(9):888-97.
17. Wu Q, Liu Y, Chen C, Ikenoue T, Qiao Y, Li CS, et al. The tuberous sclerosis complex-mammalian target of rapamycin pathway maintains the quiescence and survival of naive T cells. *J Immunol.* 2011;187(3):1106-12.
18. Araki K, Morita M, Bederman AG, Konieczny BT, Kissick HT, Sonenberg N, and Ahmed R. Translation is actively regulated during the differentiation of CD8(+) effector T cells. *Nat Immunol.* 2017;18(9):1046-57.
19. Wolf T, Jin W, Zoppi G, Vogel IA, Akhmedov M, Bleck CKE, et al. Dynamics in protein translation sustaining T cell preparedness. *Nat Immunol.* 2020;21(8):927-37.
20. Howden AJM, Hukelmann JL, Brenes A, Spinelli L, Sinclair LV, Lamond AI, and Cantrell DA. Quantitative analysis of T cell proteomes and environmental sensors during T cell differentiation. *Nat Immunol.* 2019;20(11):1542-54.
21. Damasio MP, Marchingo JM, Spinelli L, Hukelmann JL, Cantrell DA, and Howden AJM. Extracellular signal-regulated kinase (ERK) pathway control of CD8+ T cell differentiation. *Biochem J.* 2021;478(1):79-98.
22. Marchingo JM, Sinclair LV, Howden AJ, and Cantrell DA. Quantitative analysis of how Myc controls T cell proteomes and metabolic pathways during T cell activation. *Elife.* 2020;9.
23. Ron-Harel N, Santos D, Ghergurovich JM, Sage PT, Reddy A, Lovitch SB, et al. Mitochondrial Biogenesis and Proteome Remodeling Promote One-Carbon Metabolism for T Cell Activation. *Cell Metab.* 2016;24(1):104-17.
24. Tan H, Yang K, Li Y, Shaw TI, Wang Y, Blanco DB, et al. Integrative Proteomics and Phosphoproteomics Profiling Reveals Dynamic Signaling Networks and Bioenergetics Pathways Underlying T Cell Activation. *Immunity.* 2017;46(3):488-503.
25. Ma EH, Verway MJ, Johnson RM, Roy DG, Steadman M, Hayes S, et al. Metabolic Profiling Using Stable Isotope Tracing Reveals Distinct Patterns of Glucose Utilization by Physiologically Activated CD8(+) T Cells. *Immunity.* 2019;51(5):856-70 e5.
26. van der Windt GJ, Everts B, Chang CH, Curtis JD, Freitas TC, Amiel E, et al. Mitochondrial respiratory capacity is a critical regulator of CD8+ T cell memory development. *Immunity.* 2012;36(1):68-78.
27. Kalia V, Penny LA, Yuzefpolskiy Y, Baumann FM, and Sarkar S. Quiescence of Memory CD8(+) T Cells Is Mediated by Regulatory T Cells through Inhibitory Receptor CTLA-4. *Immunity.* 2015;42(6):1116-29.
28. Sarkar S, Kalia V, Haining WN, Konieczny BT, Subramaniam S, and Ahmed R. Functional and genomic profiling of effector CD8 T cell subsets with distinct memory fates. *J Exp Med.* 2008;205(3):625-40.
29. Joshi NS, Cui W, Chandele A, Lee HK, Urso DR, Hagman J, et al. Inflammation directs memory precursor and short-lived effector CD8(+) T cell fates via the graded expression of T-bet transcription factor. *Immunity.* 2007;27(2):281-95.

30. Kaech SM, Tan JT, Wherry EJ, Konieczny BT, Surh CD, and Ahmed R. Selective expression of the interleukin 7 receptor identifies effector CD8 T cells that give rise to long-lived memory cells. *Nat Immunol.* 2003;4(12):1191-8.
31. Herndler-Brandstetter D, Ishigame H, Shinnakasu R, Plajer V, Stecher C, Zhao J, et al. KLRG1(+) Effector CD8(+) T Cells Lose KLRG1, Differentiate into All Memory T Cell Lineages, and Convey Enhanced Protective Immunity. *Immunity.* 2018;48(4):716-29 e8.
32. Gaud G, Lesourne R, and Love PE. Regulatory mechanisms in T cell receptor signalling. *Nat Rev Immunol.* 2018;18(8):485-97.
33. Doering TA, Crawford A, Angelosanto JM, Paley MA, Ziegler CG, and Wherry EJ. Network analysis reveals centrally connected genes and pathways involved in CD8+ T cell exhaustion versus memory. *Immunity.* 2012;37(6):1130-44.
34. Sen DR, Kaminski J, Barnitz RA, Kurachi M, Gerdemann U, Yates KB, et al. The epigenetic landscape of T cell exhaustion. *Science.* 2016;354(6316):1165-9.
35. Omilusik KD, Best JA, Yu B, Goossens S, Weidemann A, Nguyen JV, et al. Transcriptional repressor ZEB2 promotes terminal differentiation of CD8+ effector and memory T cell populations during infection. *J Exp Med.* 2015;212(12):2027-39.
36. Banerjee A, Gordon SM, Intlekofer AM, Paley MA, Mooney EC, Lindsten T, et al. Cutting edge: The transcription factor eomesodermin enables CD8+ T cells to compete for the memory cell niche. *J Immunol.* 2010;185(9):4988-92.
37. Cruz-Guilloty F, Pipkin ME, Djuretic IM, Levanon D, Lotem J, Lichtenheld MG, et al. Runx3 and T-box proteins cooperate to establish the transcriptional program of effector CTLs. *J Exp Med.* 2009;206(1):51-9.
38. Intlekofer AM, Banerjee A, Takemoto N, Gordon SM, Dejong CS, Shin H, et al. Anomalous type 17 response to viral infection by CD8+ T cells lacking T-bet and eomesodermin. *Science.* 2008;321(5887):408-11.
39. Intlekofer AM, Takemoto N, Wherry EJ, Longworth SA, Northrup JT, Palanivel VR, et al. Effector and memory CD8+ T cell fate coupled by T-bet and eomesodermin. *Nat Immunol.* 2005;6(12):1236-44.
40. Zhou X, Yu S, Zhao DM, Harty JT, Badovinac VP, and Xue HH. Differentiation and persistence of memory CD8(+) T cells depend on T cell factor 1. *Immunity.* 2010;33(2):229-40.
41. Kallies A, Xin A, Belz GT, and Nutt SL. Blimp-1 transcription factor is required for the differentiation of effector CD8(+) T cells and memory responses. *Immunity.* 2009;31(2):283-95.
42. Rutishauser RL, Martins GA, Kalachikov S, Chandele A, Parish IA, Meffre E, et al. Transcriptional repressor Blimp-1 promotes CD8(+) T cell terminal differentiation and represses the acquisition of central memory T cell properties. *Immunity.* 2009;31(2):296-308.
43. Ichii H, Sakamoto A, Kuroda Y, and Tokuhisa T. Bcl6 acts as an amplifier for the generation and proliferative capacity of central memory CD8+ T cells. *J Immunol.* 2004;173(2):883-91.
44. Williams MA, Tyznik AJ, and Bevan MJ. Interleukin-2 signals during priming are required for secondary expansion of CD8+ memory T cells. *Nature.* 2006;441(7095):890-3.

45. Giri JG, Ahdieh M, Eisenman J, Shanebeck K, Grabstein K, Kumaki S, et al. Utilization of the beta and gamma chains of the IL-2 receptor by the novel cytokine IL-15. *EMBO J.* 1994;13(12):2822-30.
46. Grabstein KH, Eisenman J, Shanebeck K, Rauch C, Srinivasan S, Fung V, et al. Cloning of a T cell growth factor that interacts with the beta chain of the interleukin-2 receptor. *Science.* 1994;264(5161):965-8.
47. Rathmell JC, Farkash EA, Gao W, and Thompson CB. IL-7 enhances the survival and maintains the size of naive T cells. *J Immunol.* 2001;167(12):6869-76.
48. Schluns KS, Kieper WC, Jameson SC, and Lefrancois L. Interleukin-7 mediates the homeostasis of naive and memory CD8 T cells in vivo. *Nat Immunol.* 2000;1(5):426-32.
49. Vivien L, Benoist C, and Mathis D. T lymphocytes need IL-7 but not IL-4 or IL-6 to survive in vivo. *Int Immunol.* 2001;13(6):763-8.
50. Cui G, Staron MM, Gray SM, Ho PC, Amezquita RA, Wu J, and Kaech SM. IL-7-Induced Glycerol Transport and TAG Synthesis Promotes Memory CD8+ T Cell Longevity. *Cell.* 2015;161(4):750-61.
51. Alves NL, Derks IAM, Berk E, Spijker R, van Lier RAW, and Eldering E. The Noxa/Mcl-1 axis regulates susceptibility to apoptosis under glucose limitation in dividing T cells. *Immunity.* 2006;24(6):703-16.
52. Rathmell JC, Vander Heiden MG, Harris MH, Frauwirth KA, and Thompson CB. In the absence of extrinsic signals, nutrient utilization by lymphocytes is insufficient to maintain either cell size or viability. *Mol Cell.* 2000;6(3):683-92.
53. Vander Heiden MG, Plas DR, Rathmell JC, Fox CJ, Harris MH, and Thompson CB. Growth factors can influence cell growth and survival through effects on glucose metabolism. *Mol Cell Biol.* 2001;21(17):5899-912.
54. Delpoux A, Marcel N, Hess Michelini R, Katayama CD, Allison KA, Glass CK, et al. FOXO1 constrains activation and regulates senescence in CD8 T cells. *Cell Rep.* 2021;34(4):108674.
55. Bennett TJ, Udupa VAV, and Turner SJ. Running to Stand Still: Naive CD8(+) T Cells Actively Maintain a Program of Quiescence. *Int J Mol Sci.* 2020;21(24).
56. Wang R, Dillon CP, Shi LZ, Milasta S, Carter R, Finkelstein D, et al. The transcription factor Myc controls metabolic reprogramming upon T lymphocyte activation. *Immunity.* 2011;35(6):871-82.
57. Ardawi MS, and Newsholme EA. Maximum activities of some enzymes of glycolysis, the tricarboxylic acid cycle and ketone-body and glutamine utilization pathways in lymphocytes of the rat. *Biochem J.* 1982;208(3):743-8.
58. Ardawi MS, and Newsholme EA. Glutamine metabolism in lymphocytes of the rat. *Biochem J.* 1983;212(3):835-42.
59. Jacobs SR, Herman CE, Maciver NJ, Wofford JA, Wieman HL, Hammen JJ, and Rathmell JC. Glucose uptake is limiting in T cell activation and requires CD28-mediated Akt-dependent and independent pathways. *J Immunol.* 2008;180(7):4476-86.
60. Wieman HL, Wofford JA, and Rathmell JC. Cytokine stimulation promotes glucose uptake via phosphatidylinositol-3 kinase/Akt regulation of Glut1 activity and trafficking. *Mol Biol Cell.* 2007;18(4):1437-46.
61. Frauwirth KA, Riley JL, Harris MH, Parry RV, Rathmell JC, Plas DR, et al. The CD28 signaling pathway regulates glucose metabolism. *Immunity.* 2002;16(6):769-77.

62. Chang CH, Curtis JD, Maggi LB, Jr., Faubert B, Villarino AV, O'Sullivan D, et al. Posttranscriptional control of T cell effector function by aerobic glycolysis. *Cell.* 2013;153(6):1239-51.
63. Buck MD, O'Sullivan D, Klein Geltink RI, Curtis JD, Chang CH, Sanin DE, et al. Mitochondrial Dynamics Controls T Cell Fate through Metabolic Programming. *Cell.* 2016;166(1):63-76.
64. Klein Geltink RI, O'Sullivan D, Corrado M, Bremser A, Buck MD, Buescher JM, et al. Mitochondrial Priming by CD28. *Cell.* 2017;171(2):385-97 e11.
65. van der Windt GJ, O'Sullivan D, Everts B, Huang SC, Buck MD, Curtis JD, et al. CD8 memory T cells have a bioenergetic advantage that underlies their rapid recall ability. *Proc Natl Acad Sci U S A.* 2013;110(35):14336-41.
66. O'Sullivan D, van der Windt GJ, Huang SC, Curtis JD, Chang CH, Buck MD, et al. Memory CD8(+) T cells use cell-intrinsic lipolysis to support the metabolic programming necessary for development. *Immunity.* 2014;41(1):75-88.
67. Xu S, Chaudhary O, Rodriguez-Morales P, Sun X, Chen D, Zappasodi R, et al. Uptake of oxidized lipids by the scavenger receptor CD36 promotes lipid peroxidation and dysfunction in CD8(+) T cells in tumors. *Immunity.* 2021;54(7):1561-77 e7.
68. Manzo T, Prentice BM, Anderson KG, Raman A, Schalck A, Codreanu GS, et al. Accumulation of long-chain fatty acids in the tumor microenvironment drives dysfunction in intrapancreatic CD8+ T cells. *J Exp Med.* 2020;217(8).
69. Scharping NE, Menk AV, Moreci RS, Whetstone RD, Dadey RE, Watkins SC, et al. The Tumor Microenvironment Represses T Cell Mitochondrial Biogenesis to Drive Intratumoral T Cell Metabolic Insufficiency and Dysfunction. *Immunity.* 2016;45(2):374-88.
70. Bengsch B, Johnson AL, Kurachi M, Odorizzi PM, Pauken KE, Attanasio J, et al. Bioenergetic Insufficiencies Due to Metabolic Alterations Regulated by the Inhibitory Receptor PD-1 Are an Early Driver of CD8(+) T Cell Exhaustion. *Immunity.* 2016;45(2):358-73.
71. Cogliati S, Frezza C, Soriano ME, Varanita T, Quintana-Cabrera R, Corrado M, et al. Mitochondrial cristae shape determines respiratory chain supercomplexes assembly and respiratory efficiency. *Cell.* 2013;155(1):160-71.
72. Humblin E, Korpas I, Lu J, Filipescu D, van der Heide V, Goldstein S, et al. Sustained CD28 costimulation is required for self-renewal and differentiation of TCF-1(+) PD-1(+) CD8 T cells. *Sci Immunol.* 2023;8(86):eadg0878.
73. Hunt EG, Andrews AM, Larsen SR, and Thaxton JE. The ER-Mitochondria Interface as a Dynamic Hub for T Cell Efficacy in Solid Tumors. *Front Cell Dev Biol.* 2022;10:867341.
74. Chakrabarti R, Ji WK, Stan RV, de Juan Sanz J, Ryan TA, and Higgs HN. INF2-mediated actin polymerization at the ER stimulates mitochondrial calcium uptake, inner membrane constriction, and division. *J Cell Biol.* 2018;217(1):251-68.
75. Bantug GR, Fischer M, Grahlert J, Balmer ML, Unterstab G, Develioglu L, et al. Mitochondria-Endoplasmic Reticulum Contact Sites Function as Immunometabolic Hubs that Orchestrate the Rapid Recall Response of Memory CD8(+) T Cells. *Immunity.* 2018;48(3):542-55 e6.
76. Nava Lauson CB, Tiberti S, Corsetto PA, Conte F, Tyagi P, Machwirth M, et al. Linoleic acid potentiates CD8(+) T cell metabolic fitness and antitumor immunity. *Cell Metab.* 2023;35(4):633-50 e9.

77. Yang JF, Xing X, Luo L, Zhou XW, Feng JX, Huang KB, et al. Mitochondria-ER contact mediated by MFN2-SERCA2 interaction supports CD8(+) T cell metabolic fitness and function in tumors. *Sci Immunol.* 2023;8(87):eabq2424.
78. Rossi A, Pizzo P, and Filadi R. Calcium, mitochondria and cell metabolism: A functional triangle in bioenergetics. *Biochim Biophys Acta Mol Cell Res.* 2019;1866(7):1068-78.
79. Trebak M, and Kinet JP. Calcium signalling in T cells. *Nat Rev Immunol.* 2019;19(3):154-69.
80. Nowell PC. Phytohemagglutinin: an initiator of mitosis in cultures of normal human leukocytes. *Cancer Res.* 1960;20:462-6.
81. Marchingo JM, and Cantrell DA. Protein synthesis, degradation, and energy metabolism in T cell immunity. *Cell Mol Immunol.* 2022;19(3):303-15.
82. Widjaja CE, Olvera JG, Metz PJ, Phan AT, Savas JN, de Bruin G, et al. Proteasome activity regulates CD8+ T lymphocyte metabolism and fate specification. *J Clin Invest.* 2017;127(10):3609-23.
83. Hetz C. The unfolded protein response: controlling cell fate decisions under ER stress and beyond. *Nat Rev Mol Cell Biol.* 2012;13(2):89-102.
84. Yoshida H, Matsui T, Hosokawa N, Kaufman RJ, Nagata K, and Mori K. A time-dependent phase shift in the mammalian unfolded protein response. *Dev Cell.* 2003;4(2):265-71.
85. Yoshida H, Matsui T, Yamamoto A, Okada T, and Mori K. XBP1 mRNA is induced by ATF6 and spliced by IRE1 in response to ER stress to produce a highly active transcription factor. *Cell.* 2001;107(7):881-91.
86. Kamimura D, and Bevan MJ. Endoplasmic reticulum stress regulator XBP-1 contributes to effector CD8+ T cell differentiation during acute infection. *J Immunol.* 2008;181(8):5433-41.
87. Ma X, Bi E, Lu Y, Su P, Huang C, Liu L, et al. Cholesterol Induces CD8(+) T Cell Exhaustion in the Tumor Microenvironment. *Cell Metab.* 2019;30(1):143-56 e5.
88. Song M, Sandoval TA, Chae CS, Chopra S, Tan C, Rutkowski MR, et al. IRE1alpha-XBP1 controls T cell function in ovarian cancer by regulating mitochondrial activity. *Nature.* 2018;562(7727):423-8.
89. Cao Y, Trillo-Tinoco J, Sierra RA, Anadon C, Dai W, Mohamed E, et al. ER stress-induced mediator C/EBP homologous protein thwarts effector T cell activity in tumors through T-bet repression. *Nat Commun.* 2019;10(1):1280.
90. Han J, Back SH, Hur J, Lin YH, Gildersleeve R, Shan J, et al. ER-stress-induced transcriptional regulation increases protein synthesis leading to cell death. *Nat Cell Biol.* 2013;15(5):481-90.
91. Harding HP, Zhang Y, Zeng H, Novoa I, Lu PD, Calfon M, et al. An integrated stress response regulates amino acid metabolism and resistance to oxidative stress. *Mol Cell.* 2003;11(3):619-33.
92. Marciniak SJ, Yun CY, Oyadomari S, Novoa I, Zhang Y, Jungreis R, et al. CHOP induces death by promoting protein synthesis and oxidation in the stressed endoplasmic reticulum. *Genes Dev.* 2004;18(24):3066-77.
93. Hurst KE, Lawrence KA, Essman MT, Walton ZJ, Leddy LR, and Thaxton JE. Endoplasmic Reticulum Stress Contributes to Mitochondrial Exhaustion of CD8(+) T Cells. *Cancer Immunol Res.* 2019;7(3):476-86.

94. Hurst KE, Lawrence KA, Reyes Angeles L, Ye Z, Zhang J, Townsend DM, et al. Endoplasmic Reticulum Protein Disulfide Isomerase Shapes T Cell Efficacy for Adoptive Cellular Therapy of Tumors. *Cells.* 2019;8(12).
95. Cormier JH, Tamura T, Sunryd JC, and Hebert DN. EDEM1 recognition and delivery of misfolded proteins to the SEL1L-containing ERAD complex. *Mol Cell.* 2009;34(5):627-33.
96. Wu X, Siggel M, Ovchinnikov S, Mi W, Svetlov V, Nudler E, et al. Structural basis of ER-associated protein degradation mediated by the Hrd1 ubiquitin ligase complex. *Science.* 2020;368(6489).
97. Christianson JC, Olzmann JA, Shaler TA, Sowa ME, Bennett EJ, Richter CM, et al. Defining human ERAD networks through an integrative mapping strategy. *Nat Cell Biol.* 2011;14(1):93-105.
98. Wang Q, Liu Y, Soetandyo N, Baek K, Hegde R, and Ye Y. A ubiquitin ligase-associated chaperone holdase maintains polypeptides in soluble states for proteasome degradation. *Mol Cell.* 2011;42(6):758-70.
99. Francisco AB, Singh R, Li S, Vani AK, Yang L, Munroe RJ, et al. Deficiency of suppressor enhancer Lin12 1 like (SEL1L) in mice leads to systemic endoplasmic reticulum stress and embryonic lethality. *J Biol Chem.* 2010;285(18):13694-703.
100. Kim H, Kim M, Im SK, and Fang S. Mouse Cre-LoxP system: general principles to determine tissue-specific roles of target genes. *Lab Anim Res.* 2018;34(4):147-59.
101. Qi L, Tsai B, and Arvan P. New Insights into the Physiological Role of Endoplasmic Reticulum-Associated Degradation. *Trends Cell Biol.* 2017;27(6):430-40.
102. Wei X, Lu Y, Lin LL, Zhang C, Chen X, Wang S, et al. Proteomic screens of SEL1L-HRD1 ER-associated degradation substrates reveal its role in glycosylphosphatidylinositol-anchored protein biogenesis. *Nat Commun.* 2024;15(1):659.
103. Zhou Z, Torres M, Sha H, Halbrook CJ, Van den Bergh F, Reinert RB, et al. Endoplasmic reticulum-associated degradation regulates mitochondrial dynamics in brown adipocytes. *Science.* 2020;368(6486):54-60.
104. Liu Q, Yang X, Long G, Hu Y, Gu Z, Boisclair YR, and Long Q. ERAD deficiency promotes mitochondrial dysfunction and transcriptional rewiring in human hepatic cells. *J Biol Chem.* 2020;295(49):16743-53.
105. Liu L, Inoki A, Fan K, Mao F, Shi G, Jin X, et al. ER-associated degradation preserves hematopoietic stem cell quiescence and self-renewal by restricting mTOR activity. *Blood.* 2020;136(26):2975-86.
106. Xu L, Liu X, Peng F, Zhang W, Zheng L, Ding Y, et al. Protein quality control through endoplasmic reticulum-associated degradation maintains haematopoietic stem cell identity and niche interactions. *Nat Cell Biol.* 2020;22(10):1162-9.
107. Sun S, Shi G, Han X, Francisco AB, Ji Y, Mendonca N, et al. Sel1L is indispensable for mammalian endoplasmic reticulum-associated degradation, endoplasmic reticulum homeostasis, and survival. *Proc Natl Acad Sci U S A.* 2014;111(5):E582-91.
108. Pircher H, Baenziger J, Schilham M, Sado T, Kamisaku H, Hengartner H, and Zinkernagel RM. Characterization of virus-specific cytotoxic T cell clones from allogeneic bone marrow chimeras. *Eur J Immunol.* 1987;17(2):159-66.
109. Pircher H, Michalopoulos EE, Iwamoto A, Ohashi PS, Baenziger J, Hengartner H, et al. Molecular analysis of the antigen receptor of virus-specific cytotoxic T cells and identification of a new V alpha family. *Eur J Immunol.* 1987;17(12):1843-6.

110. Carty SA, Gohil M, Banks LB, Cotton RM, Johnson ME, Stelekati E, et al. The Loss of TET2 Promotes CD8(+) T Cell Memory Differentiation. *J Immunol.* 2018;200(1):82-91.
111. Roederer M, Nozzi JL, and Nason MC. SPICE: exploration and analysis of post-cytometric complex multivariate datasets. *Cytometry A.* 2011;79(2):167-74.
112. Martin M. Cutadapt removes adapter sequences from high-throughput sequencing reads. *2011.* 2011;17(1):3.
113. Dobin A, Davis CA, Schlesinger F, Drenkow J, Zaleski C, Jha S, et al. STAR: ultrafast universal RNA-seq aligner. *Bioinformatics.* 2013;29(1):15-21.
114. Li B, and Dewey CN. RSEM: accurate transcript quantification from RNA-Seq data with or without a reference genome. *BMC Bioinformatics.* 2011;12:323.
115. Benjamin C. Hitz J-WL, Otto Jolanki, Meenakshi S. Kagda, Keenan Graham, Paul Sud, Idan Gabdank, J. Seth Strattan, Cricket A. Sloan, Timothy Dreszer, Laurence D. Rowe, Nikhil R. Podduturi, Venkat S. Malladi, Esther T. Chan, Jean M. Davidson, Marcus Ho, Stuart Miyasato, Matt Simison, Forrest Tanaka, Yunhai Luo, Ian Whaling, Eurie L. Hong, Brian T. Lee, Richard Sandstrom, Eric Rynes, Jemma Nelson, Andrew Nishida, Alyssa Ingersoll, Michael Buckley, Mark Frerker, Daniel S Kim, Nathan Boley, Diane Trout, Alex Dobin, Sorena Rahmanian, Dana Wyman, Gabriela Balderrama-Gutierrez, Fairlie Reese, Neva C. Durand, Olga Dudchenko, David Weisz, Suhas S. P. Rao, Alyssa Blackburn, Dimos Gkountaroulis, Mahdi Sadr, Moshe Olshansky, Yossi Eliaz, Dat Nguyen, Ivan Bochkov, Muhammad Saad Shamim, Ragini Mahajan, Erez Aiden, Tom Gingeras, Simon Heath, Martin Hirst, W. James Kent, Anshul Kundaje, Ali Mortazavi, Barbara Wold, J. Michael Cherry. The ENCODE Uniform Analysis Pipelines. *bioRxiv* 2023.
116. Ewels P, Magnusson M, Lundin S, and Kaller M. MultiQC: summarize analysis results for multiple tools and samples in a single report. *Bioinformatics.* 2016;32(19):3047-8.
117. Lee C, Patil S, and Sartor MA. RNA-Enrich: a cut-off free functional enrichment testing method for RNA-seq with improved detection power. *Bioinformatics.* 2016;32(7):1100-2.
118. Stirling DR, Swain-Bowden MJ, Lucas AM, Carpenter AE, Cimini BA, and Goodman A. CellProfiler 4: improvements in speed, utility and usability. *BMC Bioinformatics.* 2021;22(1):433.
119. McCausland MM, and Crotty S. Quantitative PCR technique for detecting lymphocytic choriomeningitis virus in vivo. *J Virol Methods.* 2008;147(1):167-76.
120. Fogo GM, Anzell AR, Maheras KJ, Raghunayakula S, Wider JM, Emaus KJ, et al. Machine learning-based classification of mitochondrial morphology in primary neurons and brain. *Sci Rep.* 2021;11(1):5133.
121. Schindelin J, Arganda-Carreras I, Frise E, Kaynig V, Longair M, Pietzsch T, et al. Fiji: an open-source platform for biological-image analysis. *Nat Methods.* 2012;9(7):676-82.
122. Arganda-Carreras I, Kaynig V, Rueden C, Eliceiri KW, Schindelin J, Cardona A, and Sebastian Seung H. Trainable Weka Segmentation: a machine learning tool for microscopy pixel classification. *Bioinformatics.* 2017;33(15):2424-6.
123. Legland D, Arganda-Carreras I, and Andrey P. MorphoLibJ: integrated library and plugins for mathematical morphology with ImageJ. *Bioinformatics.* 2016;32(22):3532-4.
124. Ollion J, Cochennec J, Loll F, Escude C, and Boudier T. TANGO: a generic tool for high-throughput 3D image analysis for studying nuclear organization. *Bioinformatics.* 2013;29(14):1840-1.

125. Cignoni PaC, Marco and Corsini, Massimiliano and Dellepiane, Matteo and Ganovelli, Fabio and Ranzuglia, Guido. MeshLab: an Open-Source Mesh Processing Tool. *Eurographics Italian Chapter Conference.* 2008.
126. Kurd NS, He Z, Louis TL, Milner JJ, Omilusik KD, Jin W, et al. Early precursors and molecular determinants of tissue-resident memory CD8(+) T lymphocytes revealed by single-cell RNA sequencing. *Sci Immunol.* 2020;5(47).
127. Wolf FA, Angerer P, and Theis FJ. SCANPY: large-scale single-cell gene expression data analysis. *Genome Biol.* 2018;19(1):15.
128. Badia IMP, Velez Santiago J, Braunger J, Geiss C, Dimitrov D, Muller-Dott S, et al. decoupleR: ensemble of computational methods to infer biological activities from omics data. *Bioinform Adv.* 2022;2(1):vbac016.
129. Liberzon A, Subramanian A, Pinchback R, Thorvaldsdottir H, Tamayo P, and Mesirov JP. Molecular signatures database (MSigDB) 3.0. *Bioinformatics.* 2011;27(12):1739-40.
130. Rieckmann JC, Geiger R, Hornburg D, Wolf T, Kveler K, Jarrossay D, et al. Social network architecture of human immune cells unveiled by quantitative proteomics. *Nat Immunol.* 2017;18(5):583-93.
131. Cox J, Hein MY, Luber CA, Paron I, Nagaraj N, and Mann M. Accurate proteome-wide label-free quantification by delayed normalization and maximal peptide ratio extraction, termed MaxLFQ. *Mol Cell Proteomics.* 2014;13(9):2513-26.
132. Brenes AJ, Lamond AI, and Cantrell DA. The Immunological Proteome Resource. *Nat Immunol.* 2023;24(5):731.
133. Rollings CM, Sinclair LV, Brady HJM, Cantrell DA, and Ross SH. Interleukin-2 shapes the cytotoxic T cell proteome and immune environment-sensing programs. *Sci Signal.* 2018;11(526).
134. Tsao HW, Kaminski J, Kurachi M, Barnitz RA, DiIorio MA, LaFleur MW, et al. Batf-mediated epigenetic control of effector CD8(+) T cell differentiation. *Sci Immunol.* 2022;7(68):eabi4919.
135. Giles JR, Manne S, Freilich E, Oldridge DA, Baxter AE, George S, et al. Human epigenetic and transcriptional T cell differentiation atlas for identifying functional T cell-specific enhancers. *Immunity.* 2022;55(3):557-74 e7.
136. Weber EW, Parker KR, Sotillo E, Lynn RC, Anbunathan H, Lattin J, et al. Transient rest restores functionality in exhausted CAR-T cells through epigenetic remodeling. *Science.* 2021;372(6537).
137. Ewels PA, Peltzer A, Fillinger S, Patel H, Alneberg J, Wilm A, et al. The nf-core framework for community-curated bioinformatics pipelines. *Nat Biotechnol.* 2020;38(3):276-8.
138. Love MI, Huber W, and Anders S. Moderated estimation of fold change and dispersion for RNA-seq data with DESeq2. *Genome Biol.* 2014;15(12):550.
139. Hanzelmann S, Castelo R, and Guinney J. GSVA: gene set variation analysis for microarray and RNA-seq data. *BMC Bioinformatics.* 2013;14:7.
140. Gennady Korotkevich VS, Nikolay Budin, Boris Shpak, Maxim N. Artyomov, Alexey Sergushichev. Fast gene set enrichment analysis. *bioRxiv.* 2021.
141. Philipp N, Kazerani M, Nicholls A, Vick B, Wulf J, Straub T, et al. T-cell exhaustion induced by continuous bispecific molecule exposure is ameliorated by treatment-free intervals. *Blood.* 2022;140(10):1104-18.

142. Langmead B, and Salzberg SL. Fast gapped-read alignment with Bowtie 2. *Nat Methods.* 2012;9(4):357-9.
143. Zhang Y, Liu T, Meyer CA, Eeckhoute J, Johnson DS, Bernstein BE, et al. Model-based analysis of ChIP-Seq (MACS). *Genome Biol.* 2008;9(9):R137.
144. Gray SM, Amezquita RA, Guan T, Kleinstein SH, and Kaech SM. Polycomb Repressive Complex 2-Mediated Chromatin Repression Guides Effector CD8(+) T Cell Terminal Differentiation and Loss of Multipotency. *Immunity.* 2017;46(4):596-608.
145. Kaech SM, and Ahmed R. Memory CD8+ T cell differentiation: initial antigen encounter triggers a developmental program in naive cells. *Nat Immunol.* 2001;2(5):415-22.
146. Quiros PM, Goyal A, Jha P, and Auwerx J. Analysis of mtDNA/nDNA Ratio in Mice. *Curr Protoc Mouse Biol.* 2017;7(1):47-54.
147. Liu X, Yu J, Xu L, Umphred-Wilson K, Peng F, Ding Y, et al. Notch-induced endoplasmic reticulum-associated degradation governs mouse thymocyte beta-selection. *Elife.* 2021;10.
148. Soneson C, Love MI, and Robinson MD. Differential analyses for RNA-seq: transcript-level estimates improve gene-level inferences. *F1000Res.* 2015;4:1521.
149. Tyanova S, Temu T, Sinitcyn P, Carlson A, Hein MY, Geiger T, et al. The Perseus computational platform for comprehensive analysis of (prote)omics data. *Nat Methods.* 2016;13(9):731-40.
150. Wickham H, MA, JB, WC, , McGowan LDA, et al. Welcome to the Tidyverse. *The Journal of Open Source Software.* 2019.
151. Thorvaldsdottir H, Robinson JT, and Mesirov JP. Integrative Genomics Viewer (IGV): high-performance genomics data visualization and exploration. *Brief Bioinform.* 2013;14(2):178-92.
152. Wong P, and Pamer EG. CD8 T cell responses to infectious pathogens. *Annu Rev Immunol.* 2003;21:29-70.
153. Philip M, and Schietinger A. CD8(+) T cell differentiation and dysfunction in cancer. *Nat Rev Immunol.* 2022;22(4):209-23.
154. Jameson SC, and Masopust D. Understanding Subset Diversity in T Cell Memory. *Immunity.* 2018;48(2):214-26.
155. Badovinac VP, Porter BB, and Harty JT. Programmed contraction of CD8(+) T cells after infection. *Nat Immunol.* 2002;3(7):619-26.
156. Gray SM, Kaech SM, and Staron MM. The interface between transcriptional and epigenetic control of effector and memory CD8(+) T-cell differentiation. *Immunol Rev.* 2014;261(1):157-68.
157. Reina-Campos M, Scharping NE, and Goldrath AW. CD8(+) T cell metabolism in infection and cancer. *Nat Rev Immunol.* 2021;21(11):718-38.
158. Schubert U, Anton LC, Gibbs J, Norbury CC, Yewdell JW, and Bennink JR. Rapid degradation of a large fraction of newly synthesized proteins by proteasomes. *Nature.* 2000;404(6779):770-4.
159. Lykke-Andersen J, and Bennett EJ. Protecting the proteome: Eukaryotic cotranslational quality control pathways. *J Cell Biol.* 2014;204(4):467-76.
160. Walter P, and Ron D. The unfolded protein response: from stress pathway to homeostatic regulation. *Science.* 2011;334(6059):1081-6.
161. Mueller B, Lilley BN, and Ploegh HL. SEL1L, the homologue of yeast Hrd3p, is involved in protein dislocation from the mammalian ER. *J Cell Biol.* 2006;175(2):261-70.

162. Shrestha N, Liu T, Ji Y, Reinert RB, Torres M, Li X, et al. Sel1L-Hrd1 ER-associated degradation maintains beta cell identity via TGF-beta signaling. *J Clin Invest.* 2020;130(7):3499-510.
163. Ji Y, Kim H, Yang L, Sha H, Roman CA, Long Q, and Qi L. The Sel1L-Hrd1 Endoplasmic Reticulum-Associated Degradation Complex Manages a Key Checkpoint in B Cell Development. *Cell Rep.* 2016;16(10):2630-40.
164. Thepsuwan P, Bhattacharya A, Song Z, Hippleheuser S, Feng S, Wei X, et al. Hepatic SEL1L-HRD1 ER-associated degradation regulates systemic iron homeostasis via ceruloplasmin. *Proc Natl Acad Sci U S A.* 2023;120(2):e2212644120.
165. Bhattacharya A, Sun S, Wang H, Liu M, Long Q, Yin L, et al. Hepatic Sel1L-Hrd1 ER-associated degradation (ERAD) manages FGF21 levels and systemic metabolism via CREBH. *EMBO J.* 2018;37(22).
166. Sha H, Sun S, Francisco AB, Ehrhardt N, Xue Z, Liu L, et al. The ER-associated degradation adaptor protein Sel1L regulates LPL secretion and lipid metabolism. *Cell Metab.* 2014;20(3):458-70.
167. Sun S, Lourie R, Cohen SB, Ji Y, Goodrich JK, Poole AC, et al. Epithelial Sel1L is required for the maintenance of intestinal homeostasis. *Mol Biol Cell.* 2016;27(3):483-90.
168. Yoshida S, Wei X, Zhang G, O'Connor CL, Torres M, Zhou Z, et al. Endoplasmic reticulum-associated degradation is required for nephrin maturation and kidney glomerular filtration function. *J Clin Invest.* 2021;131(7).
169. Wei J, Yuan Y, Chen L, Xu Y, Zhang Y, Wang Y, et al. ER-associated ubiquitin ligase HRD1 programs liver metabolism by targeting multiple metabolic enzymes. *Nat Commun.* 2018;9(1):3659.
170. Xu Y, Melo-Cardenas J, Zhang Y, Gau I, Wei J, Montauti E, et al. The E3 ligase Hrd1 stabilizes Tregs by antagonizing inflammatory cytokine-induced ER stress response. *JCI Insight.* 2019;4(5).
171. Dils AT, Correa LO, Gronevelt JP, Liu L, Kadiyala P, Li Q, and Carty SA. The endoplasmic reticulum associated degradation adaptor Sel1L regulates T cell homeostasis and function. 2021:2021.05.22.445275.
172. Gao Y, Li W, Wang Z, Zhang C, He Y, Liu X, et al. SEL1L preserves CD8(+) T-cell survival and homeostasis by fine-tuning PERK signaling and the IL-15 receptor-mediated mTORC1 axis. *Cell Mol Immunol.* 2023.
173. Carrio R, Bathe OF, and Malek TR. Initial antigen encounter programs CD8+ T cells competent to develop into memory cells that are activated in an antigen-free, IL-7- and IL-15-rich environment. *J Immunol.* 2004;172(12):7315-23.
174. Schuck S, Prinz WA, Thorn KS, Voss C, and Walter P. Membrane expansion alleviates endoplasmic reticulum stress independently of the unfolded protein response. *J Cell Biol.* 2009;187(4):525-36.
175. Bernales S, McDonald KL, and Walter P. Autophagy counterbalances endoplasmic reticulum expansion during the unfolded protein response. *PLoS Biol.* 2006;4(12):e423.
176. Williams DB. Beyond lectins: the calnexin/calreticulin chaperone system of the endoplasmic reticulum. *J Cell Sci.* 2006;119(Pt 4):615-23.
177. Kim S, Khoriaty R, Li L, McClune M, Kalfa TA, Wu J, et al. ER-to-Golgi transport and SEC23-dependent COPII vesicles regulate T cell alloimmunity. *J Clin Invest.* 2021;131(2).

178. Johnston JA, Ward CL, and Kopito RR. Aggresomes: a cellular response to misfolded proteins. *J Cell Biol.* 1998;143(7):1883-98.
179. Chau V, Tobias JW, Bachmair A, Marriott D, Ecker DJ, Gonda DK, and Varshavsky A. A multiubiquitin chain is confined to specific lysine in a targeted short-lived protein. *Science.* 1989;243(4898):1576-83.
180. Calfon M, Zeng H, Urano F, Till JH, Hubbard SR, Harding HP, et al. IRE1 couples endoplasmic reticulum load to secretory capacity by processing the XBP-1 mRNA. *Nature.* 2002;415(6867):92-6.
181. Blazanin N, Son J, Craig-Lucas AB, John CL, Breech KJ, Podolsky MA, and Glick AB. ER stress and distinct outputs of the IRE1alpha RNase control proliferation and senescence in response to oncogenic Ras. *Proc Natl Acad Sci U S A.* 2017;114(37):9900-5.
182. Riesenberg BP, Hunt EG, Tennant MD, Hurst KE, Andrews AM, Leddy LR, et al. Stress-Mediated Attenuation of Translation Undermines T-cell Activity in Cancer. *Cancer Res.* 2022;82(23):4386-99.
183. Li S, Francisco AB, Munroe RJ, Schimenti JC, and Long Q. SEL1L deficiency impairs growth and differentiation of pancreatic epithelial cells. *BMC Dev Biol.* 2010;10:19.
184. Ross SH, Rollings C, Anderson KE, Hawkins PT, Stephens LR, and Cantrell DA. Phosphoproteomic Analyses of Interleukin 2 Signaling Reveal Integrated JAK Kinase-Dependent and -Independent Networks in CD8(+) T Cells. *Immunity.* 2016;45(3):685-700.
185. Huber M, and Lohoff M. IRF4 at the crossroads of effector T-cell fate decision. *Eur J Immunol.* 2014;44(7):1886-95.
186. Huang S, Shen Y, Pham D, Jiang L, Wang Z, Kaplan MH, et al. IRF4 Modulates CD8(+) T Cell Sensitivity to IL-2 Family Cytokines. *Immunohorizons.* 2017;1(6):92-100.
187. Nayar R, Enos M, Prince A, Shin H, Hemmers S, Jiang JK, et al. TCR signaling via Tec kinase ITK and interferon regulatory factor 4 (IRF4) regulates CD8+ T-cell differentiation. *Proc Natl Acad Sci U S A.* 2012;109(41):E2794-802.
188. Yu B, Zhang K, Milner JJ, Toma C, Chen R, Scott-Browne JP, et al. Epigenetic landscapes reveal transcription factors that regulate CD8(+) T cell differentiation. *Nat Immunol.* 2017;18(5):573-82.
189. Akondy RS, Monson ND, Miller JD, Edupuganti S, Teuwen D, Wu H, et al. The yellow fever virus vaccine induces a broad and polyfunctional human memory CD8+ T cell response. *J Immunol.* 2009;183(12):7919-30.
190. Betts MR, Nason MC, West SM, De Rosa SC, Migueles SA, Abraham J, et al. HIV nonprogressors preferentially maintain highly functional HIV-specific CD8+ T cells. *Blood.* 2006;107(12):4781-9.
191. Jeannet G, Boudousquie C, Gardiol N, Kang J, Huelsken J, and Held W. Essential role of the Wnt pathway effector Tcf-1 for the establishment of functional CD8 T cell memory. *Proc Natl Acad Sci U S A.* 2010;107(21):9777-82.
192. Zhou X, and Xue HH. Cutting edge: generation of memory precursors and functional memory CD8+ T cells depends on T cell factor-1 and lymphoid enhancer-binding factor-1. *J Immunol.* 2012;189(6):2722-6.
193. Sallusto F, Lenig D, Forster R, Lipp M, and Lanzavecchia A. Two subsets of memory T lymphocytes with distinct homing potentials and effector functions. *Nature.* 1999;401(6754):708-12.

194. Wherry EJ, Teichgraber V, Becker TC, Masopust D, Kaech SM, Antia R, et al. Lineage relationship and protective immunity of memory CD8 T cell subsets. *Nat Immunol.* 2003;4(3):225-34.
195. Hikono H, Kohlmeier JE, Takamura S, Wittmer ST, Roberts AD, and Woodland DL. Activation phenotype, rather than central- or effector-memory phenotype, predicts the recall efficacy of memory CD8+ T cells. *J Exp Med.* 2007;204(7):1625-36.
196. Mishra P, Carelli V, Manfredi G, and Chan DC. Proteolytic cleavage of Opa1 stimulates mitochondrial inner membrane fusion and couples fusion to oxidative phosphorylation. *Cell Metab.* 2014;19(4):630-41.
197. Rowland AA, and Voeltz GK. Endoplasmic reticulum-mitochondria contacts: function of the junction. *Nat Rev Mol Cell Biol.* 2012;13(10):607-25.
198. Baixauli F, Piletic K, Puleston DJ, Villa M, Field CS, Flachsmann LJ, et al. An LKB1-mitochondria axis controls T(H)17 effector function. *Nature.* 2022;610(7932):555-61.
199. Stevens MG, Mason FM, and Bullock TNJ. The mitochondrial fission protein DRP1 influences memory CD8+ T cell formation and function. *J Leukoc Biol.* 2023.
200. Preston GC, Sinclair LV, Kaskar A, Hukelmann JL, Navarro MN, Ferrero I, et al. Single cell tuning of Myc expression by antigen receptor signal strength and interleukin-2 in T lymphocytes. *EMBO J.* 2015;34(15):2008-24.
201. Chan JD, Lai J, Slaney CY, Kallies A, Beavis PA, and Darcy PK. Cellular networks controlling T cell persistence in adoptive cell therapy. *Nat Rev Immunol.* 2021;21(12):769-84.
202. Cui W, and Kaech SM. Generation of effector CD8+ T cells and their conversion to memory T cells. *Immunol Rev.* 2010;236:151-66.
203. Akondy RS, Fitch M, Edupuganti S, Yang S, Kissick HT, Li KW, et al. Origin and differentiation of human memory CD8 T cells after vaccination. *Nature.* 2017;552(7685):362-7.
204. Fraietta JA, Nobles CL, Sammons MA, Lundh S, Carty SA, Reich TJ, et al. Disruption of TET2 promotes the therapeutic efficacy of CD19-targeted T cells. *Nature.* 2018;558(7709):307-12.
205. Restifo NP, and Gattinoni L. Lineage relationship of effector and memory T cells. *Curr Opin Immunol.* 2013;25(5):556-63.
206. Fuertes Marraco SA, Soneson C, Cagnon L, Gannon PO, Allard M, Abed Maillard S, et al. Long-lasting stem cell-like memory CD8+ T cells with a naive-like profile upon yellow fever vaccination. *Sci Transl Med.* 2015;7(282):282ra48.
207. Gattinoni L, Lugli E, Ji Y, Pos Z, Paulos CM, Quigley MF, et al. A human memory T cell subset with stem cell-like properties. *Nat Med.* 2011;17(10):1290-7.
208. Willinger T, Freeman T, Herbert M, Hasegawa H, McMichael AJ, and Callan MF. Human naive CD8 T cells down-regulate expression of the WNT pathway transcription factors lymphoid enhancer binding factor 1 and transcription factor 7 (T cell factor-1) following antigen encounter in vitro and in vivo. *J Immunol.* 2006;176(3):1439-46.
209. Pauken KE, Sammons MA, Odorizzi PM, Manne S, Godec J, Khan O, et al. Epigenetic stability of exhausted T cells limits durability of reinvigoration by PD-1 blockade. *Science.* 2016;354(6316):1160-5.
210. Chen Z, Ji Z, Ngiow SF, Manne S, Cai Z, Huang AC, et al. TCF-1-Centered Transcriptional Network Drives an Effector versus Exhausted CD8 T Cell-Fate Decision. *Immunity.* 2019;51(5):840-55 e5.

211. Yao C, Sun HW, Lacey NE, Ji Y, Moseman EA, Shih HY, et al. Single-cell RNA-seq reveals TOX as a key regulator of CD8(+) T cell persistence in chronic infection. *Nat Immunol.* 2019;20(7):890-901.
212. Yamamoto K, Suzuki N, Wada T, Okada T, Yoshida H, Kaufman RJ, and Mori K. Human HRD1 promoter carries a functional unfolded protein response element to which XBP1 but not ATF6 directly binds. *J Biochem.* 2008;144(4):477-86.
213. Lee AH, Iwakoshi NN, and Glimcher LH. XBP-1 regulates a subset of endoplasmic reticulum resident chaperone genes in the unfolded protein response. *Mol Cell Biol.* 2003;23(21):7448-59.
214. June CH, O'Connor RS, Kawalekar OU, Ghassemi S, and Milone MC. CAR T cell immunotherapy for human cancer. *Science.* 2018;359(6382):1361-5.
215. Goebeler ME, and Bargou RC. T cell-engaging therapies - BiTEs and beyond. *Nat Rev Clin Oncol.* 2020;17(7):418-34.
216. Soares Moretti AI, and Martins Laurindo FR. Protein disulfide isomerases: Redox connections in and out of the endoplasmic reticulum. *Arch Biochem Biophys.* 2017;617:106-19.
217. Jha V, Kumari T, Manickam V, Assar Z, Olson KL, Min JK, and Cho J. ERO1-PDI Redox Signaling in Health and Disease. *Antioxid Redox Signal.* 2021;35(13):1093-115.
218. Fernandez-Alfara M, Sibilio A, Martin J, Tusquets Uxo E, Malumbres M, Alcalde V, et al. Antitumor T-cell function requires CPEB4-mediated adaptation to chronic endoplasmic reticulum stress. *EMBO J.* 2023;42(9):e111494.
219. Xu Y, Zhao F, Qiu Q, Chen K, Wei J, Kong Q, et al. The ER membrane-anchored ubiquitin ligase Hrd1 is a positive regulator of T-cell immunity. *Nat Commun.* 2016;7:12073.
220. Hong HS, Mbah NE, Shan M, Loesel K, Lin L, Sajjakulnukit P, et al. OXPHOS promotes apoptotic resistance and cellular persistence in T(H)17 cells in the periphery and tumor microenvironment. *Sci Immunol.* 2022;7(77):eabm8182.
221. Wang N, Wang C, Zhao H, He Y, Lan B, Sun L, and Gao Y. The MAMs Structure and Its Role in Cell Death. *Cells.* 2021;10(3).
222. Friedman JR, Lackner LL, West M, DiBenedetto JR, Nunnari J, and Voeltz GK. ER tubules mark sites of mitochondrial division. *Science.* 2011;334(6054):358-62.
223. Guo A, Huang H, Zhu Z, Chen MJ, Shi H, Yuan S, et al. cBAF complex components and MYC cooperate early in CD8(+) T cell fate. *Nature.* 2022;607(7917):135-41.
224. Bianchi T, Gasser S, Trumpp A, and MacDonald HR. c-Myc acts downstream of IL-15 in the regulation of memory CD8 T-cell homeostasis. *Blood.* 2006;107(10):3992-9.
225. Haque M, Song J, Fino K, Wang Y, Sandhu P, Song X, et al. C-Myc regulation by costimulatory signals modulates the generation of CD8+ memory T cells during viral infection. *Open Biol.* 2016;6(1):150208.
226. Lindsten T, June CH, and Thompson CB. Multiple mechanisms regulate c-myc gene expression during normal T cell activation. *EMBO J.* 1988;7(9):2787-94.
227. Guy CS, Vignali KM, Temirov J, Bettini ML, Overacre AE, Smeltzer M, et al. Distinct TCR signaling pathways drive proliferation and cytokine production in T cells. *Nat Immunol.* 2013;14(3):262-70.
228. Rodriguez-Otero P, and San-Miguel JF. Cellular therapy for multiple myeloma: what's now and what's next. *Hematology Am Soc Hematol Educ Program.* 2022;2022(1):180-9.

229. van de Donk N, and Zweegman S. T-cell-engaging bispecific antibodies in cancer. *Lancet.* 2023;402(10396):142-58.
230. Mackensen A, Muller F, Mougiakakos D, Boltz S, Wilhelm A, Aigner M, et al. Anti-CD19 CAR T cell therapy for refractory systemic lupus erythematosus. *Nat Med.* 2022;28(10):2124-32.
231. Gumber D, and Wang LD. Improving CAR-T immunotherapy: Overcoming the challenges of T cell exhaustion. *EBioMedicine.* 2022;77:103941.
232. Wu H, Carvalho P, and Voeltz GK. Here, there, and everywhere: The importance of ER membrane contact sites. *Science.* 2018;361(6401).
233. Veiga-Fernandes H, Walter U, Bourgeois C, McLean A, and Rocha B. Response of naive and memory CD8+ T cells to antigen stimulation in vivo. *Nat Immunol.* 2000;1(1):47-53.
234. Panganiban RA, Park HR, Sun M, Shumyatcher M, Himes BE, and Lu Q. Genome-wide CRISPR screen identifies suppressors of endoplasmic reticulum stress-induced apoptosis. *Proc Natl Acad Sci U S A.* 2019;116(27):13384-93.
235. McLane LM, Abdel-Hakeem MS, and Wherry EJ. CD8 T Cell Exhaustion During Chronic Viral Infection and Cancer. *Annu Rev Immunol.* 2019;37:457-95.
236. Miller BC, Sen DR, Al Abosy R, Bi K, Virkud YV, LaFleur MW, et al. Subsets of exhausted CD8(+) T cells differentially mediate tumor control and respond to checkpoint blockade. *Nat Immunol.* 2019;20(3):326-36.
237. Maurel M, Chevet E, Tavernier J, and Gerlo S. Getting RIDD of RNA: IRE1 in cell fate regulation. *Trends Biochem Sci.* 2014;39(5):245-54.
238. Le Thomas A, Ferri E, Marsters S, Harnoss JM, Lawrence DA, Zuazo-Gaztelu I, et al. Decoding non-canonical mRNA decay by the endoplasmic-reticulum stress sensor IRE1alpha. *Nat Commun.* 2021;12(1):7310.
239. Iida Y, Fujimori T, Okawa K, Nagata K, Wada I, and Hosokawa N. SEL1L protein critically determines the stability of the HRD1-SEL1L endoplasmic reticulum-associated degradation (ERAD) complex to optimize the degradation kinetics of ERAD substrates. *J Biol Chem.* 2011;286(19):16929-39.
240. Iwakoshi NN, Pypaert M, and Glimcher LH. The transcription factor XBP-1 is essential for the development and survival of dendritic cells. *J Exp Med.* 2007;204(10):2267-75.
241. Peng JJ, Wang L, Li Z, Ku CL, and Ho PC. Metabolic challenges and interventions in CAR T cell therapy. *Sci Immunol.* 2023;8(82):eabq3016.
242. Ozcan U, Yilmaz E, Ozcan L, Furuhashi M, Vaillancourt E, Smith RO, et al. Chemical chaperones reduce ER stress and restore glucose homeostasis in a mouse model of type 2 diabetes. *Science.* 2006;313(5790):1137-40.
243. Henderson MJ, Trychta KA, Yang SM, Back S, Yasgar A, Wires ES, et al. A target-agnostic screen identifies approved drugs to stabilize the endoplasmic reticulum-resident proteome. *Cell Rep.* 2021;35(4):109040.